UNDERSTANDING THE SINGLE CHANNEL BEHAVIOR OF GLUA3 RECEPTORS

A Dissertation

Presented to the Faculty of the Graduate School

of Cornell University

In Partial Fulfillment of the Requirements for the Degree of

Doctor of Philosophy

by

Kinning Poon

January 2011

UNDERSTANDING THE BEHAVIOR OF SINGLE CHANNEL GLUA3 RECEPTORS

Kinning Poon, Ph. D.

Cornell University 2011

A tremendous amount of research has been dedicated to elucidating the functional mechanism of glutamate receptors. AMPA receptors in particular were the first in which structure was correlated to function; specifically, the structures of the isolated ligand binding domain (LBD) bound to different agonists, partial agonists, and antagonists, were compared to whole cell electrophysiological recordings. A correlation between the degree of lobe closure and maximal currents was discovered; that is, the greater the degree of LBD closure, the larger the measured currents. However, as more information relating LBD closure to channel activation began to surface, it became clear the relationship was not as direct as previously thought. The studies in this dissertation look at the single channel behavior of GluA3 receptors and supply new evidence that both full and partial agonists induce a similar mechanism of activation on AMPA receptors. These studies examine how subtle changes in the LBD can affect single channel properties.

GluA3 channels have three conductance levels and the probability of opening to any of these levels is dependent on the agonist; that is, full agonists are more likely to open the channel to the largest conductance level than partial agonists. GluA3 channels also display modal behaviors that are determined by the open probability and vary from very low to very high. A never before seen fast channel blocking effect is also reported. These modal behaviors are present at low agonist concentrations and

observed for all the agonists tested (glutamate, FW, ClW and NO_2W). The agonists tested were all able to induce full LBD closures. The stability of the closures differed in the D655/S656 peptide conformation and the M712 orientation. D655/S656 flipped conformation allows H-bonding across the lobes to occur, stabilizing LBD closures. Bulkier substituents in the 5 position of the willardiine compounds reorients M712, which could alter the M4 transmembrane helix, thereby affecting channel gating. Based on these studies, although the mechanism of activation is similar for the agonists tested, it seems that subtle dynamic conformations of amino acids in the LBD caused by agonist binding can affect the agonist induced activation.

BIOGRAPHICAL SKETCH

The author was born on one fine afternoon in the month of June of 1982, on the island of Manhattan. She was raised in a neighborhood of Brooklyn that bordered between Jewish, Latin, and Asian communities. Always an avid dreamer, she would sit on the steps that lead to the front door of her house, envisioning all the different possibilities the world contained for her, and resolving to pursue a line of work that could in any manner be beneficial to society. She didn't realize it at the time, but her potential to excel in the sciences surpassed her own opinion of herself. Her excitement for science began the day she received a perfect score on a science exam, placing even higher than the top student in her junior high school class. Unaware of what the future held, she overcame many obstacles as she journeyed her way through science and math courses at E.R. Murrow high school. She attended Stony Brook University, where she not only met her future husband, but also began to embark on a scientific journey in research. As the end to her undergraduate studies approached, the fork in the road was placed in front of her: basic science research or medicine? In the end, the author chose to pursue a career as a research scientist and placed her faith in a graduate program at Cornell University where she spent the next five years pursuing her career.

This work is dedicated to my father and my older brother who both selflessly gave me the opportunity to attain my goals. This work is also dedicated to Thomas for always staying by my side.

ACKNOWLEDGMENTS

I would first like to thank my advisor, Dr. Robert Oswald, for accepting me into his lab. He gave me space to be independent while providing much guidance and abundant help. I am grateful for the advice he gave me regarding professional matters; these experiences have prepared me for my entrance into the world of science and the politics that is involved. I would also like to acknowledge my colleagues in the laboratory, who have provided discussions on many topics and created an interesting environment to work in. I would like to acknowledge my committee members, Dr. Linda Nowak, Dr. Gregory Weiland, and Dr. David Lin, who all provided in their own ways, help, advice, and mentorship. I would like to especially thank Dr. Nowak for providing me with so many things, such as cells, CTZ, (and the list goes on). A large thank you to Susan Coombs, Dr. George Hess, and Dr. Geoffrey Sharp for the numerous amounts of lab equipment I borrowed. To Blake, Greg, Debbie, Cindy, and Val, I honestly don't know how anyone can function without any one of you, and so I humbly thank you for everything that has been done for me these past few years.

Most importantly, I saved the best for last – my family (Dad, Stepmom, Kevin and Kin). Throughout this journey, they have been my motivation to cross the finish line. My father's support can only be appreciated with his words (translated from Chinese), "If you don't have enough money to submit your paper, if it will help you graduate, Dad will help you." I have only gratitude for my older brother, who always told me that I was 'smarter than him' as motivation to chase my geeky dreams. To my loving fiancé, Thomas, where would I be if I never met you? I would not have majored in Pharmacology, gotten my first research tech job, and applied to graduate school at Cornell. You told me I could do it and I did.

Supported by a Ruth L. Kirschstein NRSA (1F31NS063518)

TABLE OF CONTENTS

Biographical Sketch iii

Dedication iv

Acknowledgements v

Table of Contents vi

List of Figures ix

List of Tables xi

List of Abbreviations xii

Chapter 1: Introduction – The Progression of Ion Channel Research in the Quest to Understand Ionotropic Glutamate Receptor Function 1

1.1 Ion Channels – Classical Biophysics 2

1.2 Ligand Gated Ion Channels 3

1.3 The Glutamate Receptor Family of Ion Channels 4

I. Classification 5

A. AMPA Receptors 5

B. Kainate Receptors 7

C. NMDA Receptors 8

D. Delta Receptors 10

II. Glutamate Receptor Structure and Function 11

A. Mechanism of Activation 13

B. Mechanism of Desensitization 19

1.4 The Role of Glutamate Receptors in Synaptic Plasticity 20

1.5 Glutamate Receptor Involvement in CNS Diseases and Disorders 22
I. Excitotoxicity Events 23
II. Amyotrophic Lateral Sclerosis 24
III. Alzheimer's Disease 25
IV. Epilepsy 26
1.6 Outline of Dissertation Research 26
References 29

Chapter 2: Characterizing Single Channel Behavior of GluA3 Receptors 48

2.1 Abstract 49
2.2 Introduction 49
2.3 Methods 51
2.4 Results 60
2.5 Discussion 80
References 86

Chapter 3: Structural and Functional Mechanism for Modal Gating Behaviors of GluA3 Receptors 91

3.1 Abstract 92
3.2. Introduction 93
3.3 Methods 94
3.4 Results 102
3.5 Discussion 127
3.6 Conclusions 130

References 132

Chapter 4: Flicker Gating Mode of Single Channel GluA3 Receptors 136

4.1 Abstract 137
4.2 Introduction 137
4.3 Methods 138
4.4 Results 146
4.5 Discussion 154
References 157

Chapter 5: Conclusions 159

5.1 Summary of findings 160
5.2 Future directions 164
References 168

Appendix: Distinct Modulations of Human Capsaicin Receptor by Protons and Magnesium through Different Domains 170

A.1 Abstract 171
A.2 Introduction 171
A.3 Methods 173
A.4 Results 176
A.5 Discussion 195
References 200

LIST OF FIGURES

Figure 1.1: Topology of a glutamate receptor subunit 12

Figure 2.1: Demonstration of three open conductance states 54

Figure 2.2: Kinetic models 56

Figure 2.3: Single channel trace and amplitude histograms acquired with glutamate and FW 61

Figure 2.4: Demonstration of three states: current – voltage relationship 64

Figure 2.5: Dwell time histogram for glutamate and FW 65

Figure 2.6: Single channel traces of modal behaviors 71

Figure 2.7: Modal transitions and modal transition matrices for one patch 72

Figure 2.8: Single channel trace of stable openings to one conductance level 79

Figure 3.1: Kinetic models 97

Figure 3.2: D655/S656 peptide conformation 103

Figure 3.3: NO_2W bound to GluA2 contributes to stability by making additional H-bonds 107

Figure 3.4: Conformation of the side chain of M712 109

Figure 3.5: GluA3 channels have three conductance levels 111

Figure 3.6: Dwell time histograms 112

Figure 3.7: Single channel traces of modal behaviors 117

Figure 4.1: Representative trace of 200 μM glutamate in flicker mode 141

Figure 4.2: Representative trace of 500 $_m$M NO_2W 147

Figure 4.3: Representative trace of glutamate, FW, ClW and NO_2W 148

Figure 4.4: Current – voltage relationship for glutamate, FW, ClW and NO_2W 150

Figure 4.5: Flicker activity in the absence of CTZ 151

Figure A.1: Protons increase the capsaicin efficacy of hTRPV1 but not that of rTRPV1 177

Figure A.2: Protons block the hTRPV1 single channel current in the presence of 100 μM capsaicin 180

Figure A.3: Capsaicin dose-response curves of wild type, chimeras, and hE536Q 181

Figure A.4: A and B, representative traces for steady-state currents of hTRPV1 and rTRPV 183

Figure A.5: TM1–4 in hTRPV1 determines the proton augmentation of capsaicin efficacy 185

Figure A.6: Mutant E536Q of hTRPV1 eliminates the proton modulation of capsaicin efficacy 187

Figure A.7: Mg^{2+} increases the capsaicin efficacy of hTRPV1 but not that of rTRPV1 190

Figure A.8: Human TM5–6 region is required for the Mg^{2+} potentiation of capsaicin efficacy 191

Figure A.9: Mg^{2+} effect on hTRPV1 is diminished when the channel is substantially opened by the combination of full-dose capsaicin and protons. 193

Figure A.10: TM5–6 determines the differential Mg^{2+} effects on the whole cell basal currents of human and rat TRPV1 194

LIST OF TABLES

Table 1.1: The relationship between the degree of LBD closure and receptor function 15

Table 2.1: Summary of single channel records 58

Table 2.2: State transition matrices 66

Table 2.3: Dwell times for glutamate and FW 68

Table 2.4: Efficacy factor for modes 75

Table 2.5: Keq values for glutamate and FW 76

Table 3.1: Summary of single channel records 98

Table 3.2: State transition matrices 114

Table 3.3: The averaged probability of the GluA3 channel visiting each conductance level in the VH mode 115

Table 3.4: Efficacy factors for modes 116

Table 3.5: Patches which exhibited an alternative kinetic behaviors 120

Table 3.6: Keq values for ClW and NO_2W 121

Table 3.7: Dwell time histograms 124

Table 4.1: Summary of all the patches acquired in flicker mode 142

Table 4.2: Kinetic behavior of flicker mode 152

Table 4.3: Flicker activity is voltage dependent 153

Table A.1: Proton and magnesium effects on the 100 μM capsaicin-induced currents of the wild type and chimeric TRPV1s 178

Table A2: Activation parameters of TRPV1 wild type and mutant receptors 184

LIST OF ABBREVIATIONS

AD	Alzheimer's disease
ALS	amyotrophic lateral sclerosis
AMPA	α-amino-3-hydroxy-5-methyl-4-isoxazolepropionic acid
BrW	Bromowillardiine
ClW	chlorowillardiine
CNS	central nervous system
CNQX	6-cyano-7-nitroquinoxaline-2,3-dione
CTZ	cyclothiazide
EPSP	excitatory post-synaptic potential
FW	fluorowillardiine
GluA	glutamate ampa receptor
GluK	glutamate kainate receptor
GluN	glutamate NMDA receptor
Gluδ	glutamate delta receptor
HEK	human embryonic kidney cells
iGluR	ionotropic glutamate receptor
IW	Iodowillardiine
LBD	ligand binding domain
LL	log likelihood units
LTD	long term depression
LTP	long term potentiation
MIL	maximum interval likelihood
ms	millisecond
mV	millivolts

nAchR	nicotinic acetylcholine receptors
NMDA	n-methyl-d-aspartate
NO_2W	nitrowillardiine
pA	picoampere
P_c	closed probability
P_o	open probability
pS	pico-siemens
SKM	segmental-k-means
TARP	transmembrane AMPAR regulatory protein
tau	dwell time
t_{crit}	critical time

CHAPTER 1

Introduction: The Progression of Ion Channel Research in the Quest to Understanding Ionotropic Glutamate Receptor Function

1.1 Ion Channels

One of the basic principles in biological systems is that cells communicate with each other through chemical and electrical means. The path to understanding cellular communication begins in 1663, when German physicist Otto von Guericke set forth the idea of electrical energy by creating the first electric generator of static electricity (1). Another two centuries had passed before Walther Nernst began testing how the diffusion of electrolytes in solution created potentials and developed the famous Nernst equation in 1888, that described the equilibrium potential of an ion as a function of the ratio of ions outside to inside the cell and the valence (1). Sidney Ringer was simultaneously running experiments on frog hearts with varying salt solutions of Na^+, K^+ and Ca^{2+}, showing that specific ion concentrations of K^+, Na^+ and Ca^{2+} are needed to keep the heart beating (1). These advances in electrochemistry positioned researchers for future studies in cellular excitation and ultimately lead to the discovery of ion channels that governed cellular communication.

Julius Bernstein was the first person to propose that cells are surrounded by a membrane that at rest is selectively permeable to K^+ ions and during excitation there is an increase in permeability to other ions (1). During the period of 1935-1952, two separate groups, Cole and Curtis, and Hodgkin, Huxley and Katz, tested this theory by using the giant squid axon to study the properties of the resting cellular membrane and the propagated action potential (2, 3). Their studies revealed three different components to the action potential which we now know to be voltage-gated Na^+ channels, K^+ channels, and various 'leak' channels. The development of the patch clamp technique by Sakmann and Neher (1, 4) and advances in molecular genetics uncovered hundreds of ion channels that are involved in chemical and electrical signaling. The knowledge gained from these initial and subsequent studies on ion

channels have shaped our current understanding of how different cells types communicate with each other.

Ion channels are now classified according to the channel's gating properties, such as voltage-gated ion channels, discovered by Hodgkin and Huxley (5), and ligand-gated ion channels, first seen by Sakmann and Neher (4). Since the focus of this dissertation is on glutamate receptors, a ligand gated ion channel, there will be no further discussion of voltage gated channels.

1.2 Ligand Gated Ion Channels

Ligand gated ion channels regulate electrical changes in response to a specific binding of a chemical messenger. The first- and best-studied are the nicotinic acetylcholine receptors (nAchR) found in the neuromuscular junction of skeletal muscle in vertebrate. These receptors have been patch clamped, purified, cloned, and imaged (6-10). These receptors were found in extremely high abundance in electric fish electric organs which supplied a giant pool of nAchR's to study. Research on nAchR's first demonstrated how a chemical message was translated into an electrical signal. Muscle movement is controlled by the release of acetylcholine from prejunctional nerve terminals onto postjunctional muscle membranes (11, 12). This results in binding to and activation of nAchR's leading to depolarization of the muscle that activates voltage gated Na^+ and Ca^{2+} channels, generating an action potential that propogates along the muscle fiber and leads to muscle contraction (12, 13).

The in-depth characterization of acetylcholine receptors was subsequently translated to studies on other ligand-gated ion channels; in other words, the principles of ligand-gated ion channel activation learned from acetylcholine receptors were also used to understand other ligand-gated ion channels. From these studies, it was found that nAChR's are a part of a super family of pentameric, transmembrane ligand gated

ion channels that include 5-HT, glycine and GABA receptors (14). These pentameric channels function in similar ways; for example, only specific subunits can bind agonist, which lead to the discovery that receptors can bind two to five ligands, depending on their subunit composition (15).

Glutamate receptors also were initially thought to be similar to acetylcholine receptors, which were later found to be untrue. Although both classes of ion channels share similar basic principles, such as ligand binding, activation, deactivation and desensitization, they also differ in how these basic functions are achieved. Acetylcholine receptors are pentameric channels in which the alpha subunit is necessary to bind an agonist (14). Glutamate receptors are tetramers in which each subunit can bind an agonist. The membrane spanning region of nAchR's consists of four membrane spanning helices (16) whereas glutamate receptors consist of three membrane spanning regions and a reentrant loop (17). The ligand binding site on nAchR's is located in between two subunits (16) whereas each glutamate receptor subunit has its own ligand binding pocket. Although both receptor types are different, their shared basic properties allowed methods used to study nAchR to translate to uncovering glutamate receptor structure and function.

1.3 The Glutamate Receptor Family

From the first discovery of L-glutamate, it was difficult to believe this amino acid played any role as a neurotransmitter in the central nervous system (CNS). It wasn't until L-glutamate was shown in 1954 by Hayashi T. to have convulsant effects in the cerebral cortex (18), that researchers began to study this amino acid as a neurotransmitter. Since that time, with the discovery of different subtypes of glutamate receptors based on pharmacology it was realized that these receptors are prevalently abundant in the CNS and are major players in excitatory neurotransmission (18).

Molecular cloning identified the molecular species of each subtype (19-21), allowed the production of genetically modified animal models to study CNS diseases and disorders, as well as provided a foundation for structure-function studies. Another important aspect of these receptors was realized when it was recognized through that they play a role in learning and memory, specifically long term potentiation (LTP) (22) and long term depression (LTD) (23). This and recent advances in uncovering the structural basis of the functioning of these receptors are opening up new avenues for potential drug discovery to treat neurological disorders and diseases.

I. Classification

There are three classes of functional ionotropic glutamate receptors (iGluR) comprised of six gene families (17) and named according to their selectivity for the full agonists: AMPA, Kainate and NMDA. A fourth class of receptors that are homologous to iGluR's are the delta receptors. Much molecular work has been undertaken to understand the structural basis of the functioning of these receptors.

A. AMPA Receptors

Ionotropic glutamate receptor of the AMPA class (GluA) binds a man-made compound called α-**a**mino-3-hydroxy-5-**m**ethyl-4-isoxazole**p**ropionic **a**cid, or AMPA, with the highest affinity (17). GluA's mediate most of the fast synaptic neurotransmission in the central nervous system (CNS). There are four mammalian AMPA receptor genes that make up the AMPA class of receptor subunits, which consists of GluA1, GluA2, GluA3 and GluA4 (24, 25). The GluA receptor subunits can form both heteromeric and homomeric tetramers.

AMPA receptors are widely expressed throughout the CNS in both neurons and glial cells, and are generally located at post synaptic sites of excitatory synapses (26).

There is significant variability in the expression of the four AMPA subunits in the brain. The most abundant and widespread subunits are GluA1 and GluA2, and the fewer, more regionally expressed subunits are GluA3 and GluA4 (24). Similar to other ion channels, AMPA receptors have activation and desensitization kinetics that are dependent on subunit composition, RNA modifications, and other factors, such as polyamine block and assembly with transmembrane AMPAR regulatory proteins (TARP) (17, 27, 28).

AMPA receptors in the CNS can be either Ca^{2+} permeable or Ca^{2+} impermeable (29). Most AMPA receptors form heteromers that contain the GluA2 subunit, which play a role in many biophysical properties of the whole receptor, including Ca^{2+} permeability, receptor kinetics, single-channel conductance, and block by polyamines (27, 30). ~95% of GluA2 subunits in the brain contain an arginine (R) in the pore loop due to pre-mRNA editing by site selective deamination of adenosine to inosine (31). This Q/R editing site is specific to the GluA2 subunit. GluA2 coassembly with other AMPA subunits greatly decreases Ca^{2+} permeability, abolishes polyamine block, and causes the channel to exhibit relatively low single channel conductance (30).

All AMPA receptors have an extracellular 38 amino acid region preceding the transmembrane segment, M3, that can exist in either a flip or flop form. The flip form is predominantly expressed early in development, whereas flop form expression is increased in adult animals (32). This phenomenon arises from alternatively spliced mRNA (32). Flop forms desensitize to a greater degree and much more rapidly than the flip forms (32).

Another site that undergoes RNA editing is the R/G editing site. In GluA2, GluA3, and GluA4, an adenosine located directly before the flip/flop splice region, also undergoes site selective deamination of adenosine to inosine, changing the amino acid

from arginine to glycine. This change increases the rate of desensitization and quickens the recovery from desensitization (33).

Functionally, AMPA receptors have rapid activation and deactivation kinetics (34-37). The single channel conductance of AMPA receptors consists of three or four sublevels and have been reported to range from 7 – 50 pS, which is dependent upon subunit composition (38-40). Receptors that co-assemble with an R-edited GluA2 subunit exhibit a maximum single channel conductance of 10 pS (38). Homomeric GluA2 receptors have very low single channel conductance on the order of a few hundred femto-siemens (38). AMPA receptors are permeable to Na^+ and K^+, as well as Ca^{2+} (so long as the receptor does not contain an edited GluA2 subunit), with a reversal potential around 0 mV in vivo (17). Activation of AMPA receptors in synapses causes a rapid increase of inward currents in the postsynaptic cell that lasts for a few hundred microseconds (41).

In neurons, AMPA receptors normally assemble with auxillary proteins called TARP's. TARP's interact with the C-terminal tails of AMPA receptors and are important in the cell surface expression of AMPA receptors in neurons (42-44). TARP's also modulate the kinetics of AMPA receptor gating which result in longer and larger currents into the cell. The main effects are a slowing of receptor activation, deactivation and desensitization (45, 46). There are currently four TARP's known to interact with AMPA receptors and result in different degrees of receptor kinetics (47).

B. Kainate Receptors

Ionotropic glutamate receptors of the kainate class (GluK) consists of five kainate receptor genes (25). The kainate receptors are involved in excitatory and inhibitory neurotransmission through activation of post- and pre-synaptic receptors. Kainate receptors are comprised of GluK1, GluK2, GluK3, KA1 (or GluK4), and KA2

(GluK5) (24), with the latter two unable to form a functional channel without GluK1-3 (48). Kainate receptors can form homo- and hetero- tetrameric channels and also contribute to fast excitatory transmission in the CNS (24). The single channel conductance of kainate receptors, depending on subunit combination and RNA editing, range from a few hundred fS to 25 pS (49).

Kainate function in the CNS is similar to, yet different from, AMPA receptor function. Kainate receptors are found both pre and post synaptically. Kainate receptors on the presynaptic nerve terminal have been shown to affect excitation or inhibition of the postsynaptic cell by modulating presynaptic glutamatergic and/or GABA-ergic neurons (50, 51). Activation of kainate receptors also affects voltage gated ion channels through a noncanonical G protein signaling mechanism (52). Although kainate receptors are found in many areas of the CNS, in neurons the expression of these receptors seem to be clustered in specific areas rather than spread out (53, 54).

GluK1-3 are known to undergo alternative splicing (55). These splice variants are found in the C-termini which may alter the physiological properties of the channel. Similar to AMPA receptors, kainate receptors also undergo Q/R editing in the reentrant pore loop on GluK2 and GluK3 subunits. Incorporation of these R-edited subunits causes the channel to be impermeable to Ca^{2+} (56), abolishes polyamine block (27), and also significantly lowers the single channel conductance to a few hundred femtosiemens (49). Two additional editing sites, I/V and Y/C, also exist for kainate receptors.

C. NMDA Receptors

Ionotropic glutamate receptors of the NMDA class (GluN) are composed of seven genes (25). NMDA receptors are responsible for the slower activation and longer duration of excitatory synaptic neurotransmission. NMDA receptors are coincidence

activators, needing to both overcome a voltage-dependent Mg^{2+} block and be activated by agonists (57). NMDA receptors are obligate tetrameric heteromers (58), needing two different agonists, glycine and glutamate, to activate. Activation of NMDA receptors can allow the influx of divalent cations into the cell, which is thought to play a role in synaptic plasticity. Two processes must occur in order for NMDA receptor activation and channel opening to occur, the first being fully bound with agonists and the second is overcoming a voltage-dependent Mg^{2+} block. At resting membrane potentials, extracellular Mg^{2+} blocks NMDA channel activation. Mg^{2+} inhibition is relieved only upon depolarization (59). This important feature of NMDA receptor activity is the basis of long term potentiation in learning and memory (60).

There are currently fourteen known variants of NMDA receptor subunits produced from alternative splicing and consisting of GluN1-3. There are eight different GluN1 isoforms which binds glycine and β-serine. There are four GluN2 gene products which bind glutamate and three GluN3 gene products which bind glycine (17). Splice variants for GluN2A-D are widely expressed in the CNS (61). GluN subunits differ in their functional properties and are also localized in different areas of the CNS (61). Various combinations of subunit assembly result in altered kinetics and sensitivity to divalent ions. For example, GluN2C and 2D have low sensitivity to Mg^{2+} block but still conducts Ca^{2+}, which is thought to enhance long term potentiation processes (62). GluN1/N2A complexes have the shortest deactivation time constant on the order of 50 ms, whereas GluN1/N2D complexes have the longest deactivation time constant ranging in seconds (63).

Posttranslational modification of glutamate receptors has been extensively studied in NMDA receptors, although much still remains to be elucidated due to the numerous splice variants and subunit combinations. Examples of such modifications include phosphorylation, glycosylation, nitrosylation, and ubiquitinization. Phosphorylation

of specific serine or tyrosine residues in the C-terminus by calmodulin can increase single channel conductance and also increase the insertion of NMDA receptors onto surface of the cell (64). Glycosylation occurs on the N-terminus and affects subunit assembly and trafficking (65). S-nitrosylation of cysteines can downregulate ion channel activity by decreasing Ca^{2+} influx (66).

Location of each expressed subunit is dependent on the developmental stage and area of the brain. For example, in the forebrain GluN2B subunits are predominant in early development, but switches over to a higher expression of GluN2A as development progresses (67). The changes in expression might ultimately play a role in synapse formation and synapse maturation during development.

D. Delta Receptors

A fourth class of nonfunctional receptors, called the orphan ionotropic glutamate receptors, denoted Gluδ1−2, have been cloned by homology screening. These receptors share 40% sequence homology with AMPA / kainate receptors and 20-30% with NMDA receptors. δ receptors are predicted to have similar structure to other iGluR's based on analysis of the transmembrane region, recent structures of the 'LBD' and sequence similarities (68, 69). Gluδ subunits are insensitive to common iGluR agonists and currently, the endogenous ligand for Gluδ has not been found (70, 71). Gluδ 1 and 2 have not been found to co-express on the same neurons, suggesting they do not assemble together. However, they have been found to co-express with other iGluR's. Although they have been shown to assemble with AMPA / kainate receptors *in vitro*, the same has not been proven *in vivo* (72).

Much controversy surrounding whether these receptors actually form functional ion channels currently exists. Support for ion channel activity arose from mutations denoted lurcher and hotfoot which result in spontaneous channel opening that is

associated with neuronal cell death (73). This point mutation is located in a highly conserved transmembrane region (SYTANLAAF) of other iGluR's (73). Similar point mutations made on AMPA receptors result in a similar phenotype as the lurcher mutation in which agonist potency increases (74).

Initial mouse knock-out studies of the δ2 subunit reveal abnormal motor coordination and learning (75). Synaptogenesis in the cerebellum is also altered and parallel fiber synapses onto Purkinje cells are decreased. These synapses are actually important in LTD, which is abolished in δ2 knockout mice (76). δ1 subunits are found abundantly in the inner ear and knockout mice lacking δ1 subunits show hearing impairment (77). Most of the recent findings suggest a metabotropic rather than ionotropic function (78).

II. Glutamate Receptor Structure and Function

Early work characterizing ionotropic glutamate receptors was slow due to the many subtypes, possible subunit combinations, RNA editing, and overall differences between the three main groups of ionotropic receptors. We now know that glutamate receptors can arrange as either tetrameric homomers or tetrameric heteromers, with NMDA receptors being obligate heteromeric channels (58). Pharmacologically, each group of iGluR's have different affinities for different compounds, and some ligand that have affinity for one group does not readily activate another group. For example, NMDA only activates NMDA receptors but not AMPA or kainate receptors, and kainate is a partial agonist at AMPA receptors but is a full agonist at kainate receptors (17).

Correlating structure with function has been difficult because of the challenge in determining the structure of a membrane bound protein. Most of the structural information about glutamate receptors was determined using various methods.

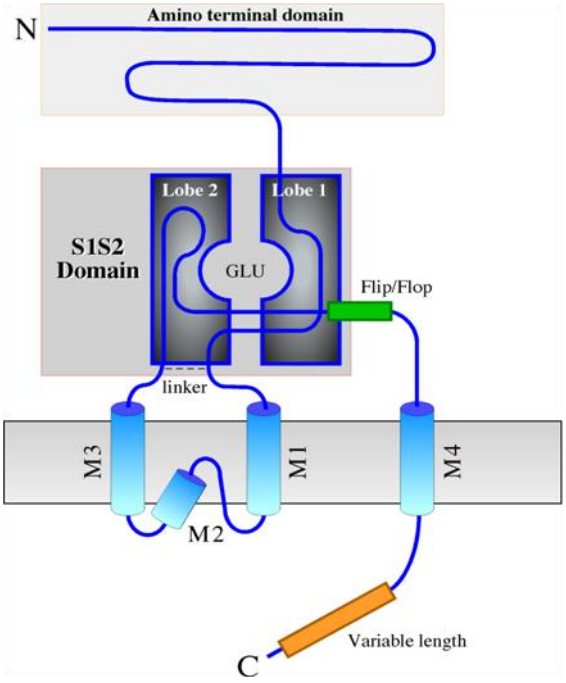

Figure 1.1

A one-dimensional topology of a single glutamate receptor subunit. A single glutamate receptor subunit consists of an N-terminal domain, a ligand binding domain (marked lobe 1 and lobe 2), a transmembrane domain and a C-terminal domain. Figure adapted from (86).

Research by various groups studying kainate (79) and AMPA (80) receptors resulted in uncovered the unexpected topology of the membrane spanning pore, which consisted of three transmembrane segments and a reentrant pore loop (79, 80), as well as solving the structure of the ligand binding domain bound to a variety of ligands (40, 81-84). Currently, the structures of the LBD of GluA2, 3, 4, GluK 1, 2, GluN1, 2A, 3A and 3B, have been solved bound to various agonists and antagonists. Recent x-ray crystallography studies pursued by Sobolevsky, *et al*. (85), resulted in an extraordinary breakthrough – the solving of the structure of a homomeric GluA2 receptor bound to an antagonist. This almost full-length structure confirmed the results of many years of research on glutamate receptors. All glutamate receptor subunits have a similar structure (Figure 1.1): an amino-terminal domain, a clam shell-like ligand binding domain (LBD), a transmembrane domain with three transmembrane segments and a reentrant pore loop, and a variable length C-terminal domain (85, 86). The structural findings along with the results from many functional studies have yielded several mechanistic models to describe the activation, deactivation and desensitization of glutamate receptors. These studies will hopefully lead to rational drug design and aid in the development of therapies for many neurological diseases and disorders (discussed in section 1.5).

A. Glutamate receptor mechanism of activation

One of the long-standing questions in neurobiology is the mechanism of glutamate receptor activation. Recording electrophysiological activity from neurons uncovered the basis of cellular excitation by way of ionotropic glutamate receptors, but did not reveal how each specific subunit contributed to activation kinetics. Functional studies on individually expressed subunits in cultured cells have yielded many properties that can be correlated with specific structural aspects of the protein.

The amino-terminal domain is a bilobate structure that is important for proper subunit assembly (87, 88) and can also bind modulators that affect channel function (89, 90). The LBD consists of two lobes that bind agonists necessary for channel activation (81). The transmembrane segments line the pore of the ion channel and are structurally similar to the pore region of voltage gated K^+ channels, but are inverted and have an extra transmembrane segment (17). The reentrant loop is also similar to the P-loop in K^+ channels and controls ion selectivity (91). The M3 segment of the transmembrane region is connected to lobe 2 of the LBD and is thought to be the channel gate. Agonist binding in the LBD causes lobe 2 to move towards lobe 1. This in turn induces conformational changes in the M3 region that opens the channel. The M3 segment is also analogous to the inner helix M2 segment in K^+ channels (92, 93). The C-terminal domain varies in length depending on the subunit type and splice variants. This region can interact with numerous intracellular proteins that are involved in signal transduction and scaffolding (94).

Isolation of the ligand binding domain (95, 96) provided much structural insight on how a ligand binds to an individual subunit (81, 97, 98). The best studied so far is the GluA2 receptor. Ligand binding to the LBD induces a 'clamping' or closure on the ligand, eventually leading to conformational changes associated with channel opening (99-101). The agonist bound state is quite similar for all the iGluR's; the region in which the ligand docks onto the LBD is on lobe 1. All ligands that can bind to iGluR's have a chemical moiety that is similar to the α-amino and α-carboxyl groups of glutamate. The closed conformation shown from agonist bound structures of the GluA2 LBD is stabilized by many direct and water-mediated hydrogen bonds (84). An arginine residue that is conserved in all AMPA receptors (R485 in GluA2) is thought to be the initial docking site for the ligand and mutation of this residue abolishes channel activity (84, 102, 103).

Table 1.1

The relationship between the degree of ligand binding domain closure and receptor function. The degree of lobe closures as measured by crystallography from (40, 81, 84, 105). Full agonists, such as glutamate and AMPA produce ~20˚ lobe closure and have maximal measured peak currents. Partial agonists induce less than 20˚ LBD closures and have less than maximal currents. All currents are normalized to the full agonist.

Ligand	Degree Lobe Closure	Degree Lobe Closure with Zn^{2+}	Ipeak / I glu
Glutamate / AMPA	--	20°	1
DNQX	2.5°	--	--
Kainate	12°	--	0.2
Willardiine	--	16.6°	0.62
Fluoro-Willardiine	15.3°	--	0.54
Bromo-Willardiine	14.8°	17.5	0.37
Iodo-Willardiine	10.8°	16.5	0.34

Structural studies on the GluA2 LBD of AMPA receptors provided evidence that the extent of lobe closure on an agonist is directly related to the efficacy measured with whole cell electrophysiology. GluA2 LBD bound to full agonists induced a cleft closure of ~20° and gave maximal whole cell electrophysiological responses (83). Partial agonists induced cleft closures ranging from 12 - 20° (83, 104, 105) and induced a whole cell electrophysiological response which corresponds to the extent of cleft closure (40); that is the less cleft closure, the smaller the measured response (Table 1.1). However, this relationship between lobe closure and efficacy may not be so simple based on more recent studies with specific mutations in the LBD, using other AMPA receptor subtypes and AMPA/kainate chimeras. For example, T686 interacts across the LBD to form a hydrogen bond with E402 in the GluA2 receptor. Mutation of T686A increases the EC_{50} values for full agonists and also changes the degree of lobe closure for certain agonists (100, 106), which suggests residues involved in stabilizing the closed LBD conformation also play a role in channel activation. These studies weaken the correlation between channel activation and the extent of LBD closure (107, 108) and indicate other mechanisms are involved. On another note, whole cell recordings can also be misleading because this technique depicts the average behavior of hundreds of active channels. To further complicate matters, each individual receptor is composed of four subunits that are equally able to bind agonist and contribute to activation. To put it simply, these initial correlations were a beginning to elucidating the function of glutamate receptors, but did not provide the best explanation for receptor activation. To obtain a better understanding of the relationship between structure and function, single channel studies are necessary, allowing quantitative analysis of the underlying kinetic behavior.

State models that describe the single channel activity of any ion channel can provide detailed kinetic information regarding receptor gating by way of transitions.

Each state represents a stable, measurable, protein conformation. NMDA receptors have been a model for single channel studies due to their large conductance and lengthy openings. Activation of NMDA receptors, unlike non-NMDA (kainate and AMPA) receptors, requires all four subunits to be bound with agonist and causes full channel openings to ~40 pS (109, 110). NMDA receptors assemble with two glycine binding subunits and two glutamate binding subunits; two glycine molecules and two glutamate molecules are needed to activate the channel (111, 112). Quite a few thorough studies on the single channel activity of NMDA receptors have been undertaken within the past few decades and have lead to the generation of kinetic models of activation. Based on the duration of closed and open time distributions, a kinetic model composed of three closed states and two open states was generated (113, 114). The combinations studied thus far also reveal modal gating behaviors which shift over time but are not agonist concentration-dependent (113). Partial agonists also induce similar modal gating behaviors but cause a decrease in the open probability of the channel (115). The few structures of NMDA LBD's bound to partial agonists reveal similar degrees of closure compared to full agonists (116). Based on these studies, it was been proposed that all four subunits need to rearrange into a high affinity conformation in order for gating to occur. Partial agonists are not as efficacious in achieving this rearrangement compared to full agonists (115). Another hypothesis has also been put forth suggesting that specific residues within the agonist binding pocket reorganize themselves to hold the two lobes together and the more efficacious the agonist, the stronger the interaction (116). Now that there is a model of activation for NMDA receptors, future studies using various mutations, pharmacological agents, and cellular factors, can clarify the effects these perturbations have on ion channel function.

Analogous studies can similarly be carried out with non-NMDA receptors to not only produce a better structure-function relationship, but also to begin elucidating the mechanism of a normally functioning receptor. However, AMPA and kainate receptors are quite different from of NMDA receptors, exhibiting smaller conductance levels and much shorter openings, making single channel data collection a difficult task. What data has been collected has lead to some initial characterization of single channel behavior. Non-NMDA receptors have multiple open conductance levels that correlate with the number of active (agonist-bound) subunits. At least two active subunits are necessary to observe the smallest conductance level, with each subsequent active subunit causing the channel to open to the next conductance level (38, 117). There are also studies that suggest there are actually four subconductance levels (39) observable from neuronal AMPA receptors. Kainate receptors also display subconductance levels but these behaviors have not been characterized the these receptors (49). The amplitudes of openings are also dependent on the subunit combinations, which has been more thoroughly studied with AMPA receptors than kainate receptors. AMPA receptor assembly with an (R)-edited GluA2 subunit greatly decreases whole cell response and single channel conductance (17, 38). Although these studies provided some insight into channel activity, these studies ulitilized recordings from short-lived activation periods. Brief events only reveal activity of a single channel for that specific moment in time; they do not capture other possible activity schemes in that longer recordings can reveal.

Longer single channel recordings on AMPA (and future studies on kainate receptors) using full agonists as well as with partial agonists can provide much more structure-function information. Another problem in the field regarding partial agonists is the fact that most studies on AMPA receptors have been conducted using kainate, which induce such small channel openings that it becomes difficult to resolve

openings from background noise. Kainate acting on AMPA receptors is also on the extreme end of the partial agonist spectrum, not only in the way its bound in the ligand binding pocket, (kainate sterically clashes with certain residues in the binding pocket (108)), but also because its maximal activation in whole cell recordings is only 20% of that of glutamate on GluA2 receptors (84). The willardiines are a group of partial agonists which differ in the 5 position substituent, yet show a graded level of whole cell activation that is greater than kainate (40, 118). These subtle differences and higher affinity for AMPA receptors make this group of partial agonists excellent candidates for detailed single channel studies. Single channel studies collected from homomeric, wild-type receptors using partial agonists with the full agonist as a control, can provide new insights into the gating mechanism as described in the studies in chapters 2-4.

B. Mechanism of Desensitization

Desensitization is a characteristic shared by many ligand gated ion channels to shut down channels that are in the continuous presence of activating factors. AMPA and kainate receptors undergo rapid desensitization in the millisecond range (119). Structural and functional studies on AMPA/kainate subtypes have generated insight into the mechanism of desensitization.

Initial crystallography studies on the GluA2 LBD revealed these isolated domains formed dimeric complexes (84). Most of the contacts are mediated by interactions between residues in lobe 1 of two LBD's (99). Specific point mutations in lobe 1 were shown in the intact receptor to alter desensitization, for example, the L/Y mutation (L483Y in GluA2) significantly reduced desensitization. Allosteric modulators which also interact within the lobe 1 interface, such as cyclothiazide (CTZ) also suppress desensitization. LBD structures of the L/Y mutant as well as structures of LBD's in

the presence of CTZ (99) also demonstrated the formation of dimers. NMR studies with a variety of allosteric modulators also show a similar interaction (120). The crystallographic structure of the almost full-length GluA2 receptor confirmed the formation of LBD dimers which then dimerizes with an adjacent pair of LBD's forming an asymmetric extracellular, symmetric transmembrane, tetrameric channel (85). Since stabilizing this dimer interface prevented desensitization and enabled long channel openings, it was hypothesized that destabilizing this interaction would induce a desensitized state. Crystallography and NMR studies (120, 121) of various allosteric modulators bound to this interface, which were then correlated with functional studies, supported the idea that formation of this dimer interaction prevents desensitization (122, 123). Recent LRET studies on an entire GluA2 receptor concluded agonist binding precedes dimer formation (124). The question of whether cooperation between the subunits is involved in only the desensitization process or also involved in the activation and deactivation process is currently unknown.

Desensitization of NMDA receptors is much slower and occurs by several mechanisms, the first being similar to AMPA / kainate receptor desensitization in which the dimer interface collapses (125). Interestingly, the GluN1/GluN2A dimer interface contains a residue, Y535 in the GluN1 subunit which interacts with GluN2A in a similar fashion as allosteric modulators in GluA's (125). The other mechanisms of desensitization of NMDA receptors involve Zn^{2+} binding to the amino terminal domain (126, 127), the glycine binding subunit (128), and Ca^{2+} entry into the cell (129).

1.4 The Role of Glutamate Receptors in Synaptic Plasticity

The first reports of mammalian excitatory neurotransmission by amino acids came from studies in the rat hippocampus. Since then, the molecular mechanisms of

synaptic plasticity involving glutamate receptors have come mainly from research on the hippocampal area in the brain. Animal models in which NMDA receptors in the hippocampus were blocked revealed an impairment of learning; subsequently similar studies carried out on other regions of the brain have corroborated the effects NMDA receptors had on learning. For example, blockade of NMDA receptors through pharmacological means inpaired fear conditioning; the animals in these experiments were unable to learn to avoid negative environmental stimuli (130). On the cellular level, scientists have long observed that brief, intense synaptic activation of neurons is usually followed by a long, slow activation, known as long term potentiation (LTP), that can persist for hours (131). The link between NMDA receptors and LTP was demonstrated when the NMDA receptor antagonist, APV, was shown to disrupt LTP without affecting synaptic neurotransmission (132). Since then, the current understanding of LTP is that it involves a number of coincidence events (133). NMDA receptors, during resting cell conditions, are normally blocked by Mg^{2+} ions due to negative membrane potential (59), with current flowing through theough these receptors only when the membrane has been depolarized. AMPA receptors, also expressed in the same regions of NMDA receptors, are activated by glutamate released into the synaptic cleft, and is the cause of the initial depolarization which relieves the Mg^{2+} block of NMDA receptors (57). Additional waves of released glutamate produces a summed postsynaptic depolarization from the now unblocked NMDA receptors and activate intracellular biochemical pathways involved in LTP, primarily via Ca^{2+} entry into the cell through these receptors (17, 57).

The opening of NMDA channels allows the entry of Ca^{2+} into the cell, resulting in the activation of various Ca^{2+} signalling cascades. Ca^{2+} has been shown to be a necessity in LTP induction because loading the cell with EDTA, a Ca^{2+} chelator prevents the occurrence of LTP (134). Synaptic plasticity by NMDA receptors can

result in either LTP or long term depression (LTD) and is determined by the amount of Ca^{2+} influx over time. High frequency stimulation over a short time course of a few seconds result in robust Ca^{2+} entry through NMDAR's and induce LTP whereas slow frequency stimulation over a much longer period of time which could last for many minutes result in smaller Ca^{2+} entry and induce LTD (135).

Since then, more recent findings have also established other modes of synaptic strengthening and weakening. An example is an increase in the membrane insertion of AMPA receptors during LTP induction (136). In a specific study on isolated hippocampal neurons, it was found that calmodulin activity induced by NMDA activation recruits Ca^{2+} permeable AMPA channels to dendritic spines (137). Another type of synaptic plasticity is the phenomenon of silent synapses, in which presynaptic activation does not have any affect on the postsynaptic cell (138). Recent evidence suggest these silent synapses are devoid of AMPA receptors (139) and it has been speculated based on postnatal development studies that synapses with weak activation lose surface expression of AMPA receptors leading to silent synapses (140). The study of the receptors that mediate synaptic plasticity can have many beneficial consequences, such as developing treatments for diseases such as Retts disease, in which glutamatergic neurons are affected (141). Aging brains also show a decline in AMPA receptor expression (142). Targeting these receptors to increase synapse formation could potentially reverse the effects of aging.

1.5 Glutamate Receptor Involvement in CNS Diseases and Disorders

The high prevalence and diverse function of ionotropic glutamate receptors in the CNS makes it unsurprising to find many CNS diseases and disorders to be linked to ionotropic glutamate receptor activity. Overactivation of ionotropic glutamate receptors can lead to excitotoxicity whereas underactivation can lead to overall CNS

depressed states. Evidence for the role of ionotropic glutamate receptors in excitotoxicity came from studies of NMDA and AMPA receptor antagonists, which were shown to have anti-convulsant effects (143, 144). Addiction to substances of abuse has also been shown to affect glutamatergic activity and in some cases, result in permanent changes. This section briefly covers the implications for the involvement of glutamate receptors in neurodegenerative diseases and disorders and the need for subunit specific agonists and antagonists to treat these problems.

I. Excitotoxicity

The role Ca^{2+} permeable ionotropic glutamate receptors play in neuronal cell death has been explored in many disorders, one of the most prominent being hypoxic induced ischemia. One hypothesis associated with neuronal excitotoxicity involves an overabundance of intracellular Ca^{2+}. Excessive amounts of Ca^{2+} can trigger the activation of proteases, lipases, phosphatases and endonucleases which leads to the formation of oxidative radicals and cellular damage (145). Normally, the extracellular glutamate concentration is regulated by plasma membrane Na^{+}/glutamate co-transporters in which the gradient is supplied from the energy provided by a Na^{+}/K^{+} ATPase pump (146). A similar Ca^{2+} ATPase pump is also used to regulate the intracellular Ca^{2+} concentration. During periods of intracellular Ca^{2+} overload, excess ATPase activation rapidly expends the available ATP pool. Stress placed on the mitochondria to produce more ATP leads to the production of oxidative species which wreak havoc on cell (146). The inability to maintain a low extracellular glutamate concentration leads to activation of Ca^{2+} permeable glutamate channels, further exacerbating the problem.

Ca^{2+} permeable AMPA channels are also permeable to Zn^{2+}, which is normally co-released with glutamate at some synaptic terminals. Zn^{2+} effects are similar to Ca^{2+}

effects, except Zn^{2+} is more harmful in that it induces prolonged production of oxidative species (147). Prolonged Zn^{2+} exposure leads to neuronal cell death (148). Zn^{2+} has been shown to increase the binding affinity of AMPA to AMPAR's, potentiate whole cell responses, and slow AMPAR desensitization (149). Similar potentiation effects were seen in rat CA3 pyramidal neurons (150). Not much is known about the direct effects of Zn^{2+} and Ca^{2+} on the single properties of AMPA or kainate receptors.

In the case of excitotoxicity, a method of limiting neuronal cell death would be to create antagonists that block ionotropic glutamate receptor activity, particularly channels that are Ca^{2+} permeable. However, ionotropic glutamate receptors are prevalent in all areas of the CNS and antagonists would affect all brain areas. In this case, subtype selective antagonists that can target specific modes of function might reduce the side effects attributed to the current nonselective antagonists. Another avenue would be to produce a partial agonist that could potentially compete with glutamate binding, still enabling a somewhat normal function, while alleviating some of the excitotoxic events. In any case, a more thorough understanding of each specific glutamate receptor subtype can aid in drug development.

II. Amyotrophic Lateral Sclerosis

Amyotrophic lateral sclerosis (ALS) is characterized by selective degeneration of motor neurons which leads to paralysis, and eventually, death (151). Clincal symptoms include muscle weakness, muscle atrophy and spasticity. 5-10% of ALS cases are caused by mutations in either the SOD1 (152) or ALS2 (153) gene; the rest of ALS cases have unknown causes. AMPA receptors have been implicated in this disease because AMPA antagonists are able to prevent death of neurons exposed to the cerebrospinal fluid of ALS patients (the cerebrospinal fluid of ALS patients have been

shown to be toxic to neurons) (154). Edited GluA2 subunits (which decrease Ca^{2+} permeability) were also found to be decreased in ALS patients (155).

Pharmacological agents that selectively target Ca^{2+} permeable AMPA channels might alleviate ALS symptoms. However, as with the case of excitotoxicity, a more thorough understanding of each specific subtype will allow for more precise drug development.

III. Alzheimer's Disease

Alzheimer's disease (AD) is the most common neurodegenerative disease of the elderly population and is marked by progressive memory loss (156). The hallmark of this disease is characterized by excessive amyloid beta plaque formation (Aβ plaques) in the brain which leads to neuronal cell death (157). The specific cause of Alzheimer's has not been determined, although there are a few factors associated with the disease. The first is oxidative stress; brain tissue from AD patients and animal models of AD show an increase in the amount of oxidative species (158, 159). Acetylcholine and glutamate receptors are the two types of receptors thought to play the largest role in the progression of the disease. There is actually a decrease in certain nicotinic acetylcholine receptor subtypes (160). *In vitro* and mice studies have shown Aβ plaques actually enhances glutamate neurotransmission and may contribute to neuroexcitoxicity (161, 162). Memantine, an NMDA antagonist, in clinical use actually reduces neuronal cell death (163). A possibility of future theurapeutics, which include glutamate receptor antagonists and nicotinic acetylcholine agonists, might provide better treatment for this horrible disease.

IV. Epilepsy

Epilepsy is a chronic neurological disorder characterized by recurrent unprovoked seizures caused by excessive neuronal activity. Seizures can occur in any brain region and are characterized based on the whether or not the seizure spreads within the brain and whether the subject loses consciousness. Many ion channels have been linked to epilepsy, including glutamate and GABA channels. GABA channels provides inhibitory action in the CNS, whereas glutamate provides excitatory action (164). Therefore, it is easy to see why drugs targeted to glutamate and GABA receptors can be beneficial to patients who suffer from epilepsy. A problem with GABA agonists is that these drugs usually enhance the functioning of GABA channels, leading to excessive neuronal inhibition. Unwanted side effects include sedation and can also lead to tolerance (164). Glutamate antagonists offer another avenue of drug treatment.

Both NMDA and AMPA receptor antagonists have been shown to have anti-convulsant effects (165) and AMPA antagonists are preferred over other anti-epileptic drugs due to the lack of tolerance development (166). However, due to the non-specificity of these antagonists for AMPA receptors, unwanted side effects such as sedation, mild ataxia, and muscle relaxation, also occur with the anti-convulsant effects (167). In this case, subtype specific antagonists could provide partial blocking of neuronal excitation.

1.6 Outline of Dissertation Research

Research in the glutamate receptors field has made tremendous progress over the past few decades. Although much has been discovered, much information regarding the function of glutamate receptors, particularly AMPA channels, is lacking because of the unavailability of single channel data. Single channel data can be used to

generate state models, such as the case for NMDA receptors, and allow us to quantitate and characterize measurable protein conformational changes associated with each state (168). These characterizations can be used to make comparisons between structural and functional data.

The studies described in this dissertation takes advantage of a specific technique, cell-attached single channel electrophysiological recordings, and uses the data collected from these recordings to determine how glutamate receptors function. Homomeric GluA3 channels are exposed to and left to equilibrate with either the full agonist glutamate, or a partial agonist, fluorowillardiine (FW), nitrowillardiine (NO_2W), or chlorowillardiine (ClW). The data collected with glutamate not only serves as the initial single channel characterization, but it also serves as the control data. Data collected from FW, NO_2W, ClW function as a perturbation which allow us to distinguish small differences in behavior that is caused by small differences in the structure of the ligand binding domain. Single channel data is collected over several minutes, which allows most of the behavior to be captured. The data are then analyzed and state model fitted to the results.

GluA3 channels exhibit three conductance levels which are conserved across all agonists tested. These channels also exhibit five modal behaviors, Very High, High, Medium, Low, Very Low, which correspond to open probabilities of: 80-100%, 60-79%, 40-59%, 20-39%, <20%. These modes are also conserved across all agonists tested. The receptor spends the most time in the highest conductance level in the presence of glutamate and spends the least time in the highest conductance level for FW, NO_2W, and ClW. The differences in the open probabilities for the willardiines are very small. Although these differences might seem small, they become very large when averaged together over the hundreds of ion channels present in a whole cell.

From structural data of the isolated LBD, it seems all agonists examined are able to induce full LBD closures, but the three willardiines are slightly more open than glutamate by 1-4°. From the single channel data and the available structural information, we propose channel activation is governed by three factors: agonist binding, degree of lobe closure and stability of lobe closure. Specifically, agonist efficacy can be correlated to the stability of the D655/S656 peptide conformation in the LBD; flipped conformations can form hydrogen bonds across the cleft to Y453/G453 which stabilizes LBD closure. Structures of FW and ClW also reveal a stable partially closed conformation mediated by waters in the D655/S656 peptide region which can explain the occurrence of an alternative kinetic behavior seen with ClW. The structures of FW, NO_2W and ClW also reveal a rotameric change in M712, which normally points toward the ligand binding pocket in an extended state when glutamate is bound. These subtle differences in structure are related to the subtle effects on the single channel behavior. The studies in this dissertation address the anomaly in the current thinking which relates the degree of lobe closure to channel activation. These studies are meant to bridge the gap in the current research by providing functional information on the single channel level and will serve as a foundation for future single channel studies of glutamate receptors.

REFERENCES

1. Hille, B., and B. Hille. 2001. Ion channels of excitable membranes. Sinauer, Sunderland, Mass.
2. Cole, K.S., and H.J. Curtis. 1939. Electric Impedance Of The Squid Giant Axon During Activity. *J Gen Physiol.* 22:649-670.
3. Hodgkin, A.L., A.F. Huxley, and B. Katz. 1952. Measurement of current-voltage relations in the membrane of the giant axon of Loligo. *J Physiol.* 116:424-448.
4. Sakmann, B., J. Patlak, and E. Neher. 1980. Single acetylcholine-activated channels show burst-kinetics in presence of desensitizing concentrations of agonist. *Nature.* 286:71-73.
5. Hodgkin, A.L., and A.F. Huxley. 1952. Currents carried by sodium and potassium ions through the membrane of the giant axon of Loligo. *J Physiol.* 116:449-472.
6. Brisson, A., and P.N. Unwin. 1985. Quaternary structure of the acetylcholine receptor. *Nature.* 315:474-477.
7. Neher, E., and B. Sakmann. 1976. Single-channel currents recorded from membrane of denervated frog muscle fibres. *Nature.* 260:799-802.
8. Noda, M., H. Takahashi, T. Tanabe, M. Toyosato, S. Kikyotani, Y. Furutani, T. Hirose, H. Takashima, S. Inayama, T. Miyata, and S. Numa. 1983. Structural homology of Torpedo californica acetylcholine receptor subunits. *Nature.* 302:528-532.
9. Mishina, M., T. Kurosaki, T. Tobimatsu, Y. Morimoto, M. Noda, T. Yamamoto, M. Terao, J. Lindstrom, T. Takahashi, M. Kuno, and et al. 1984. Expression of functional acetylcholine receptor from cloned cDNAs. *Nature.* 307:604-608.

10. Weill, C.L., M.G. McNamee, and A. Karlin. 1974. Affinity-labeling of purified acetylcholine receptor from Torpedo californica. *Biochem Biophys Res Commun.* 61:997-1003.
11. Nachmansohn, D. 1966. Role of acetylcholine in neuromuscular transmission. *Ann N Y Acad Sci.* 135:136-149.
12. Gage, P.W. 1976. Generation of end-plate potentials. *Physiol Rev.* 56:177-247.
13. Ildefonse, M., V. Jacquemond, O. Rougier, J.F. Renaud, M. Fosset, and M. Lazdunski. 1985. Excitation contraction coupling in skeletal muscle: evidence for a role of slow Ca2+ channels using Ca2+ channel activators and inhibitors in the dihydropyridine series. *Biochem Biophys Res Commun.* 129:904-909.
14. Corringer, P.J., N. Le Novere, and J.P. Changeux. 2000. Nicotinic receptors at the amino acid level. *Annu Rev Pharmacol Toxicol.* 40:431-458.
15. Dougherty, D.A. 2008. Cys-loop neuroreceptors: structure to the rescue? *Chem Rev.* 108:1642-1653.
16. Miyazawa, A., Y. Fujiyoshi, and N. Unwin. 2003. Structure and gating mechanism of the acetylcholine receptor pore. *Nature.* 423:949-955.
17. Dingledine, R., K. Borges, D. Bowie, and S.F. Traynelis. 1999. The glutamate receptor ion channels. *Pharmacol Rev.* 51:7-61.
18. Bowie, D. 2008. Ionotropic glutamate receptors & CNS disorders. *CNS Neurol Disord Drug Targets.* 7:129-143.
19. Seeburg, P.H. 1993. The TiPS/TINS lecture: the molecular biology of mammalian glutamate receptor channels. *Trends Pharmacol Sci.* 14:297-303.
20. Hollmann, M., and S. Heinemann. 1994. Cloned glutamate receptors. *Annu Rev Neurosci.* 17:31-108.
21. Nakanishi, S., and M. Masu. 1994. Molecular diversity and functions of glutamate receptors. *Annu Rev Biophys Biomol Struct.* 23:319-348.

22. Nicoll, R.A., J.A. Kauer, and R.C. Malenka. 1988. The current excitement in long-term potentiation. *Neuron.* 1:97-103.

23. Ito, M. 1989. Long-term depression. *Annu Rev Neurosci.* 12:85-102.

24. Gereau, R.W., and G.T. Swanson. 2008. The glutamate receptors. Humana Press, Totowa, N.J.

25. Buckingham, S.D., S. Kwak, A.K. Jones, S.E. Blackshaw, and D.B. Sattelle. 2008. Edited GluR2, a gatekeeper for motor neurone survival? *Bioessays.* 30:1185-1192.

26. Bassani, S., P. Valnegri, F. Beretta, and M. Passafaro. 2009. The GLUR2 subunit of AMPA receptors: synaptic role. *Neuroscience.* 158:55-61.

27. Bowie, D., and M.L. Mayer. 1995. Inward rectification of both AMPA and kainate subtype glutamate receptors generated by polyamine-mediated ion channel block. *Neuron.* 15:453-462.

28. Tomita, S., H. Adesnik, M. Sekiguchi, W. Zhang, K. Wada, J.R. Howe, R.A. Nicoll, and D.S. Bredt. 2005. Stargazin modulates AMPA receptor gating and trafficking by distinct domains. *Nature.* 435:1052-1058.

29. Geiger, J.R., T. Melcher, D.S. Koh, B. Sakmann, P.H. Seeburg, P. Jonas, and H. Monyer. 1995. Relative abundance of subunit mRNAs determines gating and Ca2+ permeability of AMPA receptors in principal neurons and interneurons in rat CNS. *Neuron.* 15:193-204.

30. Hollmann, M., M. Hartley, and S. Heinemann. 1991. Ca2+ permeability of KA-AMPA--gated glutamate receptor channels depends on subunit composition. *Science.* 252:851-853.

31. Sommer, B., M. Kohler, R. Sprengel, and P.H. Seeburg. 1991. RNA editing in brain controls a determinant of ion flow in glutamate-gated channels. *Cell.* 67:11-19.

32. Sommer, B., K. Keinanen, T.A. Verdoorn, W. Wisden, N. Burnashev, A. Herb, M. Kohler, T. Takagi, B. Sakmann, and P.H. Seeburg. 1990. Flip and flop: a cell-specific functional switch in glutamate-operated channels of the CNS. *Science.* 249:1580-1585.

33. Lomeli, H., J. Mosbacher, T. Melcher, T. Hoger, J.R. Geiger, T. Kuner, H. Monyer, M. Higuchi, A. Bach, and P.H. Seeburg. 1994. Control of kinetic properties of AMPA receptor channels by nuclear RNA editing. *Science.* 266:1709-1713.

34. Li, G., W. Pei, and L. Niu. 2003. Channel-opening kinetics of GluR2Q(flip) AMPA receptor: a laser-pulse photolysis study. *Biochemistry.* 42:12358-12366.

35. Li, G., and L. Niu. 2004. How fast does the GluR1Qflip channel open? *J Biol Chem.* 279:3990-3997.

36. Li, G., Z. Sheng, Z. Huang, and L. Niu. 2005. Kinetic mechanism of channel opening of the GluRDflip AMPA receptor. *Biochemistry.* 44:5835-5841.

37. Pei, W., Z. Huang, and L. Niu. 2007. GluR3 flip and flop: differences in channel opening kinetics. *Biochemistry.* 46:2027-2036.

38. Swanson, G.T., R.W.t. Gereau, T. Green, and S.F. Heinemann. 1997. Identification of amino acid residues that control functional behavior in GluR5 and GluR6 kainate receptors. *Neuron.* 19:913-926.

39. Smith, T.C., L.Y. Wang, and J.R. Howe. 2000. Heterogeneous conductance levels of native AMPA receptors. *J Neurosci.* 20:2073-2085.

40. Jin, R., T.G. Banke, M.L. Mayer, S.F. Traynelis, and E. Gouaux. 2003. Structural basis for partial agonist action at ionotropic glutamate receptors. *Nat Neurosci.* 6:803-810.

41. Otis, T.S., Y.C. Wu, and L.O. Trussell. 1996. Delayed clearance of transmitter and the role of glutamate transporters at synapses with multiple release sites. *J Neurosci.* 16:1634-1644.

42. Chen, L., D.M. Chetkovich, R.S. Petralia, N.T. Sweeney, Y. Kawasaki, R.J. Wenthold, D.S. Bredt, and R.A. Nicoll. 2000. Stargazin regulates synaptic targeting of AMPA receptors by two distinct mechanisms. *Nature.* 408:936-943.

43. Bats, C., L. Groc, and D. Choquet. 2007. The interaction between Stargazin and PSD-95 regulates AMPA receptor surface trafficking. *Neuron.* 53:719-734.

44. Nicoll, R.A., S. Tomita, and D.S. Bredt. 2006. Auxiliary subunits assist AMPA-type glutamate receptors. *Science.* 311:1253-1256.

45. Priel, A., A. Kolleker, G. Ayalon, M. Gillor, P. Osten, and Y. Stern-Bach. 2005. Stargazin reduces desensitization and slows deactivation of the AMPA-type glutamate receptors. *J Neurosci.* 25:2682-2686.

46. Milstein, A.D., W. Zhou, S. Karimzadegan, D.S. Bredt, and R.A. Nicoll. 2007. TARP subtypes differentially and dose-dependently control synaptic AMPA receptor gating. *Neuron.* 55:905-918.

47. Korber, C., M. Werner, S. Kott, Z.L. Ma, and M. Hollmann. 2007. The transmembrane AMPA receptor regulatory protein gamma 4 is a more effective modulator of AMPA receptor function than stargazin (gamma 2). *J Neurosci.* 27:8442-8447.

48. Herb, A., N. Burnashev, P. Werner, B. Sakmann, W. Wisden, and P.H. Seeburg. 1992. The KA-2 subunit of excitatory amino acid receptors shows widespread expression in brain and forms ion channels with distantly related subunits. *Neuron.* 8:775-785.

49. Swanson, G.T., D. Feldmeyer, M. Kaneda, and S.G. Cull-Candy. 1996. Effect of RNA editing and subunit co-assembly single-channel properties of recombinant kainate receptors. *J Physiol.* 492 (Pt 1):129-142.

50. Malva, J.O., A.P. Carvalho, and C.M. Carvalho. 1994. Modulation of dopamine and noradrenaline release and of intracellular Ca2+ concentration by presynaptic glutamate receptors in hippocampus. *Br J Pharmacol.* 113:1439-1447.

51. Engelman, H.S., and A.B. MacDermott. 2004. Presynaptic ionotropic receptors and control of transmitter release. *Nat Rev Neurosci.* 5:135-145.

52. Rozas, J.L., A.V. Paternain, and J. Lerma. 2003. Noncanonical signaling by ionotropic kainate receptors. *Neuron.* 39:543-553.

53. Castillo, P.E., R.C. Malenka, and R.A. Nicoll. 1997. Kainate receptors mediate a slow postsynaptic current in hippocampal CA3 neurons. *Nature.* 388:182-186.

54. Vignes, M., and G.L. Collingridge. 1997. The synaptic activation of kainate receptors. *Nature.* 388:179-182.

55. Bettler, B., and C. Mulle. 1995. Review: neurotransmitter receptors. II. AMPA and kainate receptors. *Neuropharmacology.* 34:123-139.

56. Egebjerg, J., and S.F. Heinemann. 1993. Ca2+ permeability of unedited and edited versions of the kainate selective glutamate receptor GluR6. *Proc Natl Acad Sci U S A.* 90:755-759.

57. Seeburg, P.H., N. Burnashev, G. Kohr, T. Kuner, R. Sprengel, and H. Monyer. 1995. The NMDA receptor channel: molecular design of a coincidence detector. *Recent Prog Horm Res.* 50:19-34.

58. McIlhinney, R.A., E. Molnar, J.R. Atack, and P.J. Whiting. 1996. Cell surface expression of the human N-methyl-D-aspartate receptor subunit 1a requires the co-expression of the NR2A subunit in transfected cells. *Neuroscience.* 70:989-997.

59. Nowak, L., P. Bregestovski, P. Ascher, A. Herbet, and A. Prochiantz. 1984. Magnesium gates glutamate-activated channels in mouse central neurons. *Nature.* 307:462-465.

60. Martin, S.J., P.D. Grimwood, and R.G. Morris. 2000. Synaptic plasticity and memory: an evaluation of the hypothesis. *Annu Rev Neurosci.* 23:649-711.

61. Laurie, D.J., and P.H. Seeburg. 1994. Regional and developmental heterogeneity in splicing of the rat brain NMDAR1 mRNA. *J Neurosci.* 14:3180-3194.

62. Perez-Otano, I., and M.D. Ehlers. 2004. Learning from NMDA receptor trafficking: clues to the development and maturation of glutamatergic synapses. *Neurosignals.* 13:175-189.

63. Cull-Candy, S., S. Brickley, and M. Farrant. 2001. NMDA receptor subunits: diversity, development and disease. *Curr Opin Neurobiol.* 11:327-335.

64. Leonard, A.S., I.A. Lim, D.E. Hemsworth, M.C. Horne, and J.W. Hell. 1999. Calcium/calmodulin-dependent protein kinase II is associated with the N-methyl-D-aspartate receptor. *Proc Natl Acad Sci U S A.* 96:3239-3244.

65. Standley, S., and M. Baudry. 2000. The role of glycosylation in ionotropic glutamate receptor ligand binding, function, and trafficking. *Cell Mol Life Sci.* 57:1508-1516.

66. Kim, W.K., Y.B. Choi, P.V. Rayudu, P. Das, W. Asaad, D.R. Arnelle, J.S. Stamler, and S.A. Lipton. 1999. Attenuation of NMDA receptor activity and neurotoxicity by nitroxyl anion, NO. *Neuron.* 24:461-469.

67. Liu, X.B., K.D. Murray, and E.G. Jones. 2004. Switching of NMDA receptor 2A and 2B subunits at thalamic and cortical synapses during early postnatal development. *J Neurosci.* 24:8885-8895.

68. Yamazaki, M., K. Araki, A. Shibata, and M. Mishina. 1992. Molecular cloning of a cDNA encoding a novel member of the mouse glutamate receptor channel family. *Biochem Biophys Res Commun.* 183:886-892.

69. Naur, P., K.B. Hansen, A.S. Kristensen, S.M. Dravid, D.S. Pickering, L. Olsen, B. Vestergaard, J. Egebjerg, M. Gajhede, S.F. Traynelis, and J.S. Kastrup. 2007. Ionotropic glutamate-like receptor delta2 binds D-serine and glycine. *Proc Natl Acad Sci U S A.* 104:14116-14121.

70. Lomeli, H., R. Sprengel, D.J. Laurie, G. Kohr, A. Herb, P.H. Seeburg, and W. Wisden. 1993. The rat delta-1 and delta-2 subunits extend the excitatory amino acid receptor family. *FEBS Lett.* 315:318-322.

71. Mayat, E., R.S. Petralia, Y.X. Wang, and R.J. Wenthold. 1995. Immunoprecipitation, immunoblotting, and immunocytochemistry studies suggest that glutamate receptor delta subunits form novel postsynaptic receptor complexes. *J Neurosci.* 15:2533-2546.

72. Kohda, K., Y. Kamiya, S. Matsuda, K. Kato, H. Umemori, and M. Yuzaki. 2003. Heteromer formation of delta2 glutamate receptors with AMPA or kainate receptors. *Brain Res Mol Brain Res.* 110:27-37.

73. Zuo, J., P.L. De Jager, K.A. Takahashi, W. Jiang, D.J. Linden, and N. Heintz. 1997. Neurodegeneration in Lurcher mice caused by mutation in delta2 glutamate receptor gene. *Nature.* 388:769-773.

74. Taverna, F., Z.G. Xiong, L. Brandes, J.C. Roder, M.W. Salter, and J.F. MacDonald. 2000. The Lurcher mutation of an alpha-amino-3-hydroxy-5-methyl-4-isoxazolepropionic acid receptor subunit enhances potency of glutamate and converts an antagonist to an agonist. *J Biol Chem.* 275:8475-8479.

75. Kashiwabuchi, N., K. Ikeda, K. Araki, T. Hirano, K. Shibuki, C. Takayama, Y. Inoue, T. Kutsuwada, T. Yagi, Y. Kang, and et al. 1995. Impairment of motor

coordination, Purkinje cell synapse formation, and cerebellar long-term depression in GluR delta 2 mutant mice. *Cell.* 81:245-252.

76. Hirano, T., K. Kasono, K. Araki, and M. Mishina. 1995. Suppression of LTD in cultured Purkinje cells deficient in the glutamate receptor delta 2 subunit. *Neuroreport.* 6:524-526.
77. Gao, J., S.F. Maison, X. Wu, K. Hirose, S.M. Jones, I. Bayazitov, Y. Tian, G. Mittleman, D.B. Matthews, S.S. Zakharenko, M.C. Liberman, and J. Zuo. 2007. Orphan glutamate receptor delta1 subunit required for high-frequency hearing. *Mol Cell Biol.* 27:4500-4512.
78. Schmid, S.M., and M. Hollmann. 2008. To gate or not to gate: are the delta subunits in the glutamate receptor family functional ion channels? *Mol Neurobiol.* 37:126-141.
79. Wo, Z.G., and R.E. Oswald. 1994. Transmembrane topology of two kainate receptor subunits revealed by N-glycosylation. *Proc Natl Acad Sci U S A.* 91:7154-7158.
80. Hollmann, M., C. Maron, and S. Heinemann. 1994. N-glycosylation site tagging suggests a three transmembrane domain topology for the glutamate receptor GluR1. *Neuron.* 13:1331-1343.
81. Armstrong, N., Y. Sun, G.Q. Chen, and E. Gouaux. 1998. Structure of a glutamate-receptor ligand-binding core in complex with kainate. *Nature.* 395:913-917.
82. Hogner, A., J.S. Kastrup, R. Jin, T. Liljefors, M.L. Mayer, J. Egebjerg, I.K. Larsen, and E. Gouaux. 2002. Structural basis for AMPA receptor activation and ligand selectivity: crystal structures of five agonist complexes with the GluR2 ligand-binding core. *J Mol Biol.* 322:93-109.

83. Jin, R., M. Horning, M.L. Mayer, and E. Gouaux. 2002. Mechanism of activation and selectivity in a ligand-gated ion channel: structural and functional studies of GluR2 and quisqualate. *Biochemistry.* 41:15635-15643.

84. Armstrong, N., and E. Gouaux. 2000. Mechanisms for activation and antagonism of an AMPA-sensitive glutamate receptor: crystal structures of the GluR2 ligand binding core. *Neuron.* 28:165-181.

85. Sobolevsky, A.I., M.P. Rosconi, and E. Gouaux. 2009. X-ray structure, symmetry and mechanism of an AMPA-subtype glutamate receptor. *Nature.* 429:745-756.

86. Oswald, R.E. 2004. Ionotropic glutamate receptor recognition and activation. *Adv Protein Chem.* 68:313-349.

87. Leuschner, W.D., and W. Hoch. 1999. Subtype-specific assembly of alpha-amino-3-hydroxy-5-methyl-4-isoxazole propionic acid receptor subunits is mediated by their N-terminal domains. *J Biol Chem.* 274:16907-16916.

88. Ayalon, G., and Y. Stern-Bach. 2001. Functional assembly of AMPA and kainate receptors is mediated by several discrete protein-protein interactions. *Neuron.* 31:103-113.

89. Herin, G.A., and E. Aizenman. 2004. Amino terminal domain regulation of NMDA receptor function. *Eur J Pharmacol.* 500:101-111.

90. Ayalon, G., E. Segev, S. Elgavish, and Y. Stern-Bach. 2005. Two regions in the N-terminal domain of ionotropic glutamate receptor 3 form the subunit oligomerization interfaces that control subtype-specific receptor assembly. *J Biol Chem.* 280:15053-15060.

91. Kuner, T., C. Beck, B. Sakmann, and P.H. Seeburg. 2001. Channel-lining residues of the AMPA receptor M2 segment: structural environment of the Q/R site and identification of the selectivity filter. *J Neurosci.* 21:4162-4172.

92. Jones, K.S., H.M. VanDongen, and A.M. VanDongen. 2002. The NMDA receptor M3 segment is a conserved transduction element coupling ligand binding to channel opening. *J Neurosci.* 22:2044-2053.

93. Liu, Y., M. Holmgren, M.E. Jurman, and G. Yellen. 1997. Gated access to the pore of a voltage-dependent K+ channel. *Neuron.* 19:175-184.

94. Soderling, T.R., and V.A. Derkach. 2000. Postsynaptic protein phosphorylation and LTP. *Trends Neurosci.* 23:75-80.

95. Kuusinen, A., M. Arvola, and K. Keinanen. 1995. Molecular dissection of the agonist binding site of an AMPA receptor. *Embo J.* 14:6327-6332.

96. Keinanen, K., M. Arvola, A. Kuusinen, and M. Johnson. 1997. Ligand recognition in glutamate receptors: insights from mutagenesis of the soluble alpha-amino-3-hydroxy-5-methyl-4-isoxazole propionic acid (AMPA)-binding domain of glutamate receptor type D (GluR-D). *Biochem Soc Trans.* 25:835-838.

97. Chen, G.Q., and E. Gouaux. 1997. Overexpression of a glutamate receptor (GluR2) ligand binding domain in Escherichia coli: application of a novel protein folding screen. *Proc Natl Acad Sci U S A.* 94:13431-13436.

98. Chen, G.Q., Y. Sun, R. Jin, and E. Gouaux. 1998. Probing the ligand binding domain of the GluR2 receptor by proteolysis and deletion mutagenesis defines domain boundaries and yields a crystallizable construct. *Protein Sci.* 7:2623-2630.

99. Sun, Y., R. Olson, M. Horning, N. Armstrong, M. Mayer, and E. Gouaux. 2002. Mechanism of glutamate receptor desensitization. *Nature.* 417:245-253.

100. Robert, A., N. Armstrong, J.E. Gouaux, and J.R. Howe. 2005. AMPA receptor binding cleft mutations that alter affinity, efficacy, and recovery from desensitization. *J Neurosci.* 25:3752-3762.

101. Valentine, E.R., and A.G. Palmer, 3rd. 2005. Microsecond-to-millisecond conformational dynamics demarcate the GluR2 glutamate receptor bound to agonists glutamate, quisqualate, and AMPA. *Biochemistry.* 44:3410-3417.

102. Kawamoto, S., S. Uchino, K.Q. Xin, S. Hattori, K. Hamajima, J. Fukushima, M. Mishina, and K. Okuda. 1997. Arginine-481 mutation abolishes ligand-binding of the AMPA-selective glutamate receptor channel alpha1-subunit. *Brain Res Mol Brain Res.* 47:339-344.

103. Lampinen, M., O. Pentikainen, M.S. Johnson, and K. Keinanen. 1998. AMPA receptors and bacterial periplasmic amino acid-binding proteins share the ionic mechanism of ligand recognition. *Embo J.* 17:4704-4711.

104. Maltsev, A.S., A.H. Ahmed, M.K. Fenwick, D.E. Jane, and R.E. Oswald. 2008. Mechanism of partial agonism at the GluR2 AMPA receptor: Measurements of lobe orientation in solution. *Biochemistry.* 47:10600-10610.

105. Jin, R., and E. Gouaux. 2003. Probing the function, conformational plasticity, and dimer-dimer contacts of the GluR2 ligand-binding core: studies of 5-substituted willardiines and GluR2 S1S2 in the crystal. *Biochemistry.* 42:5201-5213.

106. Zhang, W., Y. Cho, E. Lolis, and J.R. Howe. 2008. Structural and single-channel results indicate that the rates of ligand binding domain closing and opening directly impact AMPA receptor gating. *J Neurosci.* 28:932-943.

107. Gill, A., A. Birdsey-Benson, B.L. Jones, L.P. Henderson, and D.R. Madden. 2008. Correlating AMPA receptor activation and cleft closure across subunits: crystal structures of the GluR4 ligand-binding domain in complex with full and partial agonists. *Biochemistry.* 47:13831-13841.

108. Armstrong, N., M. Mayer, and E. Gouaux. 2003. Tuning activation of the AMPA-sensitive GluR2 ion channel by genetic adjustment of agonist-induced conformational changes. *Proc Natl Acad Sci U S A.* 100:5736-5741.

109. Stern, P., M. Cik, D. Colquhoun, and F.A. Stephenson. 1994. Single channel properties of cloned NMDA receptors in a human cell line: comparison with results from Xenopus oocytes. *J Physiol.* 476:391-397.

110. McLarnon, J.G., and K. Curry. 1990. Single channel properties of the N-methyl-D-aspartate receptor channel using NMDA and NMDA agonists: on-cell recordings. *Exp Brain Res.* 82:82-88.

111. Kleckner, N.W., and R. Dingledine. 1988. Requirement for glycine in activation of NMDA-receptors expressed in Xenopus oocytes. *Science.* 241:835-837.

112. Clements, J.D., and G.L. Westbrook. 1991. Activation kinetics reveal the number of glutamate and glycine binding sites on the N-methyl-D-aspartate receptor. *Neuron.* 7:605-613.

113. Popescu, G., and A. Auerbach. 2003. Modal gating of NMDA receptors and the shape of their synaptic response. *Nat Neurosci.* 6:476-483.

114. Auerbach, A., and Y. Zhou. 2005. Gating reaction mechanisms for NMDA receptor channels. *J Neurosci.* 25:7914-7923.

115. Kussius, C.L., and G.K. Popescu. 2009. Kinetic basis of partial agonism at NMDA receptors. *Nat Neurosci.* 12:1114-1120.

116. Inanobe, A., H. Furukawa, and E. Gouaux. 2005. Mechanism of partial agonist action at the NR1 subunit of NMDA receptors. *Neuron.* 47:71-84.

117. Rosenmund, C., Y. Stern-Bach, and C.F. Stevens. 1998. The tetrameric structure of a glutamate receptor channel. *Science.* 280:1596-1599.

118. Patneau, D.K., M.L. Mayer, D.E. Jane, and J.C. Watkins. 1992. Activation and desensitization of AMPA/kainate receptors by novel derivatives of willardiine. *J Neurosci.* 12:595-606.

119. Robert, A., and J.R. Howe. 2003. How AMPA receptor desensitization depends on receptor occupancy. *J Neurosci.* 23:847-858.

120. Ptak, C.P., A.H. Ahmed, and R.E. Oswald. 2009. Probing the allosteric modulator binding site of GluR2 with thiazide derivatives. *Biochemistry.* 48:8594-8602.

121. Ahmed, A.H., C.P. Ptak, and R.E. Oswald. 2010. Molecular mechanism of flop selectivity and subsite recognition for an AMPA receptor allosteric modulator: structures of GluA2 and GluA3 in complexes with PEPA. *Biochemistry.* 49:2843-2850.

122. Partin, K.M., M.W. Fleck, and M.L. Mayer. 1996. AMPA receptor flip/flop mutants affecting deactivation, desensitization, and modulation by cyclothiazide, aniracetam, and thiocyanate. *J Neurosci.* 16:6634-6647.

123. Yamada, K.A., and S.M. Rothman. 1992. Diazoxide blocks glutamate desensitization and prolongs excitatory postsynaptic currents in rat hippocampal neurons. *J Physiol.* 458:409-423.

124. Gonzalez, J., M. Du, K. Parameshwaran, V. Suppiramaniam, and V. Jayaraman. 2010. Role of dimer interface in activation and desensitization in AMPA receptors. *Proc Natl Acad Sci U S A.* 107:9891-9896.

125. Furukawa, H., S.K. Singh, R. Mancusso, and E. Gouaux. 2005. Subunit arrangement and function in NMDA receptors. *Nature.* 438:185-192.

126. Zheng, F., K. Erreger, C.M. Low, T. Banke, C.J. Lee, P.J. Conn, and S.F. Traynelis. 2001. Allosteric interaction between the amino terminal domain and the ligand binding domain of NR2A. *Nat Neurosci.* 4:894-901.

127. Erreger, K., and S.F. Traynelis. 2008. Zinc inhibition of rat NR1/NR2A N-methyl-D-aspartate receptors. *J Physiol.* 586:763-778.

128. Mayer, M.L., L. Vyklicky, Jr., and J. Clements. 1989. Regulation of NMDA receptor desensitization in mouse hippocampal neurons by glycine. *Nature.* 338:425-427.

129. Krupp, J.J., B. Vissel, C.G. Thomas, S.F. Heinemann, and G.L. Westbrook. 1999. Interactions of calmodulin and alpha-actinin with the NR1 subunit modulate Ca2+-dependent inactivation of NMDA receptors. *J Neurosci.* 19:1165-1178.

130. Young, S.L., D.L. Bohenek, and M.S. Fanselow. 1994. NMDA processes mediate anterograde amnesia of contextual fear conditioning induced by hippocampal damage: immunization against amnesia by context preexposure. *Behav Neurosci.* 108:19-29.

131. Collingridge, G.L., J.T. Isaac, and Y.T. Wang. 2004. Receptor trafficking and synaptic plasticity. *Nat Rev Neurosci.* 5:952-962.

132. Collingridge, G.L., P.W. Gage, and B. Robertson. 1984. Inhibitory post-synaptic currents in rat hippocampal CA1 neurones. *J Physiol.* 356:551-564.

133. Wigstrom, H., and B. Gustafsson. 1986. Postsynaptic control of hippocampal long-term potentiation. *J Physiol (Paris).* 81:228-236.

134. Lynch, G., J. Larson, S. Kelso, G. Barrionuevo, and F. Schottler. 1983. Intracellular injections of EGTA block induction of hippocampal long-term potentiation. *Nature.* 305:719-721.

135. Malenka, R.C., and M.F. Bear. 2004. LTP and LTD: an embarrassment of riches. *Neuron.* 44:5-21.

136. Hayashi, Y., S.H. Shi, J.A. Esteban, A. Piccini, J.C. Poncer, and R. Malinow. 2000. Driving AMPA receptors into synapses by LTP and CaMKII: requirement for GluR1 and PDZ domain interaction. *Science.* 287:2262-2267.

137. Fortin, D.A., M.A. Davare, T. Srivastava, J.D. Brady, S. Nygaard, V.A. Derkach, and T.R. Soderling. 2010. Long-Term Potentiation-Dependent Spine Enlargement Requires Synaptic Ca2+-Permeable AMPA Receptors Recruited by CaM-Kinase I. *J Neurosci.* 30:11565-11575.

138. Isaac, J.T., R.A. Nicoll, and R.C. Malenka. 1995. Evidence for silent synapses: implications for the expression of LTP. *Neuron.* 15:427-434.

139. Takumi, Y., V. Ramirez-Leon, P. Laake, E. Rinvik, and O.P. Ottersen. 1999. Different modes of expression of AMPA and NMDA receptors in hippocampal synapses. *Nat Neurosci.* 2:618-624.

140. Petralia, R.S., J.A. Esteban, Y.X. Wang, J.G. Partridge, H.M. Zhao, R.J. Wenthold, and R. Malinow. 1999. Selective acquisition of AMPA receptors over postnatal development suggests a molecular basis for silent synapses. *Nat Neurosci.* 2:31-36.

141. Johnston, M.V., B. Mullaney, and M.E. Blue. 2003. Neurobiology of Rett syndrome. *J Child Neurol.* 18:688-692.

142. Magnusson, K.R., and C.W. Cotman. 1993. Age-related changes in excitatory amino acid receptors in two mouse strains. *Neurobiol Aging.* 14:197-206.

143. Palmer, G.C. 2001. Neuroprotection by NMDA receptor antagonists in a variety of neuropathologies. *Curr Drug Targets.* 2:241-271.

144. Kwak, S., and J.H. Weiss. 2006. Calcium-permeable AMPA channels in neurodegenerative disease and ischemia. *Curr Opin Neurobiol.* 16:281-287.

145. Sattler, R., and M. Tymianski. 2000. Molecular mechanisms of calcium-dependent excitotoxicity. *J Mol Med.* 78:3-13.

146. Nicholls, D.G. 2008. Oxidative stress and energy crises in neuronal dysfunction. *Ann N Y Acad Sci.* 1147:53-60.

147. Sensi, S.L., H.Z. Yin, S.G. Carriedo, S.S. Rao, and J.H. Weiss. 1999. Preferential Zn2+ influx through Ca2+-permeable AMPA/kainate channels triggers prolonged mitochondrial superoxide production. *Proc Natl Acad Sci U S A.* 96:2414-2419.

148. Frederickson, C.J., J.Y. Koh, and A.I. Bush. 2005. The neurobiology of zinc in health and disease. *Nat Rev Neurosci.* 6:449-462.

149. Bresink, I., B. Ebert, C.G. Parsons, and E. Mutschler. 1996. Zinc changes AMPA receptor properties: results of binding studies and patch clamp recordings. *Neuropharmacology.* 35:503-509.

150. Lin, D.D., A.S. Cohen, and D.A. Coulter. 2001. Zinc-induced augmentation of excitatory synaptic currents and glutamate receptor responses in hippocampal CA3 neurons. *J Neurophysiol.* 85:1185-1196.

151. Rowland, L.P., and N.A. Shneider. 2001. Amyotrophic lateral sclerosis. *N Engl J Med.* 344:1688-1700.

152. Rosen, D.R., T. Siddique, D. Patterson, D.A. Figlewicz, P. Sapp, A. Hentati, D. Donaldson, J. Goto, J.P. O'Regan, H.X. Deng, and et al. 1993. Mutations in Cu/Zn superoxide dismutase gene are associated with familial amyotrophic lateral sclerosis. *Nature.* 362:59-62.

153. Hadano, S., Y. Yanagisawa, J. Skaug, K. Fichter, J. Nasir, D. Martindale, B.F. Koop, S.W. Scherer, D.W. Nicholson, G.A. Rouleau, J. Ikeda, and M.R. Hayden. 2001. Cloning and characterization of three novel genes, ALS2CR1, ALS2CR2, and ALS2CR3, in the juvenile amyotrophic lateral sclerosis (ALS2) critical region at chromosome 2q33-q34: candidate genes for ALS2. *Genomics.* 71:200-213.

154. Couratier, P., J. Hugon, P. Sindou, J.M. Vallat, and M. Dumas. 1993. Cell culture evidence for neuronal degeneration in amyotrophic lateral sclerosis being linked to glutamate AMPA/kainate receptors. *Lancet.* 341:265-268.

155. Kawahara, Y., K. Ito, H. Sun, H. Aizawa, I. Kanazawa, and S. Kwak. 2004. Glutamate receptors: RNA editing and death of motor neurons. *Nature.* 427:801.

156. Selkoe, D.J. 2002. Alzheimer's disease is a synaptic failure. *Science.* 298:789-791.

157. Blennow, K., M.J. de Leon, and H. Zetterberg. 2006. Alzheimer's disease. *Lancet.* 368:387-403.

158. Smith, M.A., K. Hirai, K. Hsiao, M.A. Pappolla, P.L. Harris, S.L. Siedlak, M. Tabaton, and G. Perry. 1998. Amyloid-beta deposition in Alzheimer transgenic mice is associated with oxidative stress. *J Neurochem.* 70:2212-2215.

159. Smith, M.A., G. Perry, P.L. Richey, L.M. Sayre, V.E. Anderson, M.F. Beal, and N. Kowall. 1996. Oxidative damage in Alzheimer's. *Nature.* 382:120-121.

160. Guan, Z.Z., X. Zhang, R. Ravid, and A. Nordberg. 2000. Decreased protein levels of nicotinic receptor subunits in the hippocampus and temporal cortex of patients with Alzheimer's disease. *J Neurochem.* 74:237-243.

161. Smith, M.A., C.A. Rottkamp, A. Nunomura, A.K. Raina, and G. Perry. 2000. Oxidative stress in Alzheimer's disease. *Biochim Biophys Acta.* 1502:139-144.

162. Guo, Q., L. Sebastian, B.L. Sopher, M.W. Miller, C.B. Ware, G.M. Martin, and M.P. Mattson. 1999. Increased vulnerability of hippocampal neurons from presenilin-1 mutant knock-in mice to amyloid beta-peptide toxicity: central roles of superoxide production and caspase activation. *J Neurochem.* 72:1019-1029.

163. Reisberg, B., R. Doody, A. Stoffler, F. Schmitt, S. Ferris, and H.J. Mobius. 2003. Memantine in moderate-to-severe Alzheimer's disease. *N Engl J Med.* 348:1333-1341.

164. Moult, P.R. 2009. Neuronal glutamate and GABAA receptor function in health and disease. *Biochem Soc Trans.* 37:1317-1322.

165. Rogawski, M.A., and S.D. Donevan. 1999. AMPA receptors in epilepsy and as targets for antiepileptic drugs. *Adv Neurol.* 79:947-963.

166. De Sarro, G., E.D. Di Paola, P. Gareri, L. Gallelli, G. Scotto, and A. De Sarro. 1999. Effects of some AMPA receptor antagonists on the development of tolerance in epilepsy-prone rats and in pentylenetetrazole kindled rats. *Eur J Pharmacol.* 368:149-159.

167. Franciosi, S. 2001. AMPA receptors: potential implications in development and disease. *Cell Mol Life Sci.* 58:921-930.

168. MacDonald, J.F., and L.M. Nowak. 1990. Mechanisms of blockade of excitatory amino acid receptor channels. *Trends Pharmacol Sci.* 11:167-172.

CHAPTER 2

Characterizing Single Channel Behavior of GluA3 Receptors*

2.1 Abstract

AMPA receptors play a major role in excitatory neurotransmission in the CNS and are involved in numerous neurological disorders. Agonists bind to each of four bilobed ligand binding domains (LBDs) of this tetrameric receptor, and upon binding, the lobes close to envelope the agonist, leading to channel activation. However, AMPA receptors exhibit complex activation kinetics, the mechanism of which has not yet been determined. We report here single channel studies of a homomeric AMPA receptor (GluA3) activated by the full agonist, glutamate, and a partial agonist, fluorowillardiine. Both agonists activate the channel to the same three open conductance levels but with different open probabilities in each level. The closed probability (P_c) varied within records, particularly at low agonist concentrations. By sorting discrete segments of the record according to P_c using the X-means algorithm, we defined five modes of activity. The kinetic behavior could then be analyzed for both agonists over a range of agonist concentrations with a relatively simple model (three closed states and two open states for each open conductance level). The structural mechanism underlying modal behavior is not clear, however, it occurs on a timescale consistent with hydrogen bonding across the lobe interface in the LBD.

2.2 Introduction

AMPA receptors, a subtype of ligand gated ionotropic glutamate receptors (iGluAs), not only mediate the majority of excitatory neurotransmission in the central nervous system (1-4) but also play a role in peripheral function (5, 6). Dysfunction of these receptors is associated with neurological diseases such as amyotropic lateral sclerosis, Huntington's disease and disorders such as epilepsy and ischaemic brain damage (7-9). The development of effective therapeutics is hampered by the widespread CNS distribution of AMPA receptors and a lack of clear understanding of

the role of specific subtypes in neuropathologies. Understanding functional characteristics of AMPA receptors can uncover differences between subunits and may allow for the design of selective pharmacological agents that target aberrant behavior without abolishing normal function.

The four AMPA subunits, GluA1-4, can form functional homo- or hetero-tetrameric channels (1, 10). Each subunit has a ligand binding domain (LBD) capable of binding one agonist molecule, a transmembrane domain responsible for channel gating, an extracellular N-terminal domain and an intracellular C-terminal domain (1, 2, 11). Glutamate binding to the LBD leads to the opening of the ion channel and a positive inward current, consisting of Na^+, K^+, and, depending on subunit composition and RNA editing (12), Ca^{2+} (13-15). The rate of desensitization is determined in part by a short sequence in the LBD called the flip/flop region (16); the flop form desensitizes faster than the flip form (17, 18). In the case of the flip form, desensitization can be slowed with the addition of cyclothiazide (CTZ), an allosteric modulator that stabilizes dimerization between two LBDs.

The structure of both the LBD (19) and the full length tetrameric GluA2 receptor (20) has been determined, and closure of the LBD upon agonist binding is thought to trigger the activation of the ion channel (19, 21-24). Functional studies of AMPA receptors on the macroscopic level have suggested a complex gating scheme (25, 26). However, macroscopic currents reveal average ion channel activation and deactivation from a large number of channels, sometimes masking details that can only be delineated with single channel recording. Previous single channel studies of various AMPA channels (23, 26-29) have been limited by heavy filtering of the data, channel rundown in the outside-out configuration, or recording of receptors from neuronal cells for which the subunit composition was not known. Earlier single channel studies on other ion channel subtypes, such as NMDA (30) and GABA (31) channels, have

revealed considerable insight into channel kinetics and modal behaviors that have yet to be characterized in detail for AMPA receptors.

The single channel studies described here used homomeric GluA3 receptors in the cell-attached mode, simplifying our system while maintaining a physiological cytoplasmic milieu. The physiological agonist, glutamate, was used, as well as a partial agonist, fluorowillardiine (FW). The use of partial agonists has been extremely important in the comparison of functional data with the extensive structural and dynamic information on AMPA receptors (20, 23, 32, 33). We report the number of conductance levels, the minimum number of states in each conductance class, the open probability, the mean lifetimes of channel opening, modal behaviors based on open probability, and a model describing the activation mechanism. Glutamate and FW share a common mechanism of channel activation with the same open conductance levels but with different open probabilities in each level. In the presence of either agonist, concentration-dependent modal behaviors that range from a mostly inactive to a highly active channel were observed.

2.3 Methods

Cell culture

Human embryonic kidney (HEK) 293 cells were stably transfected with GluA3i (G) (S.M. Holley & L.M. Nowak, unpublished). The receptor is the flip variant, and has a G in the R/G editing site. The cells were cultured in Dulbecco's Modified Eagle's Medium (DMEM) containing 10% fetal bovine serum (FBS), 1% penicillin-streptomycin and 1 µg/mL blasticidin, pH 7.4. The addition of the antibiotic, blasticidin, in the culture media selects for the growth of cells that express GluA3 channels. Cells are passaged every 3-4 days and used within 48 hours after passage. All cultures were maintained in a 37°C incubator with 5% CO_2.

Acquisition of Single Channel Currents

All experiments were performed at room temperature (~23°C). Pipettes were pulled from thick walled borosilicate glass with filament (Sutter Instrument Company, Novato, CA, USA) to a resistance of 15-20 MΩ and firepolished. Solutions were buffered at pH 7.4 and filtered using a 2 µM sterile filtering system (Corning, Lowell, MA). The bath buffer was a 1X Dulbecco's phosphate saline buffer with either Ca^{2+} and Mg^{2+}, or Mg^{2+} only (Invitrogen, Carlsbad, CA). The pipette solution contained (in mM): 150 NaCl, 10 Hepes/NaOH, 2 KCl. Stock solutions of glutamate or fluorowillardiine (FW; Tocris Bioscience, Ellisville, MO) were made from the pipette solution and kept frozen in aliquots at -20°C until the day of the experiment. Cyclothiazide (CTZ; Tocris Bioscience, Ellisville, MO, or Ascent Scientific, Princeton, NJ) was dissolved in methanol, frozen as 50 mM stock solutions, and was added (100-150 µM) to all agonist containing pipette solutions.

Single channel currents were amplified at a gain of 100 mV/pA with an EPC-7 amplifier, low pass filtered to 10 kHz using an external 8-pole Bessel filter, and digitized at 20 kHz using pClamp 7 software (Molecular Devices, Sunnyvale, CA). Data were converted from abf to qdf format on QuB software (www.qub.buffalo.edu) for analysis.

Single channel currents were recorded for 2 to 10 minutes in the cell-attached mode with pipette holding potentials of +80 to +120 mV. To determine single channel conductance, the current amplitude was measured in 20 mV increments, between -100 mV and +120 mV. The single channel conductance was estimated as the slope of the current-voltage relationship. Open channel noise with an rmsd of approximately 0.2 pA and a frequency of 1.3-2 kHz was occasionally observed using both FW and glutamate as agonists. This was likely due to a variable amount of rapid channel blocking, but was sufficiently small to have little effect on the analysis.

Analysis of Single Channel Data

Number of conductance levels: The baseline was defined by choosing a segment of the record without channel activity using QuB. We initially tested the criteria to use for analysis, which included the number of open conductance levels by idealizing the data assuming up to four different conductance levels, filtering at frequencies ranging from 1 to 10 kHz, and altering the deadtime at a range from 50-200 μs. The results from different combinations of criteria were then analyzed, and the criteria that provided the best fits to the amplitude histogram, dwell time histograms, and the largest log likelihood (LL) units were used for all subsequent analyses. In all cases, three open conductance levels provided the best fits to the data (Figure 2.1). The addition of a fourth open conductance level consistently exhibited a lower LL, despite the increase in free parameters (see Figure 2.1). Only records with one channel were chosen for further analysis.

Idealization and modeling of data: The amplitudes for each of the open conductance levels were estimated using the Amps function from QuB (Baum-Welch algorithm (34)). Next, the file was idealized at a dead time of 150 μs using the segmental-k-means (SKM) algorithm (35) to an initial simple linear model, C↔O1↔O2↔O3 (Figure 2.2A), consisting of one closed and three open classes starting with all rates set to 100 s^{-1}. The data were analyzed with or without an additional 5 kHz filtering (effective filter of 4.5 kHz). With filtering greater than this (*e.g.*, 2 kHz), baseline noise was often mistaken for small openings by QuB (Figure2.1). A dead time of 200 μs was imposed with the patches that had additional filtering. Maximum interval likelihood (MIL) analysis (36) was applied on this initial model to determine the fit to the dwell time histograms. States were then added one at a time to each closed and open class, re-idealized, refitted using MIL, and retained if the fits to the histograms improved and/or if the LL units increased by >10 LL units.

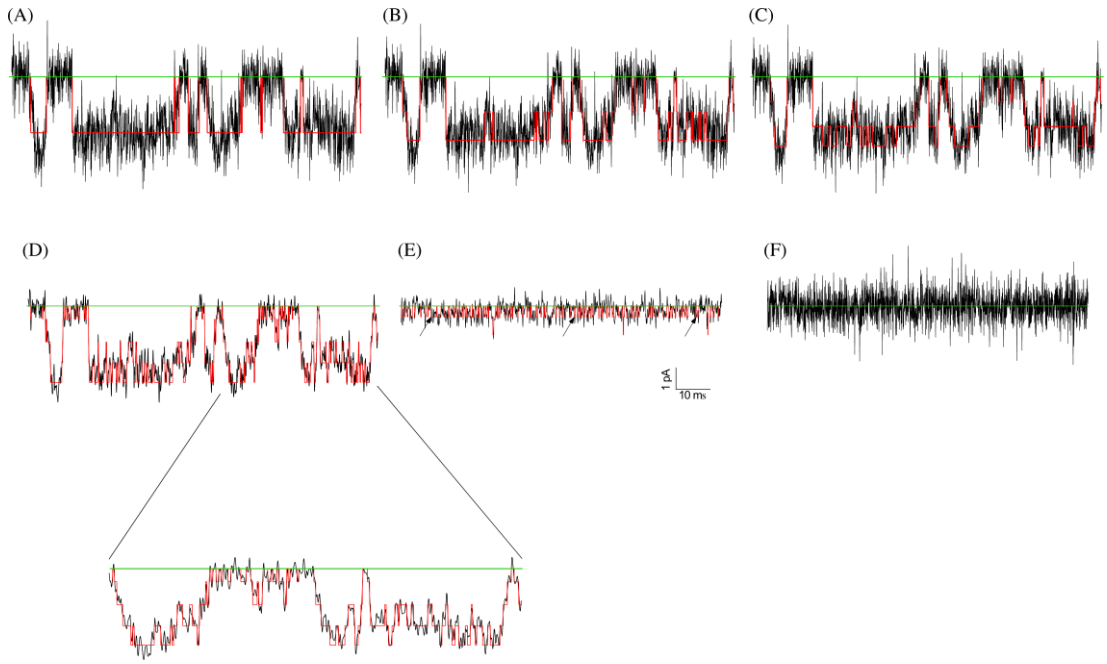

Figure 2.1.

***Demonstration of three open conductance states*: (A-C)** Idealization using the SKM algorithm is shown for one segment of data (4.5 kHz filtration) assuming one **(A)**, two **(B)**, and three **(C)** open conductances. The LL for the analysis of the entire record was 109868 for one conductance, 231758 for two conductance states, and 276996 for three conductance states. When the record was filtered to 2 kHz, four conductance states were detected **(D)**; however, the additional state was a misidentification of the noise. This is illustrated using a portion of a record filtered at 4.5 kHz with no channel **(F)** where false events (arrows indicate several representative false events) appear with 2 kHz filtering **(E)**. The idealization is superimposed in red on the current record, with the baseline shown in green.

If the addition of a state increased the LL by 10, but the rates to the new state were either close to zero or unrealistically large, then the additional state was omitted. Because of the complex behavior of GluA3 channels, this method was applied in order to determine the least complex kinetic model. This process was repeated again with rates starting at 10 s^{-1} to confirm that the final model and final rates were not affected by the starting values. From earlier studies of glutamate receptors, it is thought that at least two bound agonists are required to open the channel (11). In this case, three closed states might reflect a channel that has 0, 1, and 2 subunits with open channel gates. The fourth and sometimes a fifth closed state would reflect a deactivated or desensitized state. Our final model (Figure 2.2B) consists of three closed states and two open states in each of the open conductance levels. Loops that additionally connected closed states to the intermediate or large conductance levels in the model were tested, but in most cases worsened the fit to the dwell time histograms and/or gave unrealistic rates, so loops were not considered in our final model. Based on the transition matrices, transitions between the closed and the intermediate or large conductance levels were infrequently observed. Therefore, the final model does not include these transitions.

Segmentation of data: Inspection of the idealized traces indicated that most patches exhibited changes in activity over time, suggesting that the modal behavior observed for NMDA receptors (30) may also be a characteristic of AMPA receptors. Several different approaches were tested for sorting segments with different gating modes, including segmenting the data to 1 s segments or sorting based on mean open time (30). However, these approaches did not result in an improvement of LL within the segments. The patches that did contain activity changes had long closures between bursts. These long closures account for the fourth and sometimes fifth closed states, similar to what was found in previous studies (28). A critical time (t_{crit}), which

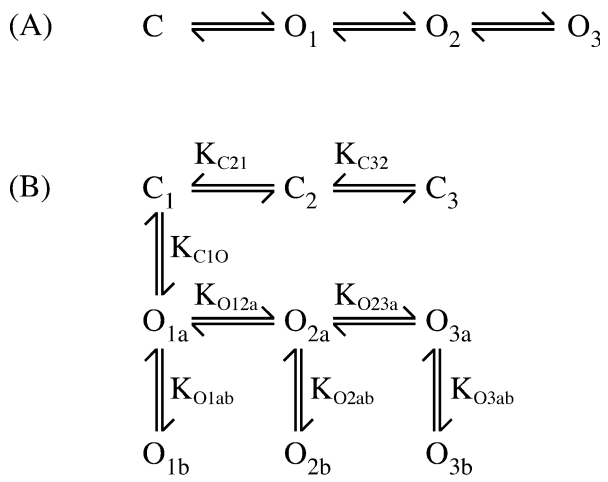

Figure 2.2

(A) Initial kinetic model used as a starting point but found not to describe the data adequately. **(B)** Final kinetic model. The notation for the equilibrium is as follows: $K_{C21} = k_{C2\to C1}/k_{C1\to C2}$, $K_{O12a} = k_{O1a\to O2a}/k_{O2a\to O1a}$, $K_{O1ab} = k_{O1a\to O1b}/k_{O1b\to O1a}$, etc.

describes the minimum closed duration between two bursts, was defined as described by Magleby and Pallotta (37).That is, t_{crit} was defined by solving:

$$a_1 e^{-t_{crit}/\tau_1} = a_2\left(1 - e^{-t_{crit}/\tau_2}\right)$$

Where a_2 and τ_2 describe the shortest closed component between bursts and a_1 and τ_1 describe the longest closed component within a burst. This choice of t_{crit} equalizes the number of closed intervals in the two components that are misclassified. It was applied only to records with more than three closed components, and a_2 and t_2 refer to the longest of the three shortest closed time components in the distribution. The closed times equal to or longer than t_{crit} were discarded in long records to yield isolated segments of bursts. These newly separated clusters were re-idealized to one closed and three open conductance classes (Figure 2.2A) to determine the closed and open probabilities of each segment. The segments were then sorted into modes using the select function in QuB. The select function uses an X-means algorithm (38) to place each segment into the appropriate mode based on P_c (P_c was used instead of P_o because of multiple conductance levels of the channel). The value of X is used to determine the number of modes by sorting the segments into similar clusters until the assignments stabilize. The modes were analyzed individually using the model described above (Figure 2.2B). Thus, the model in Figure 2.2B was applied to individual segments of data after removal of t_{crit} and sorted into modes using the X-means algorithm. In a few records having only three closed states and one mode, the model in Figure 2.2B was applied to the entire record. The files that did exhibit modal behavior did not always contain all five modes, but often a combination of less than five modes. The dwell times of similar modes were averaged, but each mode was modeled separately. Table 2.1 summarizes each record analyzed, indicating which were segmented into modes and which were analyzed as a whole. Because the number

Table 2.1

***Summary of Single Channel Records*.** Each record is shown as one row in the table. The concentration of agonist is given in the left column and the total length of the record in the second column. The total time in each of the modes is given in the next five columns, with the total time between bursts in the column on the far right. All times are in seconds and rounded to 10 ms. Records for which no entry is given in the interburst column had only three closed times and were analyzed without segmentation.

[FW] µM	Total length (s)	VH (s)	H (s)	M (s)	L (s)	VL (s)	Interburst (s)
5	207.20		105.92	42.60	5.43		53.25
	505.05		22.0		287.64		56.19
10	68.81		63.96				4.85
	209.21	140.51	22.74	9.64		3.67	32.65
	190.60		80.05	67.92	10.49		32.14
	566.26		176.88	89.15	11.67		288.56
	301.61		53.57		104.78	42.64	100.62
50	269.84		214.08				55.76
	22.14	20.86					1.28
	39.99	39.99					
	71.84	71.48					0.36
	126.51	126.51					
	397.03	228.60			12.59	24.51	71.33
	619.82	353.94	134.33	29.39	17.08	12.04	73.04
200	127.17	127.17					
	404.47	404.47					
	654.23		27.96	42.49	38.28	21.83	523.67
500	136.05	77.96				2.33	55.76
	140.18	140.18					
	144.64	144.64					
	182.52	182.52					
	176.33	176.33					

(Continued)

[glu] µM	Total length (s)	VH (s)	H (s)	M (s)	L (s)	VL (s)	Interburst (s)
50	117.83			93.32			24.51
75	268.66	29.39			9.18	14.23	215.86
100	83.20	20.10	22.66	11.26	4.10		25.08
	168.94					168.94	
	301.82			88.30		42.61	170.91
	121.26				121.26		
	73.55				73.55		
	182.66			182.66			
200	448.29				297.06		151.23
	64.08				64.08		
	211.23	35.25		58.06	30.55		87.37
	433.61					168.47	265.14
1000	180.52		36.58		10.28	24.11	109.55
	165.07			165.07			
	46.14		46.14				
	69.12	69.12					
	392.96	164.08		9.54	14.16	13.11	192.07
	31.97	31.97					
	19.94			19.94			
5000	49.78	49.78					
	63.20	63.20					
	134.08			105.06	22.69		6.33
	203.54	203.54					
	80.02	80.02					

of events in each group was necessarily less than the total number of events in the record, the LL was normalized to the number of events (LL/event) and each group was compared to the whole record. The final LL/event for each group ranged from 4.7-5.20, which is higher than that for the record as a whole by 0.05-0.30 LL/event. Five distinct modes were observed.

2.4 Results

GluA3 channels open to three distinct conductance levels

A continuous six-second segment of GluA3 single channel data recorded with 50 µM FW is shown in Figure 2.3A. As described in Methods, the largest LL value was obtained with a model that contained three open conductance levels (Figures 2.2 and 2.3), which is in agreement with most previous studies on GluA2 (23, 39), GluA4 (39), GluA3 chimeras (11), and AMPA channels in granule cells (26, 27), although four levels have been reported (40). The different conductance levels are distinguished from multi-channel patches because patches containing two or more active channels had at least double the number of open levels, were rarely closed and exhibited an amplitude that was twice the largest conductance of the single channel patch. Also, in the presence of CTZ, the channel has a high P_o (17), so that double openings are readily identified.

Amplitude probability density functions for 50 µM FW and 5 mM glutamate (both concentrations are above the corresponding EC_{50} (17, 23, 41)) bound to a single GluA3 channel are shown in Figure 2.3B. In addition to a closed level, three open conductance levels with conductance estimates of 14 ± 0.6 (6), 26 ± 1.4 (3), and 35 ± 1.8 (2) pS for FW and 14 ± 2.2 (3), 26 ± 1.3 (3), and 39 ± 0.8 (3) pS for glutamate (O_1, small; O_2, intermediate; O_3, large, respectively; number in parenthesis is the number of

Figure 2.3. (A) A representative 6 s segment of a single channel record of GluA3 activated by 50 μM FW. In this and all subsequent figures, the channel opens in a downward direction. **(B)** Amplitude histograms for an entire record obtained with 50 μM FW at 100 mV (top) and another obtained with 5 mM glutamate at 80 mV (bottom). Above each histogram is a representative 500 ms segment of the single channel record with each of the three conductance levels indicated. The inset gives the percentage of each conductance level determined from a fit of four Gaussians to the amplitude histograms. For both the FW and glutamate records shown, the channel only exhibited M mode.

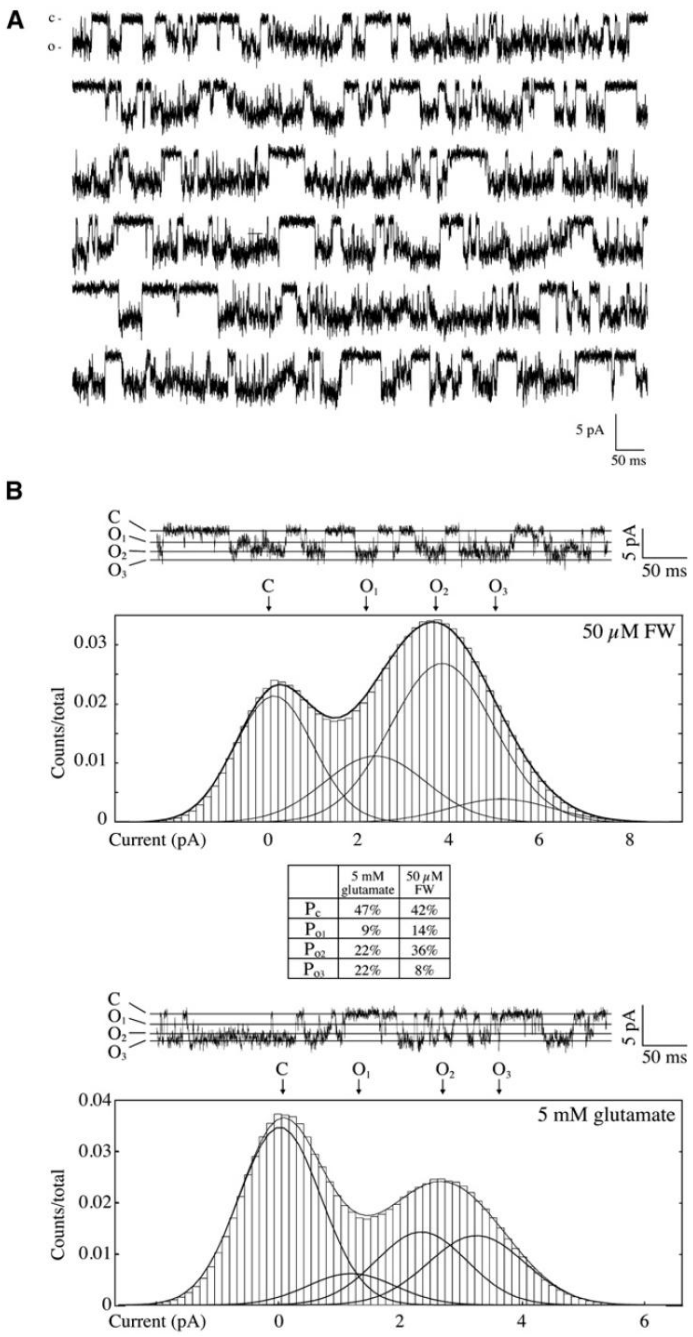

	5 mM glutamate	50 μM FW
P_c	47%	42%
P_{o1}	9%	14%
P_{o2}	22%	36%
P_{o3}	22%	8%

records used for the measurement; Figure 2.4), were observed for both FW and glutamate. However, the channel preferentially opens to the intermediate and large conductance levels when bound to glutamate, and to the small and intermediate conductance levels when bound to FW (Figure 2.3, inset). The presence of the same three conductance levels in both full and partial agonists is consistent with similar activation schemes.

GluA3 single channel currents fit to a simple model

The simplest model with the highest LL value determined from MIL analysis consists of two open states in each conductance class and three closed states (Figure 2.2B). Dwell time histograms recorded with saturating concentrations of FW (50 μM) and glutamate (5 mM) are shown in Figure 2.5. The open histograms demonstrate the presence of two exponentials (consistent with the two open states used in the MIL modeling), similar to previous studies (28). Adding loops between states resulted in either distortion of the fit to the dwell time histogram or rate constants that were either unrealistically high or close to zero. A state transition matrix from the two patches that describes the percent of transitions between states is given in Table 2.2. Based on transition matrices from all analyzed patches, the channel favors transitions between adjacent levels (stepwise opening and closing). These results are also in agreement with Zhang *et al*. (29) who reported transitions between adjacent levels for GluA2 WT and T686 mutant. At least three closed states are necessary to fit the data (Table 2.3). In some cases, depending upon the concentration of agonist, a fourth and fifth closed state can be detected. Previous studies on homomeric GluA2 and GluA4 channels detected four closed dwell times (29, 42). Patches acquired at high concentrations of agonist were uniform in activity. These patches usually had three, sometimes a fourth, closed state. At high concentrations when four closed states were observed, the long

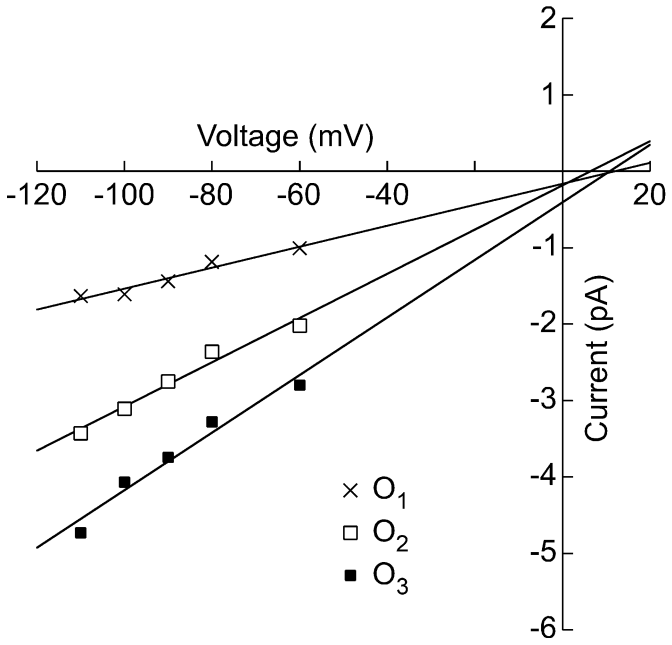

Figure 2.4

***Demonstration of three open conductance states*:** Representative current-voltage relationship acquired from the application of 5 mM glutamate. GluA3 activity was acquired over a range of holding potentials. Current amplitudes for each open level were initially estimated with 500-1000 ms of data using Amps in QuB (Baum-Welch algorithm). The amplitudes for each conductance level were then reestimated during idealization (SKM algorithm; see Methods: Idealization and modeling of the data). The current amplitudes were plotted against the holding potential to determine the conductance from the slope of the plot.

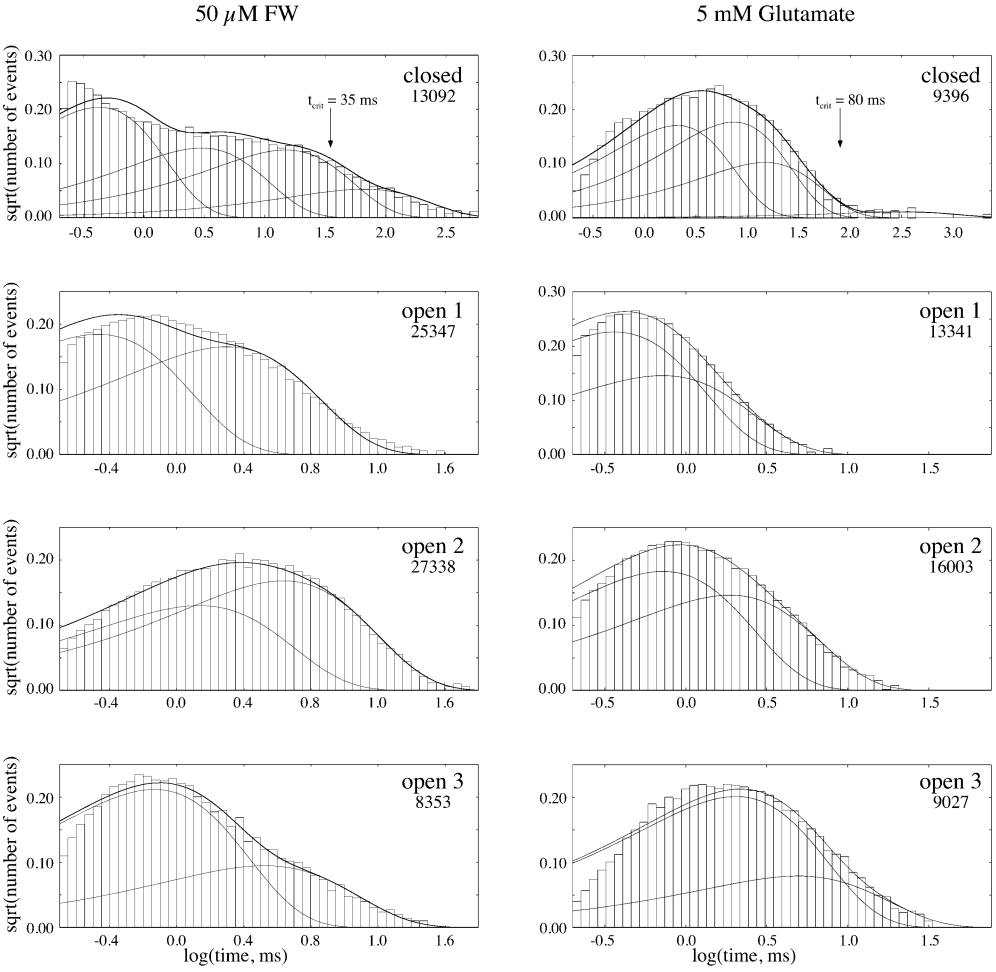

Figure 2.5

Dwell time histograms for the same records used to generate Figure 2.3B. The number in the upper left corner indicates the number of events.

Table 2.2

State transition matrices showing the percentage of transitions between each conductance level. Transitions between adjacent states are far more frequent than transitions between nonadjacent states. This constrains the model shown in Figure 1 such that transitions between closed states and O2, between closed states and O3, and between O1 and O3 are not included.

50 μM FW

	C	O1	O2	O3
C	-	13.2	6.8	0.4
O1	13.4	-	18.5	1.6
O2	6.6	18.8	-	9.4
O3	0.5	1.4	9.5	-

5 mM glutamate

	C	O1	O2	O3
C	-	13.6	4.7	0.7
O1	13.9	-	13.8	1.7
O2	4.4	13.7	-	15.5
O3	0.8	2.1	15.0	-

closures likely reflect a desensitized state for the following reasons: (i) At high concentration of agonist, the receptor is saturated with agonist so long closures do not represent unbound receptor; (ii) Due to the cell-attached patch configuration, the agonist is at equilibrium with the binding sites; (iii) The recordings are relatively long, so it is expected that the channel would eventually desensitize, as cyclothiazide slows but does not abolish desensitization. At lower concentrations of agonist, four or five closed states were observed. Since lower concentrations may reflect a nonsaturated receptor, one of the closed times could represent deactivation.To investigate whether removal of these long closures caused an alteration in the measured parameters, we compared the dwell time constants of patches with and without the long closures. The shortest three dwell time constants for the closed state and the dwell time constants for the open states are similar before and after discarding the long closures. For records with four or five closed states, the critical time (t_{crit}; see Methods) was determined and closures longer than t_{crit} were discarded.

Table 2.3 Fluorowillardiine

µM	Mode	t_{C1} (area)	t_{C2} (area)	t_{C3} (area)	t_{O1a} (area)	t_{O1b} (area)	t_{O2a} (area)	t_{O2b} (area)	t_{O3a} (area)	t_{O3b} (area)	P_o (n)
500	VH	0.98 ± 0.31 (0.73 ± 0.02)	4.4 ± 1.4 (0.21 ± 0.01)	27 ± 9.8 (0.05 ± 0.02)	1.8 ± 0.3 (0.80 ± 0.03)	13 ± 3.4 (0.20 ± 0.03)	3.0 ± 0.6 (0.81 ± 0.04)	19 ± 5.2 (0.18 ± 0.04)	3.0 ± 0.8 (0.85 ± 0.01)	17 ± 3.4 (0.15 ± 0.01)	93 ± 1.4% (5)
200	VH	1.4 ± 0.7 (0.76 ± 0.03)	5.4 ± 2.3 (0.21 ± 0.02)	32 ± 7.6 (0.24 ± 0.02)	1.5 ± 0.6 (0.74 ± 0.09)	5.4 ± 2.5 (0.25 ± 0.09)	2.4 ± 0.8 (0.77 ± 0.05)	7.7 ± 2.4 (0.22 ± 0.05)	2.5 ± 0.8 (0.80 ± 0.01)	9.9 ± 2.1 (0.19 ± 0.02)	91 ± 0.9% (3)
	H	0.59 (0.62)	2.4 (0.28)	13 (0.09)	0.91 (0.83)	3.4 (0.17)	1.5 (0.79)	4.7 (0.19)	1.3 (0.92)	9.2 (0.06)	67% (1)
	M	0.66 (0.59)	3.1 (0.30)	19 (0.11)	0.74 (0.66)	2.1 (0.34)	1.2 (0.82)	4.3 (0.14)	1.1 (0.92)	6.3 (0.06)	49% (1)
50	VH	1.2 ± 0.23 (0.76 ± 0.03)	5.7 ± 1.0 (0.20 ± 0.02)	16 ± 2.4 (0.04 ± 0.01)	1.4 ± 0.2 (0.77 ± 0.05)	5.8 ± 1.1 (0.23 ± 0.05)	2.2 ± 0.5 (0.81 ± 0.04)	6.8 ± 1.4 (0.18 ± 0.05)	2.1 ± 0.5 (0.88 ± 0.04)	9.7 ± 2.6 (0.11 ± 0.04)	88 ± 2.8% (5)
	H	0.66 ± 0.30 (0.55 ± 0.15)	2.5 ± 0.7 (0.19 ± 0.001)	11 ± 1.5 (0.24 ± 0.14)	0.62 ± 0.30 (0.55 ± 0.13)	2.5 ± 0.7 (0.45 ± 0.13)	1.6 ± 0.3 (0.50 ± 0.16)	4.9 ± 0.8 (0.48 ± 0.14)	1.9 ± 1.2 (0.84 ± 0.06)	8.1 ± 4.9 (0.15 ± 0.05)	74 ± 2% (2)
	M	1.1 (0.52)	3.7 (0.23)	12 (0.25)	1.6 (1.0)	-	1.6 (0.66)	4.9 (0.33)	3.5 (0.75)	7.6 (0.24)	53% (1)
10	VH	0.83 (0.65)	3.2 (0.3)	24 (0.05)	1.4 (0.73)	7.2 (0.27)	3.1 (0.85)	28 (0.15)	1.5 (0.82)	15 (0.17)	94% (1)
	H	1.3 ± 0.25 (0.70 ± 0.04)	4.8 ± 0.6 (0.20 ± 0.03)	17 ± 2.5 (0.07 ± 0.02)	0.93 ± 0.13 (0.80 ± 0.03)	3.1 ± 0.2 (0.19 ± 0.03)	0.85 ± 0.10 (0.84 ± 0.03)	3.7 ± 0.4 (0.15 ± 0.03)	1.2 ± 0.2 (0.85 ± 0.02)	8.0 ± 1.6 (0.12 ± 0.02)	69 ± 1.5% (5)
	M	1.4 ± 0.25 (0.68 ± 0.02)	5.7 ± 0.6 (0.21 ± 0.02)	18 ± 3.2 (0.08 ± 0.03)	1.0 ± 0.13 (0.86 ± 0.07)	5.1 ± 1.3 (0.13 ± 0.08)	0.54 ± 0.05 (0.84 ± 0.05)	1.8 ± 0.1 (0.14 ± 0.04)	0.63 ± 0.08 (0.83 ± 0.07)	2.4 ± 0.25 (0.12 ± 0.08)	45 ± 1.5% (3)
	L	1.3 (0.5)	6.3 (0.3)	16 (0.14)	0.59 (0.89)	2.9 (0.09)	0.52 (0.92)	2.0 (0.06)	0.83 (0.79)	3.1 (0.14)	37% (1)
	VL	1.9 (0.33)	3.5 (0.13)	17 (0.5)	0.69 (0.82)	3.1 (0.18)	0.46 (0.95)	2.7 (0.04)	0.81 (0.84)	2.7 (0.1)	18% (1)
5	H	1.4 ± 0.30 (0.80 ± 0.02)	8.6 ± 0.7 (0.17 ± 0.01)	52 ± 12 (0.013 ± 0.01)	1.2 ± 0.08 (0.82 ± 0.06)	5.9 ± 2.6 (0.18 ± 0.06)	1.6 ± 0.1 (0.75 ± 0.06)	6.2 ± 0.4 (0.24 ± 0.06)	3.0 ± 0.2 (0.91 ± 0.01)	23 ± 1.2 (0.07 ± 0.01)	79 ± 5% (2)
	M	2.0 (0.75)	7.5 (0.08)	13 (0.16)	1.4 (0.83)	3.5 (0.17)	1.1 (0.79)	4.5 (0.21)	2.5 (0.96)	20 (0.02)	57% (1)
	L	1.6 (0.71)	7.2 (0.26)	69 (0.02)	1.2 (0.74)	3.5 (0.26)	1.1 (0.94)	6.7 (0.05)	0.98 (0.88)	6.3 (0.1)	35% (1)
	VL	1.2 (0.52)	7.4 (0.39)	85 (0.09)	0.68 (0.79)	2.2 (0.21)	0.59 (0.85)	2.2 (0.12)	0.68 (0.92)	2.5 (0.05)	12% (1)

Table 2.3 (continued) Glutamate

µM	Mode	t_{C1} (area)	t_{C2} (area)	t_{C3} (area)	t_{O1a} (area)	t_{O1b} (area)	t_{O2a} (area)	t_{O2b} (area)	t_{O3a} (area)	t_{O3b} (area)	P_o (n)
5000	VH	0.78 ± 0.03 (0.76 ± 0.05)	3.9 ± 1.2 (0.17 ± 0.04)	45 (0.15)	0.29 ± 0.05 (0.91 ± 0.06)	1.6 ± 0.8 (0.08 ± 0.05)	0.78 ± 0.12 (0.36 ± 0.02)	2.5 ± 0.1 (0.62 ± 0.01)	1.4 ± 0.002 (0.77 ± 0.01)	5.2 ± 0.8 (0.18 ± 0.05)	93 ± 3% (2)
	M	1.9 (0.39)	5.4 (0.36)	11 (0.20)	0.34 (0.64)	0.68 (0.35)	0.68 (0.56)	1.8 (0.43)	1.9 (0.82)	4.6 (0.13)	52% (1)
1000	VH	1.2 (0.70)	6.0 (0.26)	28 (0.03)	0.96 (0.93)	2.9 (0.07)	1.1 (0.95)	3.9 (0.05)	1.0 (0.80)	4.6 (0.18)	90% (1)
	H	0.92 ± 0.26 (0.69 ± 0.01)	4.7 ± 1.4 (0.25 ± 0.01)	32 ± 4.4 (0.03 ± 0.001)	0.78 ± 0.19 (0.91 ± 0.02)	2.7 ± 0.2 (0.08 ± 0.01)	1.0 ± 0.14 (0.92 ± 0.03)	3.1 ± 0.8 (0.07 ± 0.02)	0.84 ± 0.14 (0.79 ± 0.01)	3.7 ± 0.9 (0.18 ± 0.01)	71 ± 0.5% (5)
	M	0.88 (0.43)	3.4 (0.52)	11 (0.02)	0.75 (0.87)	1.7 (0.12)	0.74 (0.90)	1.7 (0.09)	0.73 (0.82)	2.5 (0.16)	57% (2)
200	L	1.3 (0.53)	4.8 (0.35)	11 (0.08)	0.53 (0.91)	1.4 (0.08)	0.73 (0.93)	1.6 (0.05)	0.50 (0.89)	1.8 (0.06)	34% (1)
	VL	1.9 ± 0.24 (0.24 ± 0.08)	6.9 ± 1.1 (0.20 ± 0.13)	34 ± 11 (0.50 ± 0.15)	0.61 ± 0.23 (0.66 ± 0.01)	2.1 ± 0.06 (0.33 ± 0.00)	0.72 ± 0.38 (0.69 ± 0.06)	2.9 ± 0.4 (0.30 ± 0.05)	1.9 ± 1.0 (0.83 ± 0.07)	4.6 ± 1.8 (0.10 ± 0.02)	16 ± 3% (2)
100	VH	0.56 (0.63)	3.5 (0.21)	12 (0.11)	0.42 (0.86)	1.7 (0.12)	0.79 (0.86)	2.0 (0.13)	1.0 (0.76)	5.1 (0.20)	87% (1)
	H	0.62 (0.48)	2.4 (0.24)	11 (0.20)	0.39 (0.85)	1.3 (0.12)	0.75 (0.88)	1.7 (0.10)	0.77 (0.77)	3.8 (0.17)	69% (1)
	M	1.6 ± 0.5 (0.55 ± 0.07)	8.1 ± 2.9 (0.31 ± 0.03)	44 ± 17 (0.11 ± 0.05)	1.3 ± 0.5 (0.75 ± 0.09)	4.6 ± 2.0 (0.25 ± 0.09)	1.1 ± 0.2 (0.88 ± 0.02)	3.9 ± 1.5 (0.11 ± 0.02)	1.3 ± 0.5 (0.80 ± 0.04)	5.9 ± 1.8 (0.17 ± 0.05)	49 ± 2.7% (3)
	L	1.3 (0.59)	8.7 (0.32)	62 (0.08)	1.4 (0.84)	6.0 (0.16)	1.0 (0.91)	3.0 (0.08)	0.85 (0.80)	2.7 (0.19)	19% (1)
	VL	2.2 ± 0.5 (0.55 ± 0.07)	13 ± 2.4 (0.39 ± 0.19)	34 ± 0.5 (0.25 ± 0.11)	1.0 ± 0.51 (0.75 ± 0.02)	3.0 ± 1.7 (0.25 ± 0.02)	2.4 ± 1.0 (0.71 ± 0.21)	6.2 ± 2.1 (0.28 ± 0.22)	0.92 ± 0.43 (0.90 ± 0.001)	2.7 ± 1.1 (0.07 ± 0.02)	20 ± 0.8% (3)
75	VH	0.68 (0.72)	3.5 (0.20)	27 (0.01)	0.49 (0.89)	1.7 (0.09)	0.89 (0.85)	2.1 (0.13)	0.84 (0.86)	4.9 (0.08)	87% (1)
50	M	0.97 (0.53)	4.4 (0.38)	31 (0.06)	0.71 (0.90)	2.6 (0.10)	0.96 (0.79)	1.9 (0.20)	0.68 (0.81)	2.5 (0.16)	50% (1)

Analysis of modal behavior

Evidence for modal behavior as a function of concentration. The number of open states, as well as the final model, was consistent across all patches. Most patches acquired at lower concentrations of agonist exhibited fluctuation in activity over time. Analysis of patches at lower agonist concentrations as a whole did not yield fits that overlaid well to the dwell time histograms. Inspection of the records suggested that, over time, the channel operated in modes that changed abruptly from one to another, with the possibility that the rate constants differed in the various modes (Figures 2.6 and 2.7). Although a number of methods were tested for sorting records into different modes, the most successful approach was based on P_c. Bursts were separated into segments based on the t_{crit} value (see Methods), with lower concentrations of agonist having the largest range of t_{crit} values between different files (1 mM Glu 79-182 ms, 200 µM Glu 78-309 ms, 100 µM Glu 50-365 ms, 200 µM FW 73 ms, 50 µM FW 36-87 ms, 10 µM FW 53-145 ms, 5 µM FW 53-348 ms). Bursts with similar activity (based on P_c) were clustered together and analyzed separately (Figure 2.6B). The closed channel probability (P_c), the open channel probability (P_o) in each separate conductance class, as well as the length of time spent in each conductance class, varied among modes.

Five modes were observed for the full and partial agonist (Very High (VH), High (H), Medium (M), Low (L) and Very Low (VL) modes), corresponding to P_o (*i.e.*, 1 - P_c) of approximately >90%, 70%, 50%, 30%, and <20%. Although up to five different modes were detected using the X-means algorithm, the frequency of observing these modes varied with the agonist and the agonist concentration and not all records contained all five modes (Table 2.1). Figure 2.6 shows three different patches acquired at 500, 50 and 10 µM FW and the modes exhibited in each patch.

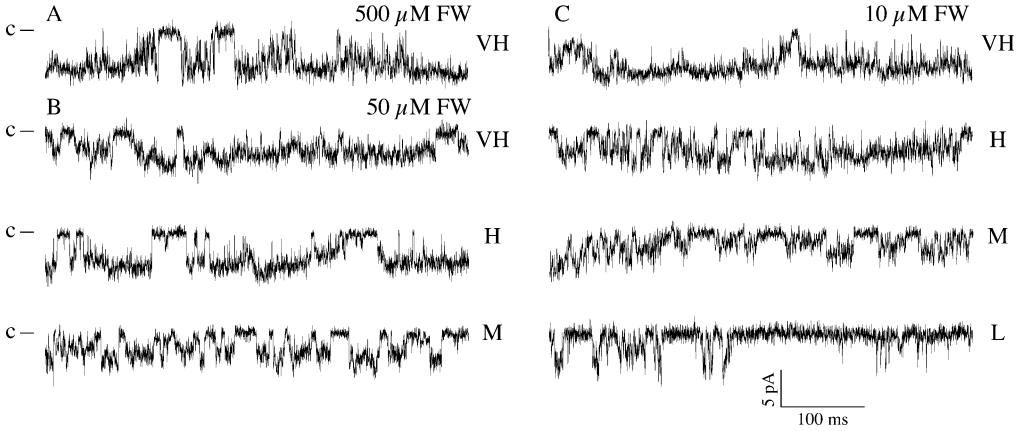

Figure 2.6

Representative segments of single channel records obtained with **(A)** 500 µM, **(B)** 50 µM, and **(C)** 10 µM FW showing different modes of activity (VH, very high mode; H, high mode; M, medium mode; L, low mode).

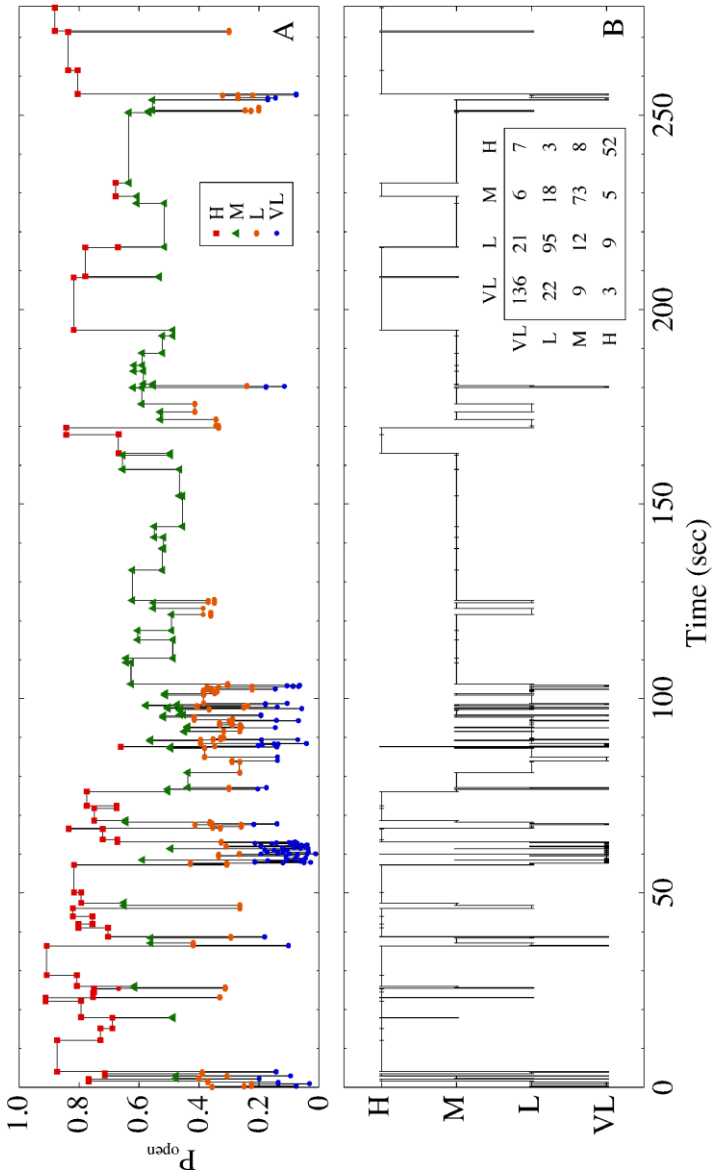

Figure 2.7

(A) P_o for segments of a single channel record with 50 µM FW. Closed times greater than t_{crit} were removed, and the horizontal lines indicate the length of the segment at a given P_o (y-axis). The plotting symbol at the beginning and the end of a segment indicates the mode as defined in the legend. **(B)** The same segment as **(A)** but classified according to mode instead of P_o. The inset is a modal transition matrix for the modes.

For each mode, the kinetic properties were similar regardless of the agonist concentration. In Figure 2.7A, the P_o values (1 - P_c) for sequential segments of one record are shown (10 μM FW). The classification into modes is indicated by the plotting symbol in Figure 2.7A, and the mode for each segment is given in the corresponding plot in Figure 2.7B. The inset shows a modal transition matrix, demonstrating that the channel is more likely to remain in the same mode than to transition to a different mode.

At very high concentrations of FW, the channel had a P_o greater than 90% and mostly resided in the VH mode of activity throughout the record. At 500 μM FW, the average P_o was 95% (n = 5) for all of the patches. At 200 μM FW, two out of three patches had a VH mode of activation and the third patch had a mixture of VH, H and M. As the agonist concentration was decreased, lower probability modes were more frequently observed. At 50 μM FW, the majority of the patches had a mixture of VH (n = 4), H (n = 2), and M (n = 1) modes. We also began to observe an L mode of activity at 50 μM FW, but with too few events to analyze. Most of the patches recorded with 10 μM FW displayed more than one mode of activation, which consisted of an assortment of all five modes, VH (n = 1), H (n = 5), M (n = 3), L (n = 2) and VL (n = 3). The application of 5 μM FW for 2 out of 7 patches resulted in the activation of the channel to all but the VH mode. The other five patches displayed activation mainly to the lowest conductance level (see section on nonbinomial activation to a single conductance level).

Modal behaviors follow a binomial distribution. Previous analyses of single channel events from GluA2 suggest that the channel opens to multiple levels and openings follow a binominal distribution (23). That is, once bound with a given number of agonist molecules (2 to 4), the channel can display openings to up to three levels. The four levels (closed plus three open) can be viewed as four trials (n) and the

level of a particular opening is defined as the number of successes (k). The probability of success (p) can then vary between agonist, at different concentrations, and, in this case, in different modes. As shown in Table 2.4, p (also referred to an "efficacy factor" (23)), is consistent across modes and increases from VL to VH mode.

Variation among modes. In VH mode, the open dwell times (τ_o) in the open states of all conductance levels are longer, and decrease as the modal activity decreases. Generally, the VH mode has the longest τ_o values whereas the VL mode has the shortest dwell times for all the conductance levels (Table 2.3). This is true both for channels activated by FW and by glutamate. With the exception of the longest closed dwell time (τ_c), (which might have been affected from discarding long closures), the shortest τ_c values were relatively similar between all the modes and concentrations. Following MIL modeling, equilibrium constants calculated from the rate constants ($K = k_f/k_r$) for the same modes were averaged across patches (Table 2.5). Overall, for the step that represents the transition from closed to open, the equilibrium constant (K_{C1O}; see Figure 1 for the definition of the equilibrium constants) varies between modes, being greatest for the VH and lowest for the VL mode at all concentrations for both glutamate and FW (Table 2.5). K_{O12a} and K_{O23a} are slightly larger for bound glutamate than FW, indicating that the energy barrier for opening in the presence of glutamate is lower. The distribution in each conductance level is independent of agonist concentration and is dependent upon the mode. The distribution shifts toward the lower conductance states in the lower modes of activation. The O_3 level is the least populated in all modes for FW relative to glutamate.

Table 2.4

Efficacy Factors for Modes. The efficacy factor (p) was calculated as described in Methods based on the conductance histograms for records separated into specific modes. The concentrations used ranged from 5 to 500 μM for FW and from 50 to 5000 μM for glutamate. The efficacy factor is synonymous with the probability of success in a bionomial distribution. The higher the value, the more likely a gate will be open.

	FW	Glutamate
VH	0.66 ± 0.02	0.73 ± 0.04
H	0.60 ± 0.02	0.71 ± 0.05
M	0.45 ± 0.05	0.59 ± 0.08
L	0.26 ± 0.11	0.42 ± 0.05
VL	0.24 ± 0.08	0.42 ± 0.11

Table 2.5 Fluorowillardiine

Conc. (μM)	Mode	K_{C32}	K_{C31}	K_{C1O}	K_{O1ab}	K_{O12a}	K_{O2ab}	K_{O23a}	K_{O3ab}
500	VH	1.6 ± 0.6	1.8 ± 0.6	7.0 ± 2.6	0.70 ± 0.44	1.5 ± 0.7	0.47 ± 0.23	0.19 ± 0.13	0.51 ± 0.23
200	VH	3.8 ± 4.3	2.6 ± 0.9	3.1 ± 0.5	0.29 ± 0.15	2.1 ± 0.4	0.25 ± 0.12	0.55 ± 0.15	0.35 ± 0.12
	H	1.1	1.3	1.8	0.25	0.80	0.22	0.25	0.27
	M	1.0	0.96	1.2	0.24	0.44	0.20	0.20	0.21
50	VH	5.2 ± 4.9	2.0 ± 0.7	4.2 ± 2.1	0.40 ± 0.22	1.8 ± 0.7	0.31 ± 0.20	0.32 ± 0.13	0.45 ± 0.36
	H	1.6 ± 0.4	0.98 ± 0.80	1.8 ± 0.01	0.69 ± 0.43	2.4 ± 1.5	0.32 ± 0.04	0.20 ± 0.10	0.29 ± 0.13
	M	2.6	1.0	1.3		0.61	0.31	0.38	0.11
10	VH	0.99	1.7	5.9	0.62	2.2	0.84	0.16	1.1
	H	3.6 ± 2.2	1.5 ± 0.9	1.7 ± 0.5	0.23 ± 0.08	0.88 ± 0.43	0.29 ± 0.13	0.34 ± 0.16	0.45 ± 0.15
	M	4.2 ± 2.2	1.6 ± 0.7	1.1 ± 0.2	0.20 ± 0.09	0.36 ± 0.23	0.17 ± 0.10	0.17 ± 0.03	0.18 ± 0.15
	L	3.9	0.97	0.58	0.21	0.62	0.10	0.57	0.23
	VL	4.8	0.83	0.32	0.34	0.28	0.12	0.29	0.13
5	H	8.4 ± 10	1.5 ± 0.6	2.4 ± 0.2	0.34 ± 0.2	1.2 ± 0.2	0.37 ± 0.09	0.38 ± 0.09	0.39 ± 0.13
	M	15	1.6	1.2	0.13	0.52	0.34	0.18	0.14
	L	1.3	0.62	0.82	0.23	0.11	0.18	0.14	0.37
	VL	0.53	0.71	0.48	0.23	0.12	0.18	0.25	0.07

Table 2.5 (Continued) Glutamate

Conc. (μM)	Mode	K_{C32}	K_{C31}	K_{C1O}	K_{O1ab}	K_{O12a}	K_{O2ab}	K_{O23a}	K_{O3ab}
5000	VH	1.2	0.83 ± 0.86	1.7 ± 0.2	0.10 ± 0.02	5.5 ± 1.7	0.38 ± 0.13	0.75 ± 0.41	0.30 ± 0.21
	M	6.4	2.1	0.3	0.1	2.0	0.23	1.1	0.10
1000	VH	2.4	2.6	3.1	0.09	2.0	0.05	0.50	0.40
	H	2.0 ± 1.6	1.4 ± 0.1	1.8 ± 0.2	0.12 ± 0.07	1.3 ± 0.2	0.07 ± 0.00	0.40 ± 0.00	0.35 ± 0.07
	M	9.3	1.8	0.93	0.06	0.77	0.05	0.57	0.20
200	VH	2.8	1.8	2.4	0.58	1.5	0.21	0.23	0.82
	M		1.4	1.3	0.32	0.26	0.23	0.15	0.93
	L	5.8	1.7	0.47	0.05	0.61	0.02	0.21	0.08
	VL	2.8 ± 1.1	0.59 ± 0.31	0.21 ± 0.15	0.31 ± 0.28	0.65 ± 0.33	0.46 ± 0.37	1.2 ± 1.7	0.08 ± 0.20
100	VH	2.5	0.78	2.2	0.18	2.9	0.09	0.87	0.48
	H	1.3	0.84	1.3	0.14	2.2	0.06	0.62	0.40
	M	1.4 ± 0.3	0.91 ± 0.11	1.2 ± 0.24	0.28 ± 0.19	0.79 ± 0.70	0.16 ± 0.10	0.27 ± 0.17	0.40 ± 0.22
	L	0.94	0.68	1.3	0.31	0.34	0.09	0.18	0.21
	VL	3.0 ± 0.6	0.62 ± 0.14	0.32 ± 0.16	0.21 ± 0.10	0.92 ± 0.32	0.11 ± 0.13	0.03 ± 0.02	0.08 ± 0.03
75	VH	1.9	1.8	2.7	0.1	2.1	0.08	0.44	0.27
50	M	1.0	1.2	1.2	0.14	0.99	0.07	0.18	0.22

Transitions between modes. The long closures between bursts represented periods of channel inactivity that may be due to desensitization and/or deactivation. In order to determine if the channel entered modes randomly following a long closure or if specific transitions were observed, a modal transition matrix for each record was generated. These showed that the channel preferentially remains in the same mode following a long closure and when a transition to a different mode is observed, it is preferentially to an adjacent mode (Inset to Figure 2.7B).

Nonbinomial activation to a single conductance level

In a number of cases, the channel opened to an individual conductance level without transitions (or having few transitions) to other levels. In the presence of 200 µM glutamate, six patches exhibited the largest conductance level without any transitions to the smallest and intermediate levels (Figure 2.8A). Four of these patches had a VH mode of activity (P_o of 93.5% ± 0.03) and long mean lifetime of channel opening (25-145 ms). Because of this high activity and long duration openings, events (transitions between open and closed) were few in number and MIL analysis was limited. The remaining two patches had a mixture of H, M and VL modes or only L mode, despite exhibiting only the highest conductance level.

In the case of FW, patches that exhibited mainly one conductance were largely in the lowest conductance level. This included 5 of 7 records with 5 µM FW (Figure 2.8B), as well as, single records at 50, 200, and 500 µM. At 5 µM FW, 3 out of 5 patches exhibited VH mode, while remaining in the lowest conductance state for 80% of the record. The remainder of these records showed other modes, but remained largely in the lowest conductance state. These records and those of glutamate cited above do not follow a binomial distribution and clearly represent an aspect of channel

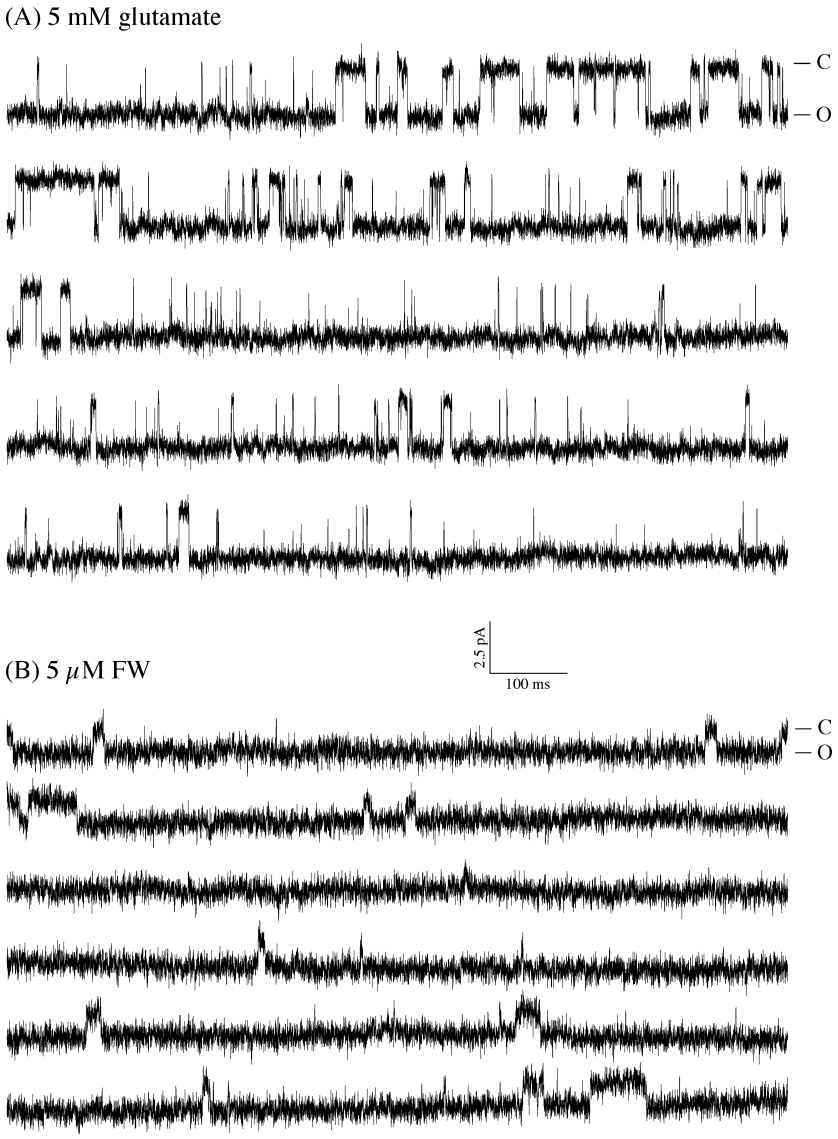

Figure 2.8

(A) Representative segment (5 s) of a record with 5 mM glutamate showing openings exclusively to the highest conductance level (O_3) and **(B)** a representative segment (5 s) with 5 μM FW showing openings exclusively to the lowest conductance level (O_1).

gating that differs from that observed with the majority of the recordings from GluA3 channels.

2.5 Discussion

While a great deal is known concerning the structure of AMPA receptors (20, 43), the details of channel activation are complex and less well characterized. The complexity arises at least in part from time-dependent changes in activity that varies with agonist concentration. Although an excess of high conductance openings at low glutamate concentrations in short records has been associated with two modes of activity (40), time-dependent changes in activity appear to be more complex and consist of a number of different modes that vary with agonist concentration.

Homomeric GluA3 channels have three open conductance classes, which are shared by the full agonist, glutamate, and the partial agonist, FW. This is similar to what has previously been reported (11, 23, 29). We show here that at high concentrations, the channel can be modeled as three closed states and three conductance levels, each with two kinetically distinct open states. At lower concentrations, the channels can be modeled with a similar number of states, but the fit to the data is not as good as at high concentrations, and the probability of opening seems to vary within a given record. As has been described for GluN and GABA channels (30, 31), dividing the record into segments (in this case, grouping segments based on P_c using the X-means function in QuB) produced much higher LL/event values for dwell time fits. Using a range of FW and glutamate concentrations, we defined five modes of activity (see Figure 2.7). The distribution of openings was consistent within each mode regardless of concentration, and the probability of observing modes of higher activity increased with increasing agonist concentration. Modeling the openings as a binomial, the "efficacy factor" (23), p, is larger in higher

modes. Furthermore, analysis of the modal behavior suggested that the channel preferentially either remains in the same mode following a long closure or changes to an adjacent mode.

The question then is what is the nature of the modal behavior? Our results clearly show that it is a graded process, with higher modes associated with higher agonist concentration and higher conductances. One possibility is that modal gating is tied to occupancy level. That is, the number of agonists bound and perhaps the distribution of bound LBDs within the tetramer may determine the mode, such that the lowest modes would have the lowest occupancy. Since the highest conductance is observed, albeit with low probability, even in VL mode, this model would suggest that the highest conductance level could be produced by tetramers that are only partially occupied by agonist. The structural basis of such a model is not obvious. Alternatively, the conductance levels could be set by the number of occupied subunits for which the LBD is in the closed lobe conformation. However, in its simplest form, this model does not explain modal gating. To account for modal gating, at least one additional factor would have to be controlling gating behavior. Although factors such as phosphorylation could play a role, at least two processes associated with the LBD could contribute to modal behavior. These include hydrogen bonding across the lobe interface and the binding of CTZ.

Extensive studies of the GluA2 LBD (21, 23, 32, 33), supported by recent crystal structures of the GluA3 LBD (44), show that two H-bonds can form across the dimer interface, stabilizing the closed lobe form. However, the lobes can be closed in the absence of these H-bonds, in which a 180˚ flip of the peptide bond between D655 and S656 (GluA3 numbering) occurs (21). Generally, the conformation in which the H-bonds can form is referred to as the "flipped form" and the 180˚ rotation of the peptide bond that cannot form H-bonds is the "unflipped form". Intermediate forms have also

been observed (21). The flipped form of the peptide bond is a dynamic process that can occur both in the presence of FW and glutamate (32). Thus, the modes may be set by both the occupancy and by the H-bonding state. The VH mode could be generated by the occupancy of all four subunits with 3-4 H-bonded subunits; whereas, the lower modes would have progressively fewer H-bonds and a tendency toward lower occupation. Depending upon the time scale of the H-bonding, a receptor could be locked into a particular mode for at least a burst of channel openings. An important question is the timescale of the transition between the flipped and unflipped form of the peptide bond. This cannot be approached by crystallography. However, relaxation measurements by NMR suggest that at least for FW and glutamate, the process is longer than a few ms (33). H/D exchange studies can provide an estimate of the timescale of the opening rate for the H-bond, but only at high pH (EX1 limit; (45)). The rates measured at high pH are on the order of 10 Hz, which approach the timescale necessary to account for the duration of the modes. Although rigorous fitting to a model with transient H-bonds that lock the LBD would not be possible with our single channel data sets due to the relatively small number of transitions between modes, different modes can easily be simulated by an additional state with locked lobe (*i.e.*, no off-rate).

An additional factor that may contribute to modal behavior is the binding of CTZ. An intact dimer interface of the LBD is thought to be necessary for channel activation and the dissociation of the interface is associated with desensitization (13). The status of the dimer interface in the resting state has been ambiguous. A recent study by Gonzalez *et al.* (46) suggests that the dimer interface is not intact in the resting state but only forms with activation. This may mean that CTZ would bind preferentially to dimers, perhaps those with agonist in both LBDs. If this were true, it would be possible at low concentrations of agonist to obtain a mode with high levels of

activation to a low conductance state by occupation of both monomers within a dimer, with CTZ bound to the dimer interface. Conversely, occupying one monomer of each potential dimer would not necessarily bind CTZ and could lead to a mode with low levels of activation.

An additional question relates to the nature of partial agonism and the transduction of the binding signal into gate opening. Clearly the closure of an LBD is associated with channel activation; however, it is not clear exactly how the LBD is coupled to channel gating. That is, an individual LBD bound to agonist is assumed to be able to activate a channel gate that is associated with an increase in channel conductance. Activation only occurs if the LBD has an intact dimer interface with the adjacent LBD. Even in the case of an intact dimer interface, individual subunit gating is unlikely to be directly coupled to occupancy of the binding site. This was recognized by Jin *et al.* (23) and, as noted above, the efficacy factor was introduced to quantitate the lower efficacy of partial agonists. Jin *et al.* (23) suggested that the efficacy factor is determined by the degree to which the lobes of the LDB were closed, in that partial agonists exhibit lower degrees of lobe closure than full agonists in many crystal structures. This was consistent with the data at the time, but the structural link to channel gating remained unclear. Zhang *et al.* (29) have suggested that channel activation is associated with the stability of the closed lobes, and Maltsev *et al.* (32) have suggested that partial agonists have a distribution of lobe closures ranging from perhaps fully closed to more open. Based on recent NMR and crystallographic evidence that a full lobe closing of GluA2 LBD can be observed under some conditions with partial agonists (*e.g.*, iodowillardiine and kainate; Ahmed and Oswald, unpublished observations), we suggest that the efficacy relates to the probability of a full lobe closure, and that in a given mode or distribution of LBD occupancy, the conductance level is set by the number of LBD that are in the fully closed

conformation at any given time. The LBDs that have formed H-bonds as described above would be transiently locked (on the timescale of 100 ms) in this fully closed-lobe conformation. FW is a relatively strong partial agonist and one might expect that full lobe closure is more likely than for a weaker partial agonist such as iodowillardiine or kainate. The occupancy in the conductance levels for FW are consistently lower than for the full agonist, glutamate, but the difference is not as dramatic as observed previously for iodowillardiine *vs*. glutamate (23).

In addition to the modal behavior exhibited in the majority of records, occasionally openings to a single level (or largely a single level) were observed. In the case of glutamate, these openings were to the highest conductance levels, and with FW, the openings were largely to the lowest conductance level. In at least one case, the activity changed from the typical three conductance levels to a single conductance within one record. These channels have the same conductance levels as GluA3 and have not been observed in the absence of agonist, and thus appear to be a distinct functional state of GluA3.

NMDA receptors, unlike AMPA receptors, require all four subunits to be bound to agonist (two of which are glycine-specific) for activation (47). Unlike the concentration dependence of modal behavior for GluA3, no such correlation exists for NMDA channels (30). Nevertheless, AMPA receptor activation shares some commonalities with NMDA receptor gating. Modeling of both channels requires three closed states, with one leading into an open level, and two exponentials are needed to fit to the open level (30, 48). Partial agonism at NMDA channels result in a decrease in open channel probability of a single conductance level (49); whereas, for AMPA channels, partial agonism is associated with a decrease in open probability in the largest conductance levels. Thus, although NMDA receptors open to only a single

conductance level, considerable similarities between the two classes of glutamate receptors are evident.

The single channel results obtained with GluA3 suggest that the kinetic model of activation is simple, but that the channel can exist in different modes depending, at least in part, on agonist occupation. All recordings were done in the presence of cyclothiazide, which dramatically decreases the rate of desensitization. Nevertheless, one might expect that the modal behavior may still have relevance to normal channel activation at the synapse. The half-time of desensitization of GluA3 is several milliseconds (13, 50), so that for a given EPSP, the mode would not necessarily change for any given channel. However, the EPSP is made up of synchronous activation of thousands of channels, probably activating in a distribution of modes. The development of compounds that could favor high or low modes could be of therapeutic value for neurological disorders such as Alzheimer's disease (drugs favoring high modes) or epilepsy (drugs favoring low modes).

REFERENCES

1. Dingledine, R., K. Borges, D. Bowie, and S.F. Traynelis. 1999. The glutamate receptor ion channels. *Pharmacol Rev.* 51:7-61.
2. Hollmann, M., and S. Heinemann. 1994. Cloned glutamate receptors. *Annu Rev Neurosci.* 17:31-108.
3. Nakanishi, S., and M. Masu. 1994. Molecular diversity and functions of glutamate receptors. *Annu Rev Biophys Biomol Struct.* 23:319-348.
4. Sommer, B., and P.H. Seeburg. 1992. Glutamate receptor channels: novel properties and new clones. *Trends Pharmacol Sci.* 13:291-296.
5. Weaver, C.D., T.L. Yao, A.C. Powers, and T.A. Verdoorn. 1996. Differential expression of glutamate receptor subtypes in rat pancreatic islets. *J Biol Chem.* 271:12977-12984.
6. Gill, S.S., O.M. Pulido, R.W. Mueller, and P.F. McGuire. 1998. Molecular and immunochemical characterization of the ionotropic glutamate receptors in the rat heart. *Brain Res Bull.* 46:429-434.
7. Kwak, S., and J.H. Weiss. 2006. Calcium-permeable AMPA channels in neurodegenerative disease and ischemia. *Curr Opin Neurobiol.* 16:281-287.
8. Chen, P.E., and D.J. Wyllie. 2006. Pharmacological insights obtained from structure-function studies of ionotropic glutamate receptors. *Br J Pharmacol.* 147:839-853.
9. Black, M.D. 2005. Therapeutic potential of positive AMPA modulators and their relationship to AMPA receptor subunits. A review of preclinical data. *Psychopharmacology (Berl).* 179:154-163.
10. Madden, D.R. 2002. The structure and function of glutamate receptor ion channels. *Nat Rev Neurosci.* 3:91-101.

11. Rosenmund, C., Y. Stern-Bach, and C.F. Stevens. 1998. The tetrameric structure of a glutamate receptor channel. *Science.* 280:1596-1599.
12. Schmauss, C., and J.R. Howe. 2002. RNA editing of neurotransmitter receptors in the mammalian brain. *Sci STKE.* 2002:PE26.
13. Sun, Y., R. Olson, M. Horning, N. Armstrong, M. Mayer, and E. Gouaux. 2002. Mechanism of glutamate receptor desensitization. *Nature.* 417:245-253.
14. Stern-Bach, Y., S. Russo, M. Neuman, and C. Rosenmund. 1998. A point mutation in the glutamate binding site blocks desensitization of AMPA receptors. *Neuron.* 21:907-918.
15. Paas, Y. 1998. The macro- and microarchitectures of the ligand-binding domain of glutamate receptors. *Trends Neurosci.* 21:117-125.
16. Sommer, B., K. Keinanen, T.A. Verdoorn, W. Wisden, N. Burnashev, A. Herb, M. Kohler, T. Takagi, B. Sakmann, and P.H. Seeburg. 1990. Flip and flop: a cell-specific functional switch in glutamate-operated channels of the CNS. *Science (New York, N.Y.* 249:1580-1585.
17. Pei, W., Z. Huang, and L. Niu. 2007. GluR3 flip and flop: differences in channel opening kinetics. *Biochemistry.* 46:2027-2036.
18. Pei, W., Z. Huang, C. Wang, Y. Han, J.S. Park, and L. Niu. 2009. Flip and flop: a molecular determinant for AMPA receptor channel opening. *Biochemistry.* 48:3767-3777.
19. Armstrong, N., Y. Sun, G.Q. Chen, and E. Gouaux. 1998. Structure of a glutamate-receptor ligand-binding core in complex with kainate. *Nature.* 395:913-917.
20. Sobolevsky, A.I., M.P. Rosconi, and E. Gouaux. 2009. X-ray structure, symmetry and mechanism of an AMPA-subtype glutamate receptor. *Nature.* 429:745-756.

21. Armstrong, N., and E. Gouaux. 2000. Mechanisms for activation and antagonism of an AMPA-sensitive glutamate receptor: crystal structures of the GluR2 ligand binding core. *Neuron.* 28:165-181.
22. Gouaux, E. 2004. Structure and function of AMPA receptors. *J Physiol.* 554:249-253.
23. Jin, R., T.G. Banke, M.L. Mayer, S.F. Traynelis, and E. Gouaux. 2003. Structural basis for partial agonist action at ionotropic glutamate receptors. *Nat Neurosci.* 6:803-810.
24. Jin, R., and E. Gouaux. 2003. Probing the function, conformational plasticity, and dimer-dimer contacts of the GluR2 ligand-binding core: studies of 5-substituted willardiines and GluR2 S1S2 in the crystal. *Biochemistry.* 42:5201-5213.
25. Zhang, W., A. Robert, S.B. Vogensen, and J.R. Howe. 2006. The relationship between agonist potency and AMPA receptor kinetics. *Biophys J.* 91:1336-1346.
26. Smith, T.C., L.Y. Wang, and J.R. Howe. 2000. Heterogeneous conductance levels of native AMPA receptors. *J Neurosci.* 20:2073-2085.
27. Smith, T.C., and J.R. Howe. 2000. Concentration-dependent substate behavior of native AMPA receptors. *Nat Neurosci.* 3:992-997.
28. Swanson, G.T., R.W. Gereau, T. Green, and S.F. Heinemann. 1997. Identification of amino acid residues that control functional behavior in GluR5 and GluR6 kainate receptors. *Neuron.* 19:913-926.
29. Zhang, W., Y. Cho, E. Lolis, and J.R. Howe. 2008. Structural and single-channel results indicate that the rates of ligand binding domain closing and opening directly impact AMPA receptor gating. *J Neurosci.* 28:932-943.
30. Popescu, G., and A. Auerbach. 2003. Modal gating of NMDA receptors and the shape of their synaptic response. *Nat Neurosci.* 6:476-483.

31. Lema, G.M., and A. Auerbach. 2006. Modes and models of GABA(A) receptor gating. *J Physiol.* 572:183-200.
32. Maltsev, A.S., A.H. Ahmed, M.K. Fenwick, D.E. Jane, and R.E. Oswald. 2008. Mechanism of partial agonism at the GluR2 AMPA receptor: Measurements of lobe orientation in solution. *Biochemistry.* 47:10600-10610.
33. Fenwick, M.K., and R.E. Oswald. 2008. NMR spectroscopy of the ligand-binding core of ionotropic glutamate receptor 2 bound to 5-substituted willardiine partial agonists. *J Mol Biol.* 378:673-685.
34. Baum, L.E., Petrie, T., Soules, G., and Weiss, N. 1970. A maximization technique occurring in the statistical analysis of probabilistic functions of Markov chains. *Ann. Math. Statist.* 41:164-171.
35. Qin, F., and L. Li. 2004. Model-based fitting of single-channel dwell-time distributions. *Biophys J.* 87:1657-1671.
36. Qin, F., A. Auerbach, and F. Sachs. 1996. Estimating single-channel kinetic parameters from idealized patch-clamp data containing missed events. *Biophys J.* 70:264-280.
37. Magleby, K.L., and B.S. Pallotta. 1983. Burst kinetics of single calcium-activated potassium channels in cultured rat muscle. *J Physiol.* 344:605-623.
38. Pelleg, D., Moore, A.W. 2000. X-means: Extending K-means with efficient estimation of the number of clusters. Morgan Kaufmann Publishers, Inc., San Francisco, CA. pp. 727-737.
39. Swanson, G.T., R.W. Gereau, T. Green, and S.F. Heinemann. 1997. Identification of amino acid residues that control functional behavior in GluR5 and GluR6 kainate receptors. *Neuron.* 19:913-926.
40. Prieto, M.L., and L.P. Wollmuth. Gating modes in AMPA receptors. *J Neurosci.* 30:4449-4459.

41. Patneau, D.K., M.L. Mayer, D.E. Jane, and J.C. Watkins. 1992. Activation and desensitization of AMPA/kainate receptors by novel derivatives of willardiine. *J Neurosci.* 12:595-606.
42. Swanson, G.T., S.K. Kamboj, and S.G. Cull-Candy. 1997. Single-channel properties of recombinant AMPA receptors depend on RNA editing, splice variation, and subunit composition. *J Neurosci.* 17:58-69.
43. Kubo, M., and E. Ito. 2004. Structural dynamics of an ionotropic glutamate receptor. *Proteins.* 56:411-419.
44. Ahmed, A.H., Q. Wang, H. Sondermann, and R.E. Oswald. 2009. Structure of the S1S2 glutamate binding domain of GluR3. *Proteins.* 75:628-637.
45. Fenwick, M.K., and R.E. Oswald. On the mechanisms of alpha-amino-3-hydroxy-5-methylisoxazole-4-propionic acid (AMPA) receptor binding to glutamate and kainate. *J Biol Chem.* 285:12334-12343.
46. Gonzalez, J., Du, M., Parameshwaran, K., Suppiramaniam,V. and Jayaraman, V. 2010. Role of dimer interface in activation and desensitization in AMPA receptors. *Proc. Natl. Acad. Sci.*
47. Johnson, J.W., and P. Ascher. 1987. Glycine potentiates the NMDA response in cultured mouse brain neurons. *Nature.* 325:529-531.
48. Auerbach, A., and Y. Zhou. 2005. Gating reaction mechanisms for NMDA receptor channels. *J Neurosci.* 25:7914-7923.
49. Kussius, C.L., A.M. Popescu, and G.K. Popescu. 2010. Agonist-specific gating of NMDA receptors. *Channels (Austin).* 4:78-82.
50. Robert, A., and J.R. Howe. 2003. How AMPA receptor desensitization depends on receptor occupancy. *J Neurosci.* 23:847-858.

CHAPTER 3

Structural and Functional Mechanism for Modal Activation of GluA3 Receptors

3.1 Abstract

AMPA receptors are the major excitatory neurotransmitter receptors in the CNS and are involved in numerous neurological disorders. An agonist-binding site is found in each of four subunits. Binding consists of three steps: docking of agonist to the bilobed ligand binding domain (LBD), closure of the LBD, and an increase in the stability of the closed lobe conformation through interlobe hydrogen bonding. We report single channel currents recorded with GluA3 channels in the presence of nitrowillardiine (NO_2W) and chlorowillardiine (ClW), in conjunction with crystal structures of GluA2 and GluA3 LBDs bound to fluorowillardiine (FW), ClW, and NO_2W. The GluA3 channel, when bound to NO_2W or ClW, opens to three conductance levels with comparable open probabilities and displays modal behaviors, similar to that obtained with glutamate and FW as agonists (Poon et al., 2010). At low agonist concentrations, ClW displayed an alternative kinetic behavior, consisting of high open probability (high mode of activation) to the lower conductance states. The structure of ClW bound to GluA3 LBD exhibits a unique partially open hydrogen bonding structure that may be associated with an alternative kinetic gating. NO_2W exhibits long open times in the very high modes of activation. The structure of NO_2W bound to GluA2 LBD exhibits fully closed lobes with additional interlobe interactions mediated by the nitro group of NO_2W. These results suggest that differences in GluA3 receptor activation by full and partial agonists are not simply just coupled to the degree of LBD closure but may be associated with multiple small differences within the LBD.

3.2 Introduction

AMPA receptors are a class of ionotropic glutamate receptors involved in excitatory neurotransmission in the CNS and include four different types of subunits, GluA1-4. A single subunit consists of an N-terminal domain, a ligand binding domain (LBD), a transmembrane domain, and a C-terminal domain. Four subunits associate to form a functional heteromeric or homomeric receptor in which each subunit can bind an agonist and contribute to channel activation (1).

Characterization of AMPA receptor structure and function has led to initial models of channel activation. Specifically, the closure of the LBD upon agonist binding is directly correlated to activation of the gating mechanism within the transmembrane segments (2, 3). Early studies correlated the degree of LBD closure in crystal structures to the amplitude of whole cell currents at saturating agonist concentrations. Full agonists exhibited the most closure and partial agonists exhibited partial closures (3). However, dynamic studies using NMR and crystal structures of mutant GluA2 LBDs have suggested that closed lobe stability may also determine agonist efficacy. Agonist binding to the LBD consists of at least three steps: (1) agonist binding to Lobe 1, (2) closure of the lobes and contacts with Lobe 2, and (3) interlobe contacts (including H-bonds) to stabilize the closed lobe form (2, 5, 6). The current speculation is that lobe closure is required for channel gating, but the degree of lobe closure that can trigger gating is not clear (that is, does gating require a full closure?). In addition, the role of auxiliary interlobe contacts has not been completely resolved. We recently suggested (8) that the H-bonding associated with the flip of the D655/S656 peptide bond determine the modal behavior observed in homomeric GluA3 channels activated by FW and glutamate.

Our previous studies found that both glutamate and FW activated the GluA3 channel to similar three conductance levels (8). The studies described here involve a larger spectrum of functional activity using two other partial agonists in the willardiine family of compounds, nitrowillardiine (NO_2W) and chlorowillardiine (ClW). We have also obtained crystal structures of FW and ClW bound to the LBD of GluA3 as well as NO_2W and ClW bound to the LBD of GluA2. Although overall, the structures are quite similar to the large number of published AMPA LBD structures, several details may be related to the functional properties elicited by NO_2W and ClW. The structural details that vary upon binding of different ligands are the orientation of the two lobes (*e.g.*, lobe closure and twist), the orientation of the peptide bond between D655 and S656, and the orientation of the sidechain of M712. These differences may affect the single channel properties of GluA3 receptors when bound to the willardiine compounds, specifically the probability the channel enters each conductance level and the modal behaviors.

3.3 Methods

Cell culture

Human embryonic kidney (HEK) 293 cells were stably transfected with GluA3i (G) (S.M. Holley & L.M. Nowak, manuscript in preparation). The receptor is the flip variant, and has a G in the R/G editing site. The cells were cultured in Dulbecco's Modified Eagle's Medium (DMEM) containing 10% fetal bovine serum (FBS), 1% penicillin-streptomycin and 1 µg/mL blasticidin, pH 7.4. The addition of the antibiotic, blasticidin, in the culture media selects for the growth of cells that express GluA3 channels. Cells are passaged every 3-4 days and used within 48 hours after passage. All cultures were maintained in a 37°C incubator with 5% CO_2.

Acquisition of Single Channel Currents

All experiments were performed at room temperature (~23°C). Pipettes were pulled from thick walled borosilicate glass with filament (Sutter Instrument Company, Novato, CA, USA) to a resistance of 15-20 MΩ and firepolished. Solutions were buffered at pH 7.4 and filtered using a 2 μM sterile filtering system (Corning, Lowell, MA). The bath buffer was a 1X Dulbecco's phosphate saline buffer with Mg^{2+} only (Invitrogen, Carlsbad, CA). The pipette solution contained (in mM): 150 NaCl, 10 Hepes/NaOH, 2 KCl. Stock solutions of nitrowillardiine or chlorowillardiine (NO_2W; ClW; Tocris Bioscience, Ellisville, MO, or Ascent Scientific, Princeton, NJ) were made from the pipette solution and kept frozen in aliquots at -20°C until the day of the experiment. Cyclothiazide (CTZ; Tocris Bioscience, Ellisville, MO, or Ascent Scientific, Princeton, NJ) was dissolved in methanol, frozen as 50 mM stock solutions, and was added (100-150 μM) to all agonist containing pipette solutions.

Single channel currents were amplified at a gain of 100 mV/pA with an EPC-7 amplifier, low pass filtered to 10 kHz using an external 8-pole Bessel filter, and digitized at 20 kHz using pClamp 7 software (Molecular Devices, Sunnyvale, CA). Single channel currents were recorded for 2 to 10 minutes in the cell-attached mode with pipette holding potentials of +80 to +120 mV. Data were converted from abf to qdf format on QuB software (www.qub.buffalo.edu) for analysis.

Analysis of Single Channel Data

All data were initially idealized at a dead time of 150 μs using the segmental-k-means (SKM) algorithm (9) to an initial simple linear model, C↔O1↔O2↔O3 (Figure 3.1A), consisting of one closed and three open classes starting with all rates set to 100 s^{-1}. The data were analyzed with or without an additional 5 kHz filtering (effective filter of 4.5 kHz). A dead time of 200 μs was imposed on patches that had

additional filtering. Maximum interval likelihood (MIL) analysis (10) was applied on this initial model to determine the fit to the dwell time histograms. States were then added one at a time to each closed and open class, re-idealized, refitted using MIL, and retained if the fits to the histograms improved and/or if the LL units increased by >10 LL units. If the addition of a state increased the LL by 10, but the rates to the new state were either close to zero or unrealistically large, then the additional state was omitted. This process was repeated again with rates starting at 10 s^{-1} to confirm that the final model and final rates were not affected by the starting values. Similar to our previous findings, our final model consists of three closed states and two open states in each of the open conductance levels. Loops that additionally connected closed states to the intermediate or large conductance levels in the model were tested, but in most cases worsened the fit to the dwell time histograms and/or gave unrealistic rates, so loops were not considered in our final model. Based on the transition matrices (not shown), transitions between the closed and the intermediate or large conductance levels were infrequently observed. Therefore, the final model does not include these transitions. Data were further segmented into modes based on the closed probability. Patches with long closures were modeled to four or five closed states. The critical time (t_{crit}), which describes the minimum closed duration between two bursts, was used to discard long closures. The newly separated clusters were re-idealized to one closed and three open conductance classes to determine the closed and open probabilities of each segment. The segments were then sorted into modes using an X means algorithm in QuB (11). The sorted modes were analyzed individually using the model described above. In a few records having only three closed states and one mode, the model in Figure 3.1B was applied to the entire record. The dwell times of similar modes were averaged, but each mode was modeled separately. Table 3.1 summarizes each record analyzed, indicating which were segmented into modes and which were analyzed as a

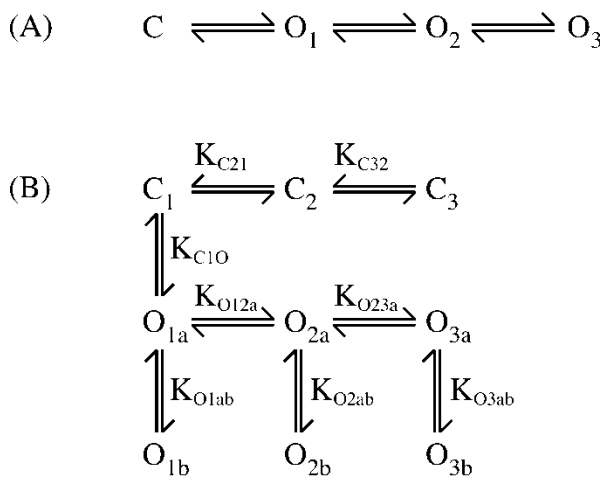

Figure 3.1

(A) Initial kinetic model used as a starting point but found not to describe the data adequately. **(B)** Final kinetic model. The notation for the equilibrium is as follows: $K_{C21} = k_{C2\to C1}/k_{C1\to C2}$, $K_{O12a} = k_{O1a\to O2a}/k_{O2a\to O1a}$, $K_{O1ab} = k_{O1a\to O1b}/k_{O1b\to O1a}$, etc.

Table 3.1

Summary of Single Channel Records

Each record is shown as one row in the table. The concentration of agonist is given in the left column and the total length of the record in the second column. The total time in each of the modes is given in the next five columns, with the total time between bursts in the column on the far right. All times are in seconds and rounded to 10 ms. Records for which no entry is given in the interburst column had only three closed times and were analyzed without segmentation.

(Continued)

[NO2W] μM	Total Length (s)	VH (s)	H (s)	M (s)	L (s)	VL (s)	Interburst (s)
1000	166.866	52.625	84.0582	12.0505		2.1706	13.646
	246.072						19.781
500	578.91		69.21	59.80	31.14		390.12
	249.64	96.30					109.64
	179.33		161.09				14.20
	286.83		88.86	91.76	4.68		101.53
	335.99		85.54	66.14	32.71	16.17	135.44
	190.74	190.74					
	180.82	180.82					
100	126.03	126.03					
	279.21	163.14	41.89	32.45	9.55	6.15	26.04
	61.94		61.94				
	31.52	30.81					0.71
	139.66		139.66				
	94.94			94.94			
	84.88	83.31					1.56
	352.86	124.95	96.60		3.91		127.40
	71.20		69.87				
	162.27	162.27					
50	98.53		98.53				
	45.60				27.64		17.96
	33.25		33.25				
	244.59		244.59				
	335.77		335.77				
	622.42	134.74	93.00	17.11	12.30	19.35	342.55

(Continued)

[ClW] μM	Total Length (s)	VH (s)	H (s)	M (s)	L (s)	VL (s)	Interburst (s)
1000	73.92	73.92					
	40.46	40.46					
	233.43	91.14	57.00	55.56		9.14	18.32
500	181.72		110.82	16.29			54.10
	149.12	149.12					
	140.34		140.34				
	233.93	214.54	12.45				6.81
	127.88	127.88					
	85.44	85.44					
	319.83	319.83					
	115.30	115.30					
100	771.80		512.52	146.04	39.47	20.22	53.49
	615.78			153.29	215.48	74.45	172.56
	356.40	143.65	93.96		11.83	35.93	68.06
	172.16		167.81				4.35
	122.69	110.84			6.94		4.90
50	366.77					335.14	31.64
	157.64					150.07	
	60.43		60.43				
	360.90		224.04		32.64	34.00	
	643.51		224.57		102.40	28.42	271.53
	217.07	217.07					
	540.87	540.87					

whole. Because the number of events in each group was necessarily less than the total number of events in the record, the LL was normalized to the number of events (LL/event) and each group was compared to the whole record. Five distinct modes were observed. For a more detailed description of the single channel analysis methods, refer to (8).

Protein Preparation and Purification

GluA2 S1S2 consists of residues N392 - K506 and P632 - S775 of the full rat $GluA2_o$ subunit (12), a 'GA' segment at the N-terminus, and a 'GT' linker connecting K506 and P632 (*12*). A similar construct of GluA3 S1S2 was prepared as described previously (13). pET-22b(+) plasmids were transformed in *E. coli* strain Origami B (DE3) cells and were grown at 37˚C to OD600 of 0.9 to 1.0 in LB medium supplemented with the antibiotics (ampicillin and kanamycin). The cultures were cooled to 20˚C for 20 min. and isopropyl-β-D-thiogalactoside (IPTG) was added to a final concentration of 0.5 mM. Cultures were allowed to grow at 20˚C for 20 h. The cells were then pelleted and the S1S2 protein purified using a Ni-NTA column, followed by a sizing column (Superose 12, XK 26/100), and finally an HT-SP-ion exchange-Sepharose column (Amersham Pharmacia). Glutamate (1 mM) was maintained in all buffers throughout purification. After the last column, the protein was concentrated and stored in 20 mM sodium acetate, 1 mM sodium azide, and 10 mM glutamate at pH 5.5.

Crystallography

For crystallization trials, the ligand was exchanged by successive dilution and concentration, and the protein was subsequently concentrated to 0.2 - 0.5 mM using a Centricon 10 centrifugal filter (Millipore, Bedford, MA). Crystals were grown at 4˚C

using the hanging drop technique, and the drops contained a 1:1 (*v*/*v*) ratio of protein solution to reservoir solution. The reservoir solution contained 14-15% PEG 8K, 0.1 M sodium cacodylate, 0.1-0.15 M zinc acetate, and 0.25 M ammonium sulfate, pH 6.5. The final concentrations of agonists were: FW, 2 mM; NO_2W, 2 mM; and ClW, 2 mM.

Data were collected at the Cornell High Energy Synchrotron Source beam line A1 using a Quantum-210 Area Detector Systems charge-coupled device detector. Data sets were indexed and scaled with HKL-2000 (14). Structures were solved with molecular replacement using Phenix (15). Refinement was performed with Phenix (15), and Coot 0.6.1 (16) was used for model building.

3.4 Results

Structures of GluA2 and GluA3 bound to FW, NO_2W and ClW

Lobe closure variability: The GluA3 and GluA2 LBD structures when bound to various agonists are quite similar, with small differences (Figure 3.2A). FW bound GluA3 (2.5 Å resolution) is 2.6˚ degree more open relative to glutamate (3DP6, B protomer, glutamate bound to GluA3, (17)). The structure of the GluA2 LBD bound to FW has been reported previously (18) and is overall very similar to the GluA3 LBD structure reported here. The FW bound GluA2 structure is 4˚ more open relative to glutamate.

Despite the fact that the nitro substituent of NO_2W is larger than the fluorine on FW, two of the three copies in the asymmetric unit for NO_2W bound to GluA2 LBD (1.78 Å resolution) are more closed than observed for FW bound to either GluA2 or GluA3 LBD. In fact, defined by the distribution of lobe orientations of GluA2 bound to glutamate (0.53˚ and 1.75˚ relative to the most closed copy; 3DP6, C and A protomers, respectively), two of the three copies of NO_2W are fully closed. The most

Figure 3.2 (continued) ***D655/S656 peptide conformation.*** **(A)** GluA2 LBD bound to NO_2W. **(B)** FW bound to GluA3 LBD. The D655/S656 is in the flipped conformation; however, an additional water is mediating a hydrogen bonding network to the backbone carbonyls of D655 and S656, the backbone amides of G453 and Y452, and the sidechain hydroxyl of S656. **(C)** ClW bound to GluA3 LBD. The D655/S656 is in the flipped conformation; however, an acetate molecule is present which forms an interlobe H-bond with the backbone carbonyls of D655 and K451, as well as three water molecules which joins the carbonyl of S656 to the amides of both Y452 and G453. **(D)** ClW bound to GluA2 LBD. The D655/S656 is in the unflipped conformation. **(E)** NO_2W bound to GluA2 LBD. The D655/S656 is in the appropriate position to form hydrogen bonds to G453 and Y452. **(F)** NO_2W bound to GluA2 LBD. The D655/S656 is in the unflipped conformation. For both ClW and NO_2W, the sidechain of D655 (D651 GluA2 equivalent) forms a salt bridge with K660 (K656 GluA2 equivalent). (All residues in the figure are numbered according to its respective subunit; all residues in legend are GluA3 numbering unless specified.)

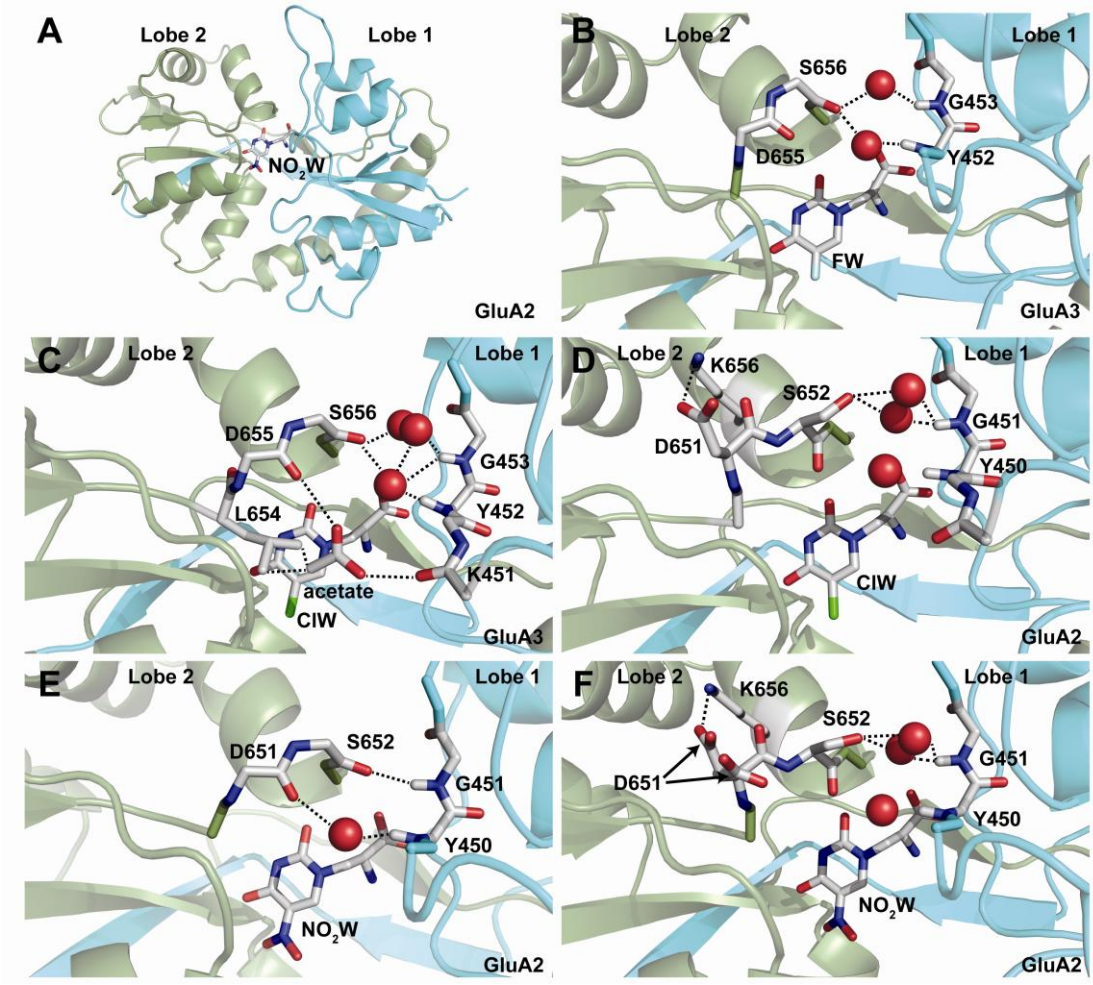
A
Lobe 2
Lobe 1
NO2W
GluA2
B
Lobe 2
Lobe 1
S656
G453
D655
Y452
FW
GluA3
C
Lobe 2
Lobe 1
S656
D655
G453
L654
Y452
K451
acetate
ClW
GluA3
D
Lobe 2
K656
Lobe 1
S652
G451
D651
Y450
ClW
GluA2
E
Lobe 2
Lobe 1
D651
S652
G451
Y450
NO2W
GluA2
F
Lobe 2
K656
Lobe 1
S652
G451
D651
Y450
NO2W
GluA2

striking aspect of the NO_2W structure is the variation observed. The range of lobe opening relative to the most closed glutamate-bound structure is more than 3˚ (0.68˚, 1.5˚, and 3.9˚; average 2.0˚ ± 1.7˚).

The structures of ClW bound to the LBDs of GluA2 and GluA3 were determined to 1.7 and 2.0, Å, respectively. Despite the somewhat smaller size of the chloride moiety, the average lobe opening relative to the most closed glutamate-bound form of GluA3 for ClW bound to GluA2 LBD (4.1˚, 2.4˚, 2.2˚; average 2.9˚ ± 1.0˚) is larger than NO_2W bound to GluA2 LBD, but the distributions overlap. The lobe opening for GluA3 LBD bound to ClW (3.7˚; one copy per asymmetric unit) is within the range observed for GluA2.

D655/S656 peptide conformation: The flipped conformation of the D655/S656 (all subsequent residues are given in GluA3 numbering), which is typically seen in full agonist structures, allows the formation of two H-bonds across the lobe interface: the carbonyl of S656 (Lobe 2) forms an H-bond with the amide of G453 (Lobe 1) and the carbonyl of D655 forms a water-mediated H-bond with the amide of Y452. This conformation has been correlated to modal behaviors; that is, the formation of these hydrogen bonds allows the channel to stably open for long periods of time, resulting in very high modes of activation in full ligand bound receptors (8). The FW bound GluA3 LBD structure reveals the D655/S656 peptide bond is in the flipped conformation (Figure 3.2B). Although this conformation has not been crystallographically observed for the GluA2 LBD bound to FW, residual dipolar coupling measurements using NMR spectroscopy (19) suggested that FW-bound GluA2 can also assume a flipped conformation for the D655/S656 peptide bond. In the case of FW bound to GluA3, the lobes are slightly more separated than glutamate so that the water-mediated D655-Y452 H-bond is maintained but the direct H-bond between S656 and G453 cannot be formed. Instead, an additional water molecule sits

in the pocket forming an H-bonding network that includes the backbone carbonyls of D655 and S656, the backbone amides of G453 and Y452, and the sidechain hydroxyl of S656 (Figure 3.2B). This may result in additional stability in this partially open form of the LBD.

The GluA3 LBD structure bound to ClW exhibits several interesting features (Figure 3.2C, D). Unlike other structures that are not fully closed but similar to the FW GluA3 LBD structure, the D655/S656 peptide bond is in the flipped conformation. The question then is whether the H-bonds typical of the flipped conformation are formed. The carbonyl of D655 probably does not participate in H-bond with the amide of Y452, although the water molecule is in the appropriate position. However, an acetate molecule is present in the cleft that forms an interlobe H-bond with the backbone carbonyls of D655 and K451 (Figure 3.2C). Also, the carbonyl of S656 is not sufficiently close to the amide of G453 to make a direct H-bond. However, an H-bonding network involving three water molecules joins the carbonyl of S656 to the amides of both Y452 and G453 (Figure 3.2C). This seems to suggest that a semi-stable partially open, flipped conformation exists. In contrast, all three structures of GluA2 LBD bound to ClW are in the unflipped conformation; however, in two of the three structures, the three water molecules are in similar positions (Figure 3.2D). The sidechain of S656 (S652 in GluA2) is rotated to form a water-mediated H-bond with G453. In all three copies, both the backbone carbonyl and the sidechain of D655 interact with K660 (Figure 3.2D).

NO_2W bound to GluA2 differs in each copy. In the most closed copy, the D655/S656 peptide bond is in the flipped conformation (Figure 3.2E). For the other two, the bond is not flipped, and two conformations of the sidechain of D655 are apparent (Figure 3.2F). The sidechain of D655 can form a salt bridge with the sidechain of K660. This is seen in the conformer with the flipped peptide bond, but

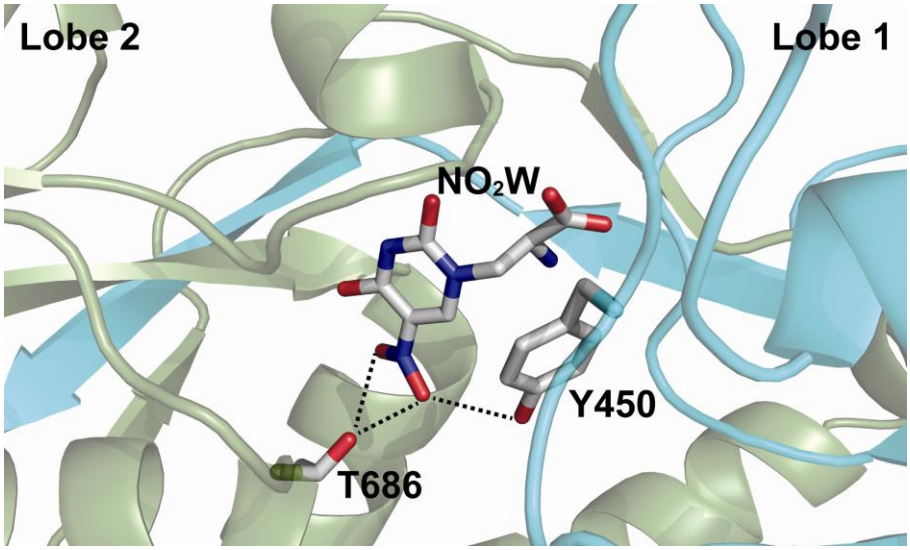

Figure 3.3

The nitro group of NO_2W bound to GluA2 contributes to stability by making additional H-bonds to T686 and Y450 (GluA2 numbering; T690 and Y452 GluA3 equivalent).

only one of the two conformations of the D655 sidechain can form this salt bridge in the two unflipped structures. In the case of the unflipped structure, the sidechain of K660 can interact with both the sidechain and backbone carbonyl of D655 (Figure 3.2F). However, in the flipped form, the carbonyl of D655 forms an interlobe H-bond with Y452, so that only the D655 sidechain is available for this interaction. In addition, the nitro group of NO_2W contributes interactions that may stabilize the closed lobe conformation; NO_2W can H-bond with the sidechain of T690 and the sidechain hydroxyl of Y452 (Figure 3.3).

Although these structures capture either the flip or unflipped conformations, it is very likely that both of these states are visited in solution. Based on the structures reported here, it seems the flip conformation of the D655/S656 peptides can exist in partially closed LBD structures and is stabilized by water molecules occupying the partially open space. NMR results (20) suggest the GluA2 LBD exhibits an equilibrium between the flipped and unflipped conformations, which means either form could be crystallized. The differences in this flip region between GluA2 and GluA3 are unlikely to be functional differences but rather both conformations are most likely present in both subtypes.

Met 712 sidechain conformation: M712 has been seen to adopt different conformations depending on the agonist that is bound (2, 18, 21). In glutamate bound and FW bound GluA2 and GluA3 structures, M712 is in an extended conformation. For NO_2W, comparison of the structure with that of the FW-bound and glutamate-bound GluA2 and GluA3 structures indicates that the larger size of NO_2W is accommodated by a change in the rotameric state of M712 at the β carbon and the exclusion of one water molecule (relative to the glutamate bound form) from the binding pocket (Figure 3.4A). This places the sidechain in a position that is

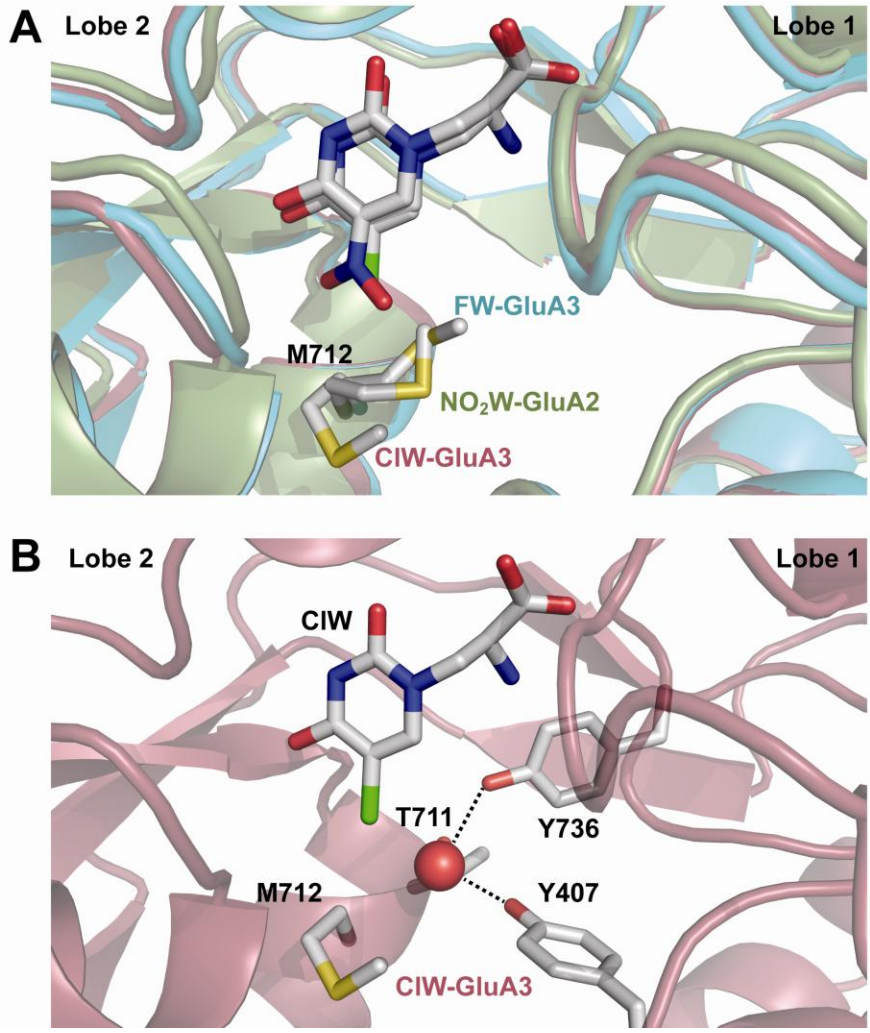

Figure 3.4

Conformation of the sidechain of M712. The sidechain of M712 is in an extended state when bound to FW. There is a rotomeric change at the β carbon when bound to NO_2W. The rotameric change is most dramatic with ClW bound.

intermediate between the glutamate-bound form and the form reported previously for BrW and IW (18)).

The rotamer of the sidechain of M712 in the ClW bound GluA3 LBD structure is similar to willardiine partial agonists such as BrW and IW. However, in the structure of GluA2 bound to ClW, two of the protomers have a conformation of M712 similar to that of the NO_2W structure and one has density corresponding to both the NO_2W conformation and that similar to the conformation seen with ClW bound to GluA3. In the case of GluA3 ClW, the rotation of the sidechain allows an additional water molecule to enter the binding pocket to interact with the sidechain hydroxyls of Y407 and Y736 (Figure 3.4B).

Single Channel Behavior of GluA3 Activated by NO_2W and ClW

NO_2W and ClW activate GluA3 channels in the same manner as glutamate and FW: The willardiine family of partial agonists shares the same structure but differ in the substituent in the 5-position and produces a graded level of whole-cell activation based on the size and electronegativity of the substituent. The electronegativity seems to affect ligand potency while the size seems to affect efficacy (22). The trend for efficacy of the willardiine compounds in whole cell studies is FW > NO_2W > ClW (22). Interestingly, our single channel studies show the willardiine compounds can all activate the homomeric GluA3 receptor to three similar conductance levels. Figure 3.5A is a 500 ms representative trace of 100 μM NO_2W. Figure 3.5B and C are amplitude histograms of 500 μM NO_2W and 500 μM ClW activating in a Very High mode. Similar to our previous findings with glutamate and FW (8), NO_2W and ClW activate GluA3 channels to three open conductance levels with conductances of: 15.6 ± 0.74, 28.8 ± 1.59, 40.4 ± 1.39 pS NO_2W (n=3); 14.5 ± 0.99, 22 ± 4, 38 ± 3 pS ClW

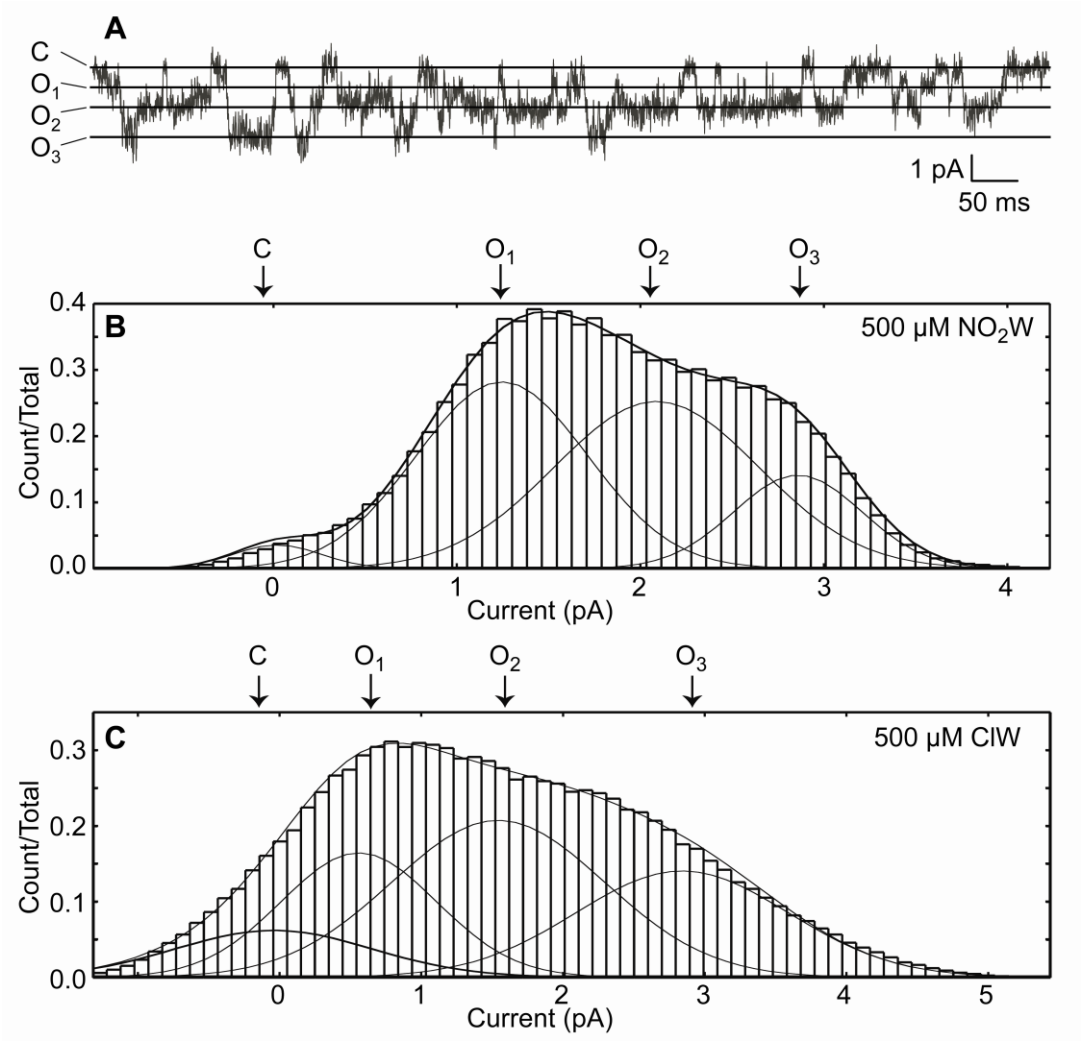

Figure 3.5

GluA3 channels have three conductance levels. **(A)** A 500 ms representative segment of a GluA3 channel activated by 100 μM NO_2W opens to three different conductance levels. **(B, C)** Amplitude histograms for an entire record obtained with 500 μM NO_2W at 100 mV **(B)** and 500 μM ClW at 80 mV **(C)**. For both the NO_2W and ClW records shown, the channel exhibited VH mode.

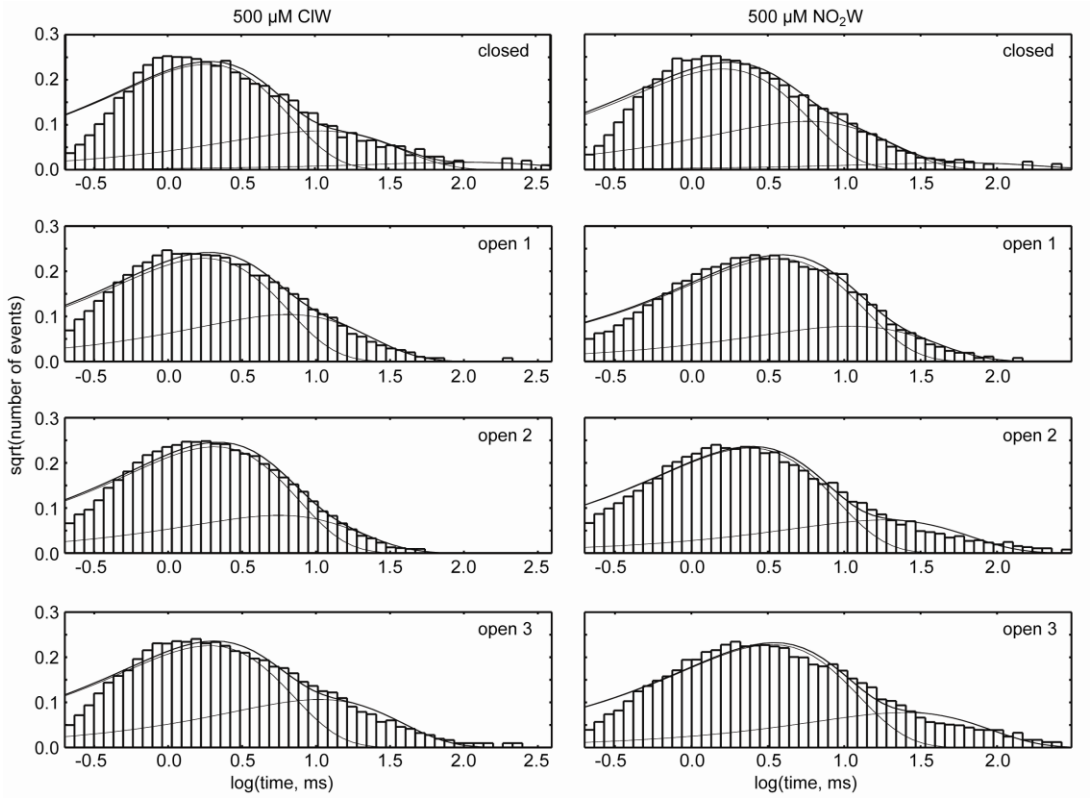

Figure 3.6

Dwell time histogram for the same records used to generate Figure 5 B and C.

(n=2) (refer to (8) for example of IV curve). The population in each conductance level is very similar for both agonists. The channel is activated largely to the small and intermediate conductance levels by NO_2W and ClW (P_C, P_{O1}, P_{O2}, P_{O3}, for these two patches are: 9%, 38%, 34%, 20%, for NO_2W and 11%, 29%, 36%, 24% for ClW).

The data also fit well to the simple model created from studies with glutamate and FW. Figure 3.6 shows dwell time histograms for the 500 μM NO_2W and ClW data. The closed histogram consists of three exponentials and the open histograms consist of two exponentials, consistent with our previous findings with glutamate and FW. Based on state transition matrices (Table 3.2), the channel when bound to NO_2W and ClW preferentially transitions between adjacent conductance levels. These results suggest the mechanism of activation is the same for both glutamate and the willardiines.

The probability in each conductance level for each agonist was averaged for the VH mode (see (8) and next section for a description of modal behaviors) to obtain a more global comparison of the occupancy in each conductance level for glutamate, FW, NO_2W and ClW (Table 3.3). All three willardiines have very similar open probabilities in all conductance levels with small subtle differences. FW and glutamate populate the highest conductance level to a greater extent than ClW and NO_2W, with glutamate being greater than all the willardiines. NO_2W and ClW both spend a similar percentage of time in the largest conductance level. The population in the intermediate conductance level is higher for FW than NO_2W. The rank order of the population of the largest conductance level is: ClW $\leq$ NO_2W $\leq$ FW < glutamate. The slightly higher efficacy of FW compared to NO_2W seems to be caused by a higher open probability in O_2. These findings correlate well with the efficacy measured in whole cell recordings and also suggests the difference in lowered efficacy of partial agonists in whole cell

Table 3.2

State transition matrices showing the percentage of transitions between each conductance level. Transitions between adjacent states are far more frequent than transitions between nonadjacent states. This constrains the model shown in Figure 3.1 such that transitions between closed states and O_2, between closed states and O_3, and between O_1 and O_3 are not included.

500 μM ClW	C	O_1	O_2	O_3
C		8.95	1.13	0.04
O_1	8.70		25.20	0.53
O_2	1.37	24.81		14.36
O_3	0.05	0.66	14.21	

500 μM NO_2W	C	O_1	O_2	O_3
C		7.99	0.41	0.01
O_1	8.22		25.14	1.24
O_2	0.19	25.64		14.96
O_3	0.00	0.97	15.23	

Table 3.3

The averaged probability of the GluA3 channel visiting each conductance level in the VH mode for glutamate, FW, NO_2W and ClW (n=3 for each agonist).

	5 mM glutamate	200 μM FW	500 μM NO2W	500 μM ClW
P_C	6% ± 3	9% ± 1	12 ± 3%	13 ± 2%
P_{O1}	6% ± 3	22% ± 5	37 ± 5%	31 ± 3%
P_{O2}	51% ± 6	47% ± 2	33 ± 4%	42 ± 3%
P_{O3}	36% ± 12	22% ± 7	17 ± 2%	14 ± 4%

Table 3.4

Efficacy Factors for Modes

The efficacy factor (p) was calculated as described in (Poon et al, 2010) based on conductance histograms for records separated into modes. The concentrations used range from 50 to 1000 μM of ClW and NO_2W. The efficacy factor is synonymous with the probability of success in a binomial distribution. The higher the value, the more likely a gate will be open.

	ClW	NO_2W
VH	0.63 ± 0.02	0.64 ± 0.02
H	0.55 ± 0.02 (0.30 ± 0.02)	0.55 ± 0.01
M	0.43 ± 0.002	0.29 ± 0.03
L	0.25 ± 0.03	0.19 ± 0.004
VL	0.24 ± 0.07	0.08 ± 0.01

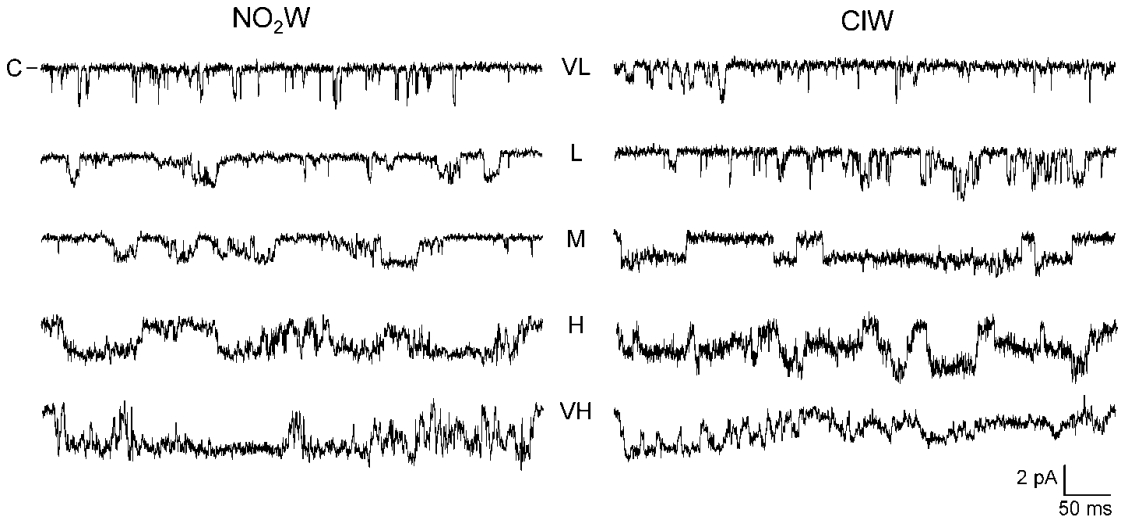

Figure 3.7

Representative 500 ms segments of single channel records showing modal behaviors for 50 μM ClW (VL), 100 μM ClW (L, M, H), 500 μM ClW (VH), and 50 μM NO_2W (VL, L), 100 μM NO_2W (M, H), 500 μM NO_2W (VH). The traces are additionally filtered at 1 kHz for viewing purposes.

studies is attributed to the differences in open probability in each of the conductance levels.

NO_2W and ClW induce modal behaviors: Modal gating of AMPA receptors has been previously described in detail for GluA3 bound to FW or glutamate and has been correlated to hydrogen bonding of the peptide flip conformation of D655 and S656 to Y452 and G453 (8). We tested if modal gating could also be observed for the lower efficacy partial agonists, NO_2W and ClW. The single channel data acquired with NO_2W and ClW were analyzed as described previously for glutamate and FW (8). Patches with long closures were segmented according to the t_{crit} (values ranging from: 1000 μM, 79 ms; 500 μM, 82 -226 ms; 100 μM, 49-170 ms; 50 μM, 50-280 ms for ClW; 1000 μM, 78ms; 500 μM, 127-295 ms; 100 μM, 81-180 ms; 50 μM, 131-169 ms for NO_2W) and sorted into the closest P_C distribution using the X means method (11). These sorted segments were then reanalyzed using the model in Figure 3.1B. Like glutamate and FW, NO_2W and ClW also exhibited five modes of behavior (Figure 3.7). The five modes are represented by P_O (where $P_O = 1 - P_C$) of: 80-100%, 60-79%, 40-59%, 20-39%, and <20%, (which correspond to Very High (VH), High (H), Medium (M), Low (L) and Very Low (VL) modes). Patches were also recorded in which a specific mode of activity was retained throughout the record, independent of agonist concentration. The kinetic data acquired from these patches were averaged with other similar P_O modes of behavior. The values for each patch and mode are given in Table 3.1. Interestingly, the LBD structures reported here show both flipped and unflipped conformations of the D655/S656 peptide region and either conformation can be visited in solution for NO_2W and ClW (19). The modal behaviors reported here for NO_2W and ClW were similar to those reported for FW and thus may also be correlated to the H-bonding of this flip region.

ClW and NO_2W, similar to FW and glutamate, also follow a binomial distribution, which is referred to as an 'efficacy factor' (Table 3.4). The efficacy factors remain constant for a given mode regardless of concentration, and are similar for ClW and NO_2W. The exceptions are the M, L and VL modes for NO_2W. This is likely due to the small sampling size of those modes for NO_2W; in comparison to ClW, most of the M, L and VL activity for NO_2W are short in duration (Table 3.1). The efficacy compared to FW and glutamate (0.66 ± 0.02, 0.60 ± 0.02, 0.45 ± 0.05, 0.26 ± 0.1 0.24 ± 0.08 for FW; 0.73 ± 0.04, 0.71 ± 0.05, 0.59 ± 0.08, 0.42 ± 0.05, 0.42 ± 0.11 for glutamate; VH, H, M, L, VL respectively) is lower for ClW and NO_2W. This also follows the trend for efficacy in whole cell mode.

The equilibrium constants also show differences among modes. The K_{eq} for both ClW and NO_2W favor channel opening to the smallest conductance level in all modes with the exception of L and VL modes (Table 3.6). Interestingly, at the VH mode, the K_{eq} for ClW is actually greater than one from the smallest to the intermediate conductance level. This is in contrast to NO_2W, in which the majority of the K_{eq} from O_1 to O_2 are less than one (K_{eq} is a forward equilibrium constant so that a value greater than one indicates a relatively greater population of O_2 than O_1). For both agonists, the forward K_{eq} dramatically decreases when the channel transitions from O_2 to O_3. As the modal behavior descends in activity, the K_{eq} also decreases.

ClW exhibits an alternative kinetic behaviors at lower concentrations of agonist: ClW activity generally follows the same modal pattern as glutamate; however, an anomaly was detected at lower concentrations of agonist. Table 3.5 highlights the P_O of ClW acquired at 50 μM ClW activating in H mode. In the H mode, ClW seems to exhibit two populations of activity; one with a high P_o in the largest conductance level

Table 3.5

Patches which exhibited an alternative kinetic behaviors when bound with either ClW, FW or NO_2W in the High mode of activation. The sub-modes are in italics or bold.

μM ClW	C	P_{O1}	P_{O2}	P_{O3}
100	31%	32%	26%	11%
	27%	32%	28%	13%
	32%	**55%**	**13%**	**0.17%**
50	24%	28%	35%	13%
	26%	36%	28%	10%
	33%	**47%**	**19%**	**0.96%**
	37%	**49%**	**14%**	**0.39%**
	35%	**49%**	**16%**	**0.67%**
μM FW	C	P_{O1}	P_{O2}	P_{O3}
10	29%	25%	29%	17%
	30%	23%	30%	17%
	31%	28%	29%	12%
	36%	40%	19%	5%
	27%	49%	21%	3%
μM NO_2W	C	P_{O1}	P_{O2}	P_{O3}
100	26%	36%	27%	12%
	22%	34%	32%	12%
	20%	34%	34%	12%
	31%	31%	27%	11%
	24%	25%	37%	14%
	31%	37%	26%	6%
50	23%	38%	28%	12%
	34%	30%	25%	10%
	32%	39%	22%	7%
	38%	32%	24%	6%
	27%	39%	26%	8%

Table 3.6 *NO_2W*

Equilibrium constants as defined in Figure 1 were calculated using NO_2W and ClW as the agonist. All constants are unitless.

Conc. (μM)	Mode	K_{C32}	K_{C31}	K_{C1O}	K_{O1ab}	K_{O12a}	K_{O2ab}	K_{O23a}	K_{O3ab}
1000	VH	1.86 ± 1.32	2.16 ± 1.52	5.72 ± 4.04	0.12 ± 0.09	0.83 ± 0.59	0.20 ± 0.14	0.27 ± 0.19	0.24 ± 0.17
	H	2.962	2.032	1.989	0.1712	0.4829	0.1052	0.1733	0.3434
500	VH	3.66	4.97 ± 1.67	7.71 ± 2.61	0.21 ± 0.08	0.65 ± 0.04	0.35 ± 0.11	0.55 ± 0.02	0.52 ± 0
	H	5.37 ± 3.9	1.76 ± 0.08	2.14 ± 0.20	0.25 ± 0.05	0.87 ± 0.14	0.37 ± 0.18	0.27 ± 0.02	0.39 ± 0.05
	M	13.23 ± 11	1.64 ± 0.29	1.22 ± 0.04	0.18 ± 0.04	0.31 ± 0.05	0.20 ± 0.04	0.18 ± 0.04	0.33 ± 0.02
	L	2.16	1.17 ± 0.04	0.67 ± 0.02	0.13 ± 0.04	0.15 ± 0.005	0.21 ± 0.12	0.16 ± 0.01	0.23 ± 0.03
100	VH	4.03 ± 1.28	1.85 ± 0.28	3.26 ± 0.40	0.42 ± 0.07	1.51 ± 0.18	0.43 ± 0.10	0.49 ± 0.11	0.57 ± 0.13
	H	4.77 ± 1.39	1.73 ± 0.31	1.76 ± 0.11	0.30 ± 0.09	0.91 ± 0.05	0.31 ± 0.11	0.36 ± 0.06	0.34 ± 0.09
	M		1.77	1.02	0.26	0.18	0.24	0.11	0.21
50	VH	3.14	0.67	1.43	0.82	0.85	0.82	0.37	0.99
	H	3.24 ± 0.50	0.78 ± 0.08	2.42 ± 0.50	0.42 ± 0.08	0.82 ± 0.00	0.19 ± 0.04	0.30 ± 0.06	0.34 ± 0.12
	L	1.51	0.84	0.48	1.40	0.28	0.29	0.17	0.27

(continued) *ClW*

Conc. (μM)	Mode	K_{C32}	K_{C31}	K_{C10}	K_{O1ab}	K_{O12a}	K_{O2ab}	K_{O23a}	K_{O3ab}
1000	VH	1.87 ± 0.69	2.83 ± 0.23	2.44 ± 1.27	1.30 ± 0.98	4.42 ± 2.79	0.22 ± 0.06	0.25 ± 0.08	0.21 ± 0.12
	H	1.40	1.42	1.77	0.10	0.63	0.07	0.32	0.26
	M	1.99	1.06	1.02	0.14	0.49	0.08	0.32	0.24
500	VH	1.76 ± 0.37	1.87 ± 0.25	4.20 ± 0.60	0.23 ± 0.03	1.55 ± 0.21	0.11 ± 0.01	0.29 ± 0.08	0.32 ± 0.09
	H	1.56 ± 0.06	1.43 ± 0.05	2.45 ± 0.41	0.16 ± 0.07	0.65 ± 0.01	0.19 ± 0.05	0.15 ± 0.04	0.28 ± 0.08
100	VH	2.84 ± 0.86	2.79 ± 0.34	4.19 ± 0.51	0.36 ± 0.04	1.14 ± 0.14	0.28 ± 0.16	0.34 ± 0.14	0.37 ± 0.09
	H	3.30 ± 1.82	1.70 ± 0.21	2.02 ± 0.18	0.26 ± 0.09	0.66 ± 0.18	0.17 ± 0.02	0.25 ± 0.12	0.37 ± 0.04
	M	2.20 ± 0.5	1.21 ± 0.07	1.38 ± 0.06	0.16 ± 0.04	0.49 ± 0.01	0.13 ± 0.003	0.24 ± 0.003	0.35 ± 0.02
	L	1.60 ± 0.27	0.88 ± 0.09	0.99 ± 0.03	0.18 ± 0.04	0.27 ± 0.03	0.15 ± 0.02	0.13 ± 0.02	0.31 ± 0.01
	VL	1.47	0.75	0.47	0.18	0.14	0.21	0.10	0.39
50	H	10.9 ± 5.8	1.96 ± 0.24	1.92 ± 0.11	0.17 ± 0.04	0.57 ± 0.17	0.27 ± 0.07	0.14 ± 0.07	0.53 ± 0.21
	M	2.76	1.34	0.84	0.23	0.12	0.19	0.04	
	L	1.78	1.03	1.16	0.14	0.22	0.10	0.09	0.40
	VL	2.52 ± 0.71	1.10 ± 0.07	0.30 ± 0.11	0.19 ± 0.04	0.30 ± 0.15	0.06 ± 0.01	0.08 ± 0.04	0.31 ± 0.09

and another with a very low P_O in the largest conductance level. The possibility that other agonists also displayed this alternative kinetic behavior led to the decision to reanalyze the P_O's for glutamate, FW and NO_2W in the VH and H modes at lower concentrations. Interestingly, FW and NO_2W also presented this type of alternative kinetic behavior, but to a much smaller, less observable degree (Table 3.5). The alternative kinetic behavior was not present with glutamate. Two efficacy factors are given for ClW in H mode, arising from the two behaviors seen at lower concentration of agonist and having a lower efficacy.

NO_2W and FW have long dwell times: Similar to previous glutamate and FW results, the dwell times in the open states of all conductance levels measured with NO_2W and ClW are longer in the VH modes and shorten with a decrease in modal activity (Table 3.7). The longest dwell time (the second time constant, $\tau_{O1,2,3b}$)) in each of the conductance levels in the VH mode for NO_2W is much longer than those observed for glutamate and ClW. $\tau_{O1,2,3b}$ for NO_2W ranges from 10-30 ms for all three conductance levels. $\tau_{O1,2,3b}$ for ClW range from 2-12ms. Comparing this with previous findings (8); $\tau_{O1,2,3b}$ for glutamate, similar to ClW, ranges from 2-6 ms, whereas FW ranges from 5-28 ms. The order of $\tau_{O1,2,3b}$ in increasing length is: NO_2W > FW > ClW > glutamate.

Table 3.7

Exponential fits to the dwell time histograms for different concentrations of NO_2W and ClW separated by modes. The dwell times are averaged. The open probability (P_O) is $1 - P_C$. τ values are in ms.

(continued)

NO_2W

µM	Mode	τ_{C1} (Area)	τ_{C2} (Area)	τ_{C3} (Area)	τ_{O1a} (Area)	τ_{O1b} (Area)	τ_{O2a} (Area)	τ_{O2b} (Area)	τ_{O3a} (Area)	τ_{O3b} (Area)	Po (n)
		0.73 ± 0.25	3.13 ± 0.08	17.58 ± 4.36	2.18 ± 0.93		1.98 ± 0.80	5.97 ± 2.29	2.06 ± 0.84	8.65 ± 2.25	
1000	VH	(0.76 ± 0.10)	(0.22 ± 0.08)	(0.03 ± 0.01)	(0.94 ± 0.06)	3.53 (0.12)	(0.78 ± 0.12)	(0.21 ± 0.12)	(0.90 ± 0.003)	(0.10 ± 0.003)	87 ± 3.5%
	H	1.49 (0.81)	6.52 (0.17)	25.05 (0.03)	1.54 (0.87)	4.93 (0.13)	1.14 (0.92)	3.49 (0.08)	0.86 (0.87)	4.29 (0.13	69%
		1.45 ± 0.04	4.96 ± 0.43		3.18 ± 0.26	9.60 ± 0.62	1.97 ± 0.28	23.21 ± 6.36	2.69 ± 0.43	27.98 ± 4.81	91 ± 1%
500	VH	(0.83 ± 0.04)	(0.16 ± 0.04)	52.05 (0.004)	(0.79 ± 0.10)	(0.21 ± 0.10)	(0.94 ± 0.04)	(0.06 ± 0.04)	(0.92 ± 0.03)	(0.08 ± 0.03)	(2)
		1.29 ± 0.16	5.62 ± 0.55	31.7 ± 4.64	1.17 ± 0.08	4.41 ± 0.75	1.23 ± 0.19	7.73 ± 4.05	1.04 ± 0.16	5.17 ± 0.63	74 ± 3%
	H	(0.75 ± 0.01)	(0.21 ± 0.02)	(0.03 ± 0.01)	(0.8 ± 0.03)	(0.19 ± 0.03)	(0.84 ± 0.03)	(0.15 ± 0.03)	(0.83 ± 0.02)	(0.15 ± 0.02)	(5)
		1.54 ± 0.20	6.92 ± 1.28	29.77 ± 9.87	1.4 ± 0.16	4.31 ± 0.86	0.88 ± 0.18	3.04 ± 0.65	0.80 ± 0.17	3.85 ± 0.58	53 ± 1%
	M	(0.69 ± 0.01)	(0.27 ± 0.005)	(0.04 ± 0.01)	(0.82 ± 0.02)	(0.17 ± 0.02)	(0.84 ± 0.02)	(0.16 ± 0.03)	(0.83 ± 0.03)	(0.15 ± 0.03)	(3)
		2.09 ± 0.37	9.22 ± 0.21		1.48 ± 0.25	3.75 ± 0.91	0.78 ± 0.10	3.54 ± 1.23	0.72 ± 0.04	4.53 ± 2.32	32 ± 1%
	L	(0.56 ± 0.01)	(0.37 ± 0.08)	30.38 (0.14)	(0.82 ± 0.03)	(0.18 ± 0.03)	(0.90 ± 0.02)	(0.09 ± 0.02)	(0.84 ± 0.10)	(0.14 ± 0.10)	(2)
		1.54 ± 0.28	6.38 ± 0.90	22.17 ± 1.40	1.83 ± 0.51	10.18 ± 3.82	2.11 ± 0.56	12.91 ± 6.58	2.27 ± 0.57	15.95 ± 5.76	88 ± 2%
100	VH	(0.73 ± 0.02)	(0.22 ± 0.02)	(0.04 ± 0.01)	(0.77 ± 0.04)	(0.23 ± 0.04)	(0.72 ± 0.08)	(0.27 ± 0.08)	(0.81 ± 0.04)	(0.18 ± 0.05)	(6)
		1.91 ± 0.35	9.14 ± 1.78	39.32 ± 8.93	1.51 ± 0.31	6.13 ± 1.37	1.48 ± 0.34	4.13 ± 0.76	1.56 ± 0.12	6.68 ± 0.59	
	H	(0.72 ± 0.04)	(0.22 ± 0.02)	(0.04 ± 0.03)	(0.79 ± 0.06)	(0.21 ± 0.06)	(0.67 ± 0.07)	(0.32 ± 0.07)	(0.79 ± 0.05)	(0.19 ± 0.06)	73 ± 2 (5)
	M		7.20 (0.73)	33.9 (0.27)	4.0 (0.64)	11.14 (0.36	1.56 (0.87)	6.40 (0.13)	1.15 (0.94)	7.11 (0.06)	50% (1)
		2.37 ± 0.01	12.76 ± 0.77	39.74 ± 1.51	1.89 ± 0.24	9.42 ± 2.05	2.33 ± 0.03	10.82 ± 2.66	1.93 ± 0.14	9.87 ± 0.87	90 ± 2%
50	VH	(0.66 ± 0.14)	(0.24 ± 0.06)	(0.10 ± 0.07)	(0.71 ± 0.09)	(0.29 ± 0.09)	(0.78 ± 0.10)	(0.21 ± 0.10)	(0.71 ± 0.12)	(0.28 ± 0.12)	(2)
		1.70 ± 0.19	8.34 ± 1.43	29.77 ± 5.49	1.91 ± 0.20	7.36 ± 0.48	2.05 ± 0.22	6.18 ± 0.49	1.56 ± 0.25	7.41 ± 1.46	70 ± 3%
	H	(0.61 ± 0.04)	(0.26 ± 0.05)	(0.13 ± 0.05)	(0.66 ± 0.06)	(0.33 ± 0.06)	(0.80 ± 0.03)	(0.20 ± 0.03)	(0.83 ± 0.05)	(0.17 ± 0.05)	(4)
	L	2.31 (0.51	9.87 (0.29)	40.71 (0.18)	0.95 (0.76)	10.06 (0.23)	0.70 (0.83)	2.96 (0.16)	0.87 (0.85)	3.94 (0.13)	31% (1)

(continued)

ClW

μM	Mode	τ_{C1} (Area)	τ_{C2} (Area)	τ_{C3} (Area)	τ_{O1a} (Area)	τ_{O1b} (Area)	τ_{O2a} (Area)	τ_{O2b} (Area)	τ_{O3a} (Area)	τ_{O3b} (Area)	Po (n)
		0.88 ± 0.21	3.76 ± 0.80	24.68 ± 8.16	0.45 ± 0.20	1.94 ± 0.77	1.23 ± 0.20	3.75 ± 0.50	1.34 ± 0.42	4.97 ± 0.62	
1000	VH	(0.81 ± 0.01)	(0.13 ± 0.01)	(0.02 ± 0.00)	(0.49 ± 0.23)	(0.50 ± 0.24)	(0.64 ± 0.13)	(034 ± 0.13)	(0.87 ± 0.04)	(0.09 ± 0.04)	86 ± 3% (3)
	H	0.63 (0.64)	2.89 (0.27)	18.28 (0.04)	0.74 (0.90)	2.35 (0.08	0.62 (0.89)	1.70 (0.08)	0.61 (0.80)	2.53 (0.15)	68% (1)
	M	0.77 (0.55)	3.85 (0.34)	18.06 (0.06)	0.64 (0.87)	2.14 (0.12)	0.54 (0.86)	1.38 (0.11)	0.59 (0.80)	2.46 (0.13)	44% (1)
		0.91 ± 0.14	4.48 ± 0.57	35.58 ± 6.91	1.26 ± 0.15	4.80 ± 0.53	1.90 ± 0.26	4.74 ± 0.73	1.45 ± 0.19	7.08 ± 1.38	
500	VH	(0.78 ± 0.02)	(0.19 ± 0.02)	(0.02 ± 0.01)	(0.83 ± 0.05)	(0.17 ± 0.05)	(0.78 ± 0.06)	(0.21 ± 0.06)	(0.87 ± 0.02)	(0.13 ± 0.02	86 ± 2% (6)
		1.13 ± 0.23	5.47 ± 1.37	39.85 ± 13.79	1.72 ± 0.58	5.38 ± 1.95	1.88 ± 0.82	6.69 ± 3.28	0.96 ± 0.12	4.47 ± 0.62	
	H	(0.72 ± 0.01)	(0.24 ± 0.01)	(0.03 ± 0.01)	(0.85 ± 0.07)	(0.15 ± 0.07)	(0.86 ± 0.03)	(0.13 ± 0.03)	(0.86 ± 0.04)	(0.13 ± 0.04)	70 ± 2% (3)
		0.84 ± 0.10	3.24 ± 0.19	18.77 ± 3.62	1.66 ± 0.46	7.15 ± 2.22	2.29 ± 0.72	8.0 ± 1.16	2.40 ± 0.09	11.17 ± 1.41	
100	VH	(0.78 ± 0.01)	(0.20 ± 0.01)	(0.01 ± 0)	(0.81 ± 0.01)	(0.19 ± 0.01)	(0.82 ± 0.07)	(0.17 ± 0.07)	(0.84 ± 0.03)	(0.16 ± 0.02)	90 ± 0% (2)
		1.67 ± 0.65	6.60 ± 1.79	32.0 ± 0.23	1.43 ± 0.32	5.61 ± 1.28	1.06 ± 0.13	3.55 ± 0.54	1.23 ± 0.45	7.37 ± 3.43	
	H	(0.65 ± 0.06)	(0.30 ± 0.07)	(0.03 ± 0.01)	(0.83 ± 0.07)	(0.17 ± 0.07)	(0.86 ± 0.01)	(0.13 ± 0.02)	(0.83 ± 0.04)	(0.15 ± 0.04)	70 ± 1% (3)
		1.41 ± 0.33	7.07 ± 1.38	31.88 ± 0.30	1.22 ± 0.15	3.76 ± 0.55	0.95 ± 0.04	3.18 ± 0.02	1.01 ± 0.06	5.50 ± 0.08	
	M	(0.68 ± 0.02)	(0.26 ± 0.02)	(0.05 ± 0)	(0.85 ± 0.03)	(0.14 ± 0.03)	(0.90 ± 0.04)	(0.10 ± 0)	(0.86 ± 0.01)	(0.12 ± 0.02)	54 ± 4 (2)
		1.41 ± 0.30	7.52 ± 0.91	40.36 ± 4.79	1.32 ± 0.14	4.36 ± 0.19	1.11 ± 0.25	3.63 ± 0.81	1.05 ± 0.10	4.58 ± 0.19	
	L	(0.58 ± 0.04)	(0.33 ± 0.05)	(0.08 ± 0.02)	(0.84 ± 0.05)	(0.16 ± 0.05)	(0.87 ± 0.02)	(0.12 ± 0.02	(0.90 ± 0.05)	(0.13 ± 0.01)	34 ± 1% (3)
	VL	2.10 (0.45)	8.35 (0.28)	35.29 (0.26)	1.19 (0.76)	3.21 (0.24	0.77 (0.83)	2.60 (0.17)	1.23 (0.89)	8.46 (0.09)	16 (1)
		1.32 ± 0.17	5.46 ± 0.95	30.95 ± 8.27	1.83 ± 0.33	6.07 ± 1.99	1.68 ± 0.26	7.72 ± 2.04	0.91 ± 0.15	5.73 ± 1.54	
50	H	(0.67 ± 0.03)	(0.29 ± 0.02)	(0.04 ± 0.02)	(0.82 ± 0.03)	(0.18 ± 0.03)	(0.83 ± 0.05)	(0.16 ± 0.05)	(0.82 ± 0.04)	(0.17 ± 0.05)	69 ± 2% (5)
	L	1.41 ± 0.60	5.67 ± 0.31	18.4 ± 0.09	1.26 ± 0.76	3.76 ± 0.24	1.24 ± 0.87	4.55 ± 0.12	0.54 ± 0.99		36% (1)
		1.46 ± 0.32	6.46 ± 1.39	19.02 ± 2.81	0.53 ± 0.14	2.11 ± 0.71	0.72 ± 0.08	3.03 ± 0.74	0.63 ± 0.16	4.01 ± 0.60	
	VL	(0.31 ± 0.06)	(0.44 ± 0.04)	(0.22 ± 0.01)	(0.85 ± 0.04)	(0.15 ± 0.04)	(0.94 ± 0)	(0.04 ± 0.01)	(0.87 ± 0.05)	(0.11 ± 0.02)	15 ± 4% (3)

3.5 Discussion

Efficacy of partial agonists

The original hypothesis concerning the mechanism of partial agonism was that efficacy correlates with the degree of lobe closure (3). While this was consistent with the original data, more recent work has supported a model in which the stability of full lobe closure determines efficacy (4, 5), such that partial closures more likely represent intermediate states of low energy in the crystal. The evidence supporting the stability argument includes a demonstration that at least some partial agonists can exist in a wide range of lobe orientations (19) that are in equilibrium (13, 23, 20) and that even the lowest efficacy agonists can access a fully closed state (Ahmed, Wang, Chuang & Oswald, manuscript in preparation). The crystal structures presented here show that FW, ClW and NO_2W–bound LBD can access a range of lobe orientations, one of which was essentially fully closed. Furthermore, all structures show multiple side chain orientations near the lobe interface, suggesting that the LBD is not held in a fixed conformation but is in equilibrium between distinct states. This suggests the differences in conductance level population are less likely to be affected by the extent of lobe closure but rather other structural and dynamic differences within the LBD. The question is how often these states are visited for each agonist. The fact that GluA2 can be crystallized in the fully closed state when bound to NO_2W, may suggest that this state is of low energy. However, if this is the case, then why is the efficacy of FW, albeit to a small degree, greater than NO_2W yet the single channel open probabilities are very similar? There are three potential structural differences between the bound form of FW and that of NO_2W. These include (1) the orientation of M712, (2) the additional interactions with Lobe 2 by virtue of the nitro group in NO_2W, and (3) possible differences in H-bonding across the lobe interface.

Considering first the orientation of M712, the rotameric state for this sidechain in both the ClW and NO_2W structures of GluA2 differs from previous structures of full and partial agonists (3). The M712 sidechain rotates slightly around the β carbon and by about 60˚ around the γ carbon relative to the FW-bound structure, providing space for the nitro moiety in NO_2W. Although the functional significance of this change in rotameric state is difficult to assess, M712 is part of Helix I, which undergoes a bending motion when bound to weak partial agonists, such as IW (24). At the other end of Helix I, a disulfide bond connects Helix I to the C-terminal portion of the LBD, which in the intact protein is beginning of the linker to the M4 helix. The M4 helix of one subunit is actually associated with the ion channel gating region of an adjacent subunit (26) and this slight change in M712 could alter gating kinetics. In fact, mutations in the M4 segment in NMDA receptors alters function (25).

With RDC measurement using NMR spectroscopy, Maltsev et al. (2008) estimated the proportion of the flipped conformation of the D655/S656 peptide bond varies with agonist as follows: 0.54, 0.44, 0.46, 0.45, 0.28, and 0.29 for HW, FW, ClW, BrW, IW, and NO_2W, respectively. This would suggest that the D655/S656 bond would be in a position to form H-bonds more often for FW and ClW than NO_2W; however, as demonstrated by the GluA3 structures bound to FW and ClW, the flipped peptide bond does not always correspond to a fully closed lobe. It is possible that the additional contacts made by NO_2W in Lobe 2 (H-bonding to E705 and Y452) could stabilize lobe closure and compensate for the lower propensity to form a flipped conformation. Preliminary ITC studies (Romero B., unpublished results) do show that the binding of NO_2W is driven by enthalphy to a larger extent than FW and ClW, possibly suggesting the importance of additional contacts in the bound state.

Modal gating and the peptide flip conformation

Like glutamate and FW, activation of the channel by NO_2W and ClW exhibits five distinct modes of activation (VL, L, M, H, and VH). We previously postulated (8) that modal behavior could arise from locking a specified number of LBD's closed as a result of the flip of the D655/S656 peptide bond. This flipping results in the formation of two H-bonds between the carbonyl of S656 (Lobe 2) and the amide of G453 (Lobe 1), and between the carbonyl of D655 and the amide of Y452 through a water molecule. This H-bonding pattern is seen in one of three protomers of the structure of NO_2W bound to GluA2 LBD, similar to that reported for glutamate bound to the same construct (2). FW and ClW bound to GluA3 LBD show a variation on this H-bonding pattern. In both cases, the peptide bond is flipped in the context of lobes that are slightly open (about 3˚ relative to the glutamate structure that is the most closed), making the H-bonds difficult to form. However, additional water molecules enter the cleft (and, in one case, an acetate molecule) and mediate the H-bonds between the two lobes. These hybrid H-bonded conformations have not been previously reported for partial agonists and may result in subtle functional effects. One possibility is the sub-modes observed with ClW and to a lesser extent FW and NO_2W. If one assumes that the modes are set by the occupancy and H-bonding state as we suggested previously (8), the existence of this hybrid H-bonding state increases the number of possibilities. The fully closed, previously reported H-bonding pattern exists on the timescale of approximately 100 ms (23), suggesting that this stabilization is on the same timescale as modal gating. If the hybrid H-bonding states have the same stability as the fully closed pattern but actually are a conformation that does not permit channel activation, then the H and VH modes that are observed with extremely low probability for the largest conductance state may arise from a fully occupied tetramer with two to three subunits in the standard H-bonding conformation and one or two in the hybrid

conformation. In fact, ClW has three water molecules tethering this hybrid conformation whereas FW has only one water molecule and the single channel results show ClW has the greatest effect on inducing the alternative kinetic behavior than FW, with NO_2W being the least affected.

Dwell time variation between agonists

In the VH mode, NO_2W exhibits relatively long channel lifetimes in the large conductance state and the overall efficacy is slightly better than ClW. The size of the nitro group is larger than the chloro substituent, but the lobes are, on average, more closed for NO_2W and ClW. The fraction of bound NO_2W in the flipped conformation calculated from RDC measurements suggest NO_2W was 0.29 (similar to that of relatively low efficacy partial agonist, iodowillardiine); whereas, the fraction for ClW and FW was 0.46 and 0.44, respectively (19). However, the additional contacts of NO_2W to the sidechains of T690 and Y452 may help stabilize the fully closed state and may contribute to longer openings in each of the conductance levels. These interactions are not present in the other willardiine partial agonists and may compensate for the decreased population of the flipped conformation.

3.6 Conclusions

The structures of the willardiines bound to GluA2 and GluA3 LBD suggest full lobe closures are possible for partial agonists. Crystal structures of kainate bound to the LBD of a kainate receptor reveal 3° less closure than glutamate and yet kainate is a full agonist at kainate receptors (27), further implying crystal structures are only representative of a specific conformation that is in a low energy state and other conformations are possible. Partial agonists at NMDA receptors exhibit full lobe closures (28). Although NMDA receptors have very different activation kinetics (slow activation, long openings) compared to AMPA receptors, the mechanism leading to a

gating event may be conserved for all subtypes of glutamate receptors. Taken together with our results, these findings imply that agonist-induced activation of AMPA channels is not necessarily dependent on any specific attribute in the LBD but rather on the 'push and pull' of various factors, such as, agonist affinity, lobe closure, and interdomain contacts.

In summary, although the differences in single channel activity between FW, ClW and NO_2W are small, these small differences can multiply into large whole cell differences and have an impact on neuronal function. ClW and NO_2W show similar conductance levels, mechanism of activation, and modal behaviors as glutamate and FW. The small disparities in single function can be compared to specific structural dissimilarities and provide new insights into the range of channel activation.

REFERENCES

1. Dingledine, R., K. Borges, D. Bowie, and S.F. Traynelis. 1999. The glutamate receptor ion channels. *Pharmacol Rev.* 51:7-61.
2. Armstrong, N., and E. Gouaux. 2000. Mechanisms for activation and antagonism of an AMPA-sensitive glutamate receptor: crystal structures of the GluR2 ligand binding core. *Neuron.* 28:165-181.
3. Jin, R., T.G. Banke, M.L. Mayer, S.F. Traynelis, and E. Gouaux. 2003. Structural basis for partial agonist action at ionotropic glutamate receptors. *Nat Neurosci.* 6:803-810.
4. Zhang, W., Y. Cho, E. Lolis, and J.R. Howe. 2008. Structural and single-channel results indicate that the rates of ligand binding domain closing and opening directly impact AMPA receptor gating. *J Neurosci.* 28:932-943.
5. Robert, A., N. Armstrong, J.E. Gouaux, and J.R. Howe. 2005. AMPA receptor binding cleft mutations that alter affinity, efficacy, and recovery from desensitization. *J Neurosci.* 25:3752-3762.
6. Weston, M.C., C. Gertler, M.L. Mayer, and C. Rosenmund. 2006. Interdomain interactions in AMPA and kainate receptors regulate affinity for glutamate. *J Neurosci.* 26:7650-7658.
7. Abele, R., K. Keinanen, and D.R. Madden. 2000. Agonist-induced isomerization in a glutamate receptor ligand-binding domain. A kinetic and mutagenetic analysis. *J Biol Chem.* 275:21355-21363.
8. Poon, K., L.M. Nowak, and R.E. Oswald. 2010. Characterizing single-channel behavior of GluA3 receptors. *Biophys J.* 99:1437-1446.

9. Qin, F., and L. Li. 2004. Model-based fitting of single-channel dwell-time distributions. *Biophys J.* 87:1657-1671.
10. Qin, F., A. Auerbach, and F. Sachs. 1996. Estimating single-channel kinetic parameters from idealized patch-clamp data containing missed events. *Biophys J.* 70:264-280.
11. Pelleg, D., and A.W. Moore. 2000. X-means: Extending K-means with efficient estimation of the number of clusters. Morgan Kaufmann Publishers, Inc., San Francisco, CA. pp. 727-737.
12. Hollmann, M., and S. Heinemann. 1994. Cloned glutamate receptors. *Annu Rev Neurosci.* 17:31-108.
13. Ahmed, A.H., Q. Wang, H. Sondermann, and R.E. Oswald. 2009. Structure of the S1S2 glutamate binding domain of GluR3. *Proteins: Structure, Function, and Bioinformatics.* 75:628-637.
14. Otwinowski, Z., and W. Minor. 1997. Processing of X-ray diffraction data collected in oscillation mode. *In* Methods in Enzymology, Vol. 276, Macromolecular Crystallography, part A. Carter CW, Sweet RM, editors. Academic Press, New York. 307-326.
15. Adams, P.D., R.W. Grosse-Kunstleve, L.W. Hung, T.R. Ioerger, A.J. McCoy, N.W. Moriarty, R.J. Read, J.C. Sacchettini, N.K. Sauter, and T.C. Terwilliger. 2002. PHENIX: building new software for automated crystallographic structure determination. *Acta Crystallogr D Biol Crystallogr.* 58:1948-1954.
16. Emsley, P., and K. Cowtan. 2004. Coot: model-building tools for molecular graphics. *Acta Crystallogr D Biol Crystallogr.* 60:2126-2132.
17. Ahmed, A.H., Q. Wang, H. Sondermann, and R.E. Oswald. 2009. Structure of the S1S2 glutamate binding domain of GLuR3. *Proteins.* 75:628-637.

18. Jin, R., and E. Gouaux. 2003. Probing the function, conformational plasticity, and dimer-dimer contacts of the GluR2 ligand-binding core: studies of 5-substituted willardiines and GluR2 S1S2 in the crystal. *Biochemistry.* 42:5201-5213.
19. Maltsev, A.S., A.H. Ahmed, M.K. Fenwick, D.E. Jane, and R.E. Oswald. 2008. Mechanism of partial agonism at the GluR2 AMPA receptor: Measurements of lobe orientation in solution. *Biochemistry.* 47:10600-10610.
20. Maltsev, A.S., and R.E. Oswald. 2010. Hydrophobic side chain dynamics of a glutamate receptor ligand binding domain. *J Biol Chem.* 285:10154-10162.
21. Jin, R., M. Horning, M.L. Mayer, and E. Gouaux. 2002. Mechanism of activation and selectivity in a ligand-gated ion channel: structural and functional studies of GluR2 and quisqualate. *Biochemistry.* 41:15635-15643.
22. Patneau, D.K., M.L. Mayer, D.E. Jane, and J.C. Watkins. 1992. Activation and desensitization of AMPA/kainate receptors by novel derivatives of willardiine. *J Neurosci.* 12:595-606.
23. Fenwick, M.K., and R.E. Oswald. 2010. On the mechanisms of alpha-amino-3-hydroxy-5-methylisoxazole-4-propionic acid (AMPA) receptor binding to glutamate and kainate. *J Biol Chem.* 285:12334-12343.
24. Fenwick, M.K., and R.E. Oswald. 2008. NMR spectroscopy of the ligand-binding core of ionotropic glutamate receptor 2 bound to 5-substituted willardiine partial agonists. *J Mol Biol.* 378:673-685.
25. Ren, H., Y. Honse, B.J. Karp, R.H. Lipsky, and R.W. Peoples. 2003. A site in the fourth membrane-associated domain of the N-methyl-D-aspartate receptor regulates desensitization and ion channel gating. *J Biol Chem.* 278:276-283.
26. Sobolevsky, A.I., M.P. Rosconi, and E. Gouaux. 2009. X-ray structure, symmetry and mechanism of an AMPA-subtype glutamate receptor. *Nature.*

27. Mayer, M.L. 2005. Crystal structures of the GluR5 and GluR6 ligand binding cores: molecular mechanisms underlying kainate receptor selectivity. *Neuron.* 45:539-552.
28. Inanobe, A., H. Furukawa, and E. Gouaux. 2005. Mechanism of partial agonist action at the NR1 subunit of NMDA receptors. *Neuron.* 47:71-84.

CHAPTER 4

Flicker Gating Mode of Single Channel GluA3 Receptors

4.1 Abstract

Single channel studies on ion channels have revealed a plethora of information on their possible *in vivo* mechanisms of function, including modal gating behaviors, mechanisms of allosteric modulation, and single channel block. Systemic characterization has only recently begun for AMPA receptors. AMPA receptor-channel block has never been characterized on the single channel level. We report here a flicker mode of activity that corresponds to a fast open channel block by an intrinsic HEK 293 cell factor and is independent of the agonist or agonist concentration. We also show that the block is voltage-dependent, with increasing negative membrane potentials reducing the level of block. Development of drugs that mimick this behavior could potentially prove useful in treating various CNS diseases and disorders.

4.2 Introduction

AMPA receptors are a class of ionotropic glutamate receptors that play a major role in excitatory neurotransmission in the CNS. AMPA receptors form functional homo- or hetero-tetrameric channels (1). Upon binding of agonist, AMPA channels open and flux Na^+, K^+ and Ca^{2+}. Assembly with an R-edited GluA2 subunit affects AMPA channel including weak permeability to Ca^{2+}, decreases in the channel conductance and resistance to intracellular polyamine block (1, 2). The majority of neurons in the CNS contain AMPA receptors which co-assemble with GluA2 subunits (1, 2). However, there are populations of neurons that do not assemble with GluA2 and are Ca^{2+} permeable. These Ca^{2+} permeable AMPA channels are susceptible to ion channel block that is reminiscent of block on other ion channels that have been characterized in whole cell studies (3).

Blockade of ion channels, including K^+ channels, Ca^{2+} channels, and NMDA channels is not a new concept (4, 5). There are many types of channel block induced

by a variety of different factors, such as toxins or extracellular ions. One particular type of block, open channel block, is caused by a charged species that enters the pore of the ion channel. There are three types of open channel blockers, slow, intermediate and fast, in which each affect activation in distinct ways (6). Slow open channel blockers have a slow dissociation rate leading to long blocking periods that result in a mostly closed state throughout the record. Intermediate channel blockers generate periods of rapid channel opening and closing seen as flickers (6). Fast open channel blockers have fast rates of association and dissociation; they tend to decrease the apparent amplitude of opening and also cause a flickering effect (5, 6). Although these types of block have been reported on the single channel level for other ion channel subtypes, they have not been seen at a single channel level in AMPA receptors.

Recent studies on GluA3 homomeric channels have revealed modal gating behavior which ranged from very low to very high open probability that is dependent on the concentration of the agonist. However, single channel blocking behavior has not been recorded for any AMPA receptor. The studies highlighted here have captured a flicker mode of activity for GluA3 receptors that reflect a fast open channel block. The activity was seen only when using AMPA receptor agonists. This section characterizes the block and provides some possible factors that could be associated with this activity.

4.3 Methods

Cell Culture

Human embryonic kidney (HEK) 293 cells were stably transfected with r/m GluA3i (G). The cells were cultured in Dulbecco's Modified Eagle's Medium (DMEM) containing 10% fetal bovine serum (FBS), 1% penicillin-streptomycin and

1μg/mL blasticidin, pH 7.4. The addition of the antibiotic, blasticidin, in the culture media selects for the growth of cells that express GluA3 channels. Cells are passaged every 3-4 days and used within 36-48 hours. All cultures were kept in a 37°C incubator with 5% CO_2.

Acquisition of Single Channel Data

All experiments were performed at room temperature (~23°C). Pipettes were pulled from thick-walled borosilicate glass with filament (Sutter Instrument Company, Novato, CA, USA) to a resistance of 15-20 MΩ and firepolished. All solutions were buffered at pH 7.4 and filtered using a 2 μM sterile filtering system (Corning, Lowell, MA). The bath buffer is 1X Dulbecco's phosphate saline buffer (DPBS) with either Ca^{2+} and Mg^{2+}, or Mg^{2+} only (Invitrogen, Carlsbad, CA). The pipette solution contained: 150 mM NaCl, 10 mM Hepes / NaOH, 2 mM KCl. Stock solutions of glutamate, fluorowillardiine (FW), chlorowillardiine (ClW) and nitrowillardiine (NO_2W) (Tocris Bioscience, Ellisville, MO or Ascent Scientific, Princeton, NJ) were made from the pipette solution and kept frozen in aliquots at -20°C until the day of the experiment. Cyclothiazide (CTZ; Tocris Bioscience, Ellisville, MO, or Ascent Scientific, Princeton, NJ) was solubilized in methanol and frozen as 50 mM stock solutions and was added (100-150 μM) to all agonist containing pipette solutions.

Single channel currents were acquired in the cell-attached configuration. Single channel currents were amplified at a gain of 100 mV/pA with an EPC-7 amplifier, low pass filtered to 10 kHz using an external 8-pole Bessel filter, and digitized at 20 kHz using pClamp 7 software (Molecular Devices, Sunnyvale, CA) and stored directly on a PC hard drive. Data were converted from abf to qdf format on QuB software (www.qub.buffalo.edu) for analysis. Single channel currents were recorded from 30

seconds to 2 minutes at holding potentials ranging from 80 to 130 mV. The single channel conductance was estimated from the slope of the current-voltage relationship.

Analysis of Single Channel Data

The data were analyzed in steps: first, the baseline was set; next, the amplitude of the open level was estimated using AMP function from QuB (Baum-Welch algorithm (7)). Visual inspection of the data revealed more than one open conductance level, but the kinetics of channel openings and closures were so rapid that these levels could not be resolved (Figure 4.1A). Instead, the data was then idealized using the segmental-k-means (SKM) algorithm (8) to an initial model of one closed state and one open conductance state using a dead time of 150 μs (Figure 4.1B). Patches with lower to signal-to-noise ratio were additionally filtered at 5 kHz (effective filter of 4.5 kHz) and idealized using a dead time of 200 μs. Maximum interval likelihood (MIL) (9) analysis was applied to this initial model to determine the fit to the dwell time histograms. Additional closed and open states were added one at a time, re-idealized, re-fitted using MIL, and kept if the addition of the state increased by >10 units. If the addition of the state increased the LL by 10 but yielded rates that were close to zero or unrealistically large, then the additional state was omitted. The results of all the patches that exhibited the flicker mode are in Table 1.

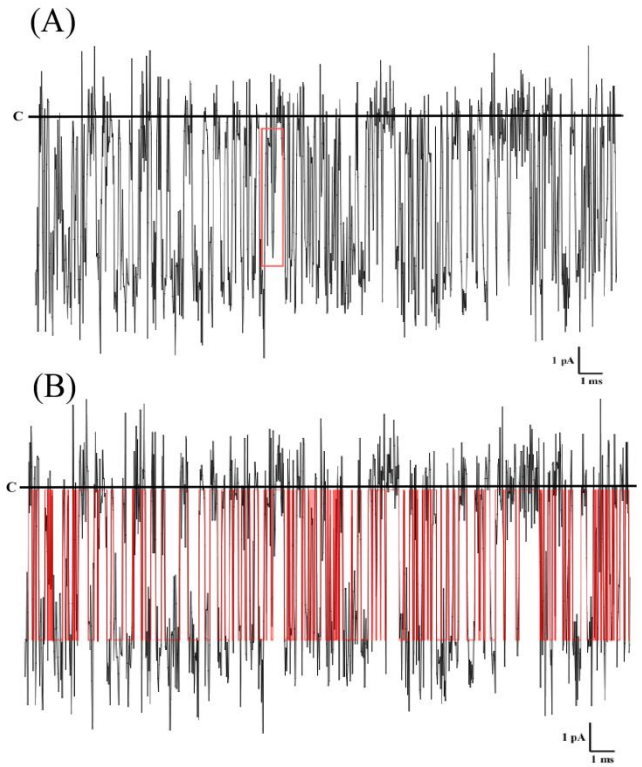

Figure 4.1

A 50 ms representative trace of GluA3 with 200 μM glutamate at a holding potential of 100 mV. **(A)** The red box highlights subconductance levels within the flicker mode that were too brief to be resolved. **(B)** The same trace as A, with idealization to one closed and one open state overlaid in red.

Table 4.1

A summary of all the patches acquired in flicker mode The * denotes a patch acquired without the addition of cyclothiazide. The highlighted data are the anomalies.

Glutamate

Cell #	Vhold (mV)	Conc (μM)	P_C	P_O	Closed Lifetime (ms)	Open Lifetime (ms)	Closed Amp (pA)	Open Amp (pA)
1	100	50	0.48	0.52	0.21	0.23	0.51	6.07
	110	50	0.43	0.57	0.18	0.24	0.49	6.42
2	100	50	0.79	0.21	0.68	0.18	0.19	3.24
3	100	50	0.53	0.47	0.31	0.28	0.16	4.05
4	100	50	0.78	0.22	1.26	0.36	0.06	1.89
5	100	50	0.52	0.48	0.27	0.25	0.35	5.34
6	100	50	0.48	0.52	0.30	0.32	0.22	4.29
7	80	50	0.78	0.22	1.20	0.33	0.02	2.98
8	100	100	0.54	0.46	0.26	0.22	0.22	5.39
9	100	200	0.42	0.58	0.23	0.31	0.43	5.47
	110	200	0.33	0.67	0.17	0.34	0.64	6.10
	90	200	0.42	0.58	0.29	0.40	0.37	5.00
10	90	200	0.59	0.41	0.55	0.38	0.12	3.10
11	100	200	0.59	0.41	0.39	0.27	0.14	4.28
12	100	200	0.63	0.37	0.43	0.26	0.04	4.40
13	90	200	0.67	0.33	0.72	0.35	0.30	2.96
	100	200	0.79	0.21	0.83	0.22	0.42	2.87

(continued)

FW

Cell #	Vhold (mV)	Conc (μM)	P_C	P_O	Closed Lifetime (ms)	Open Lifetime (ms)	Closed Amp (pA)	Open Amp (pA)
1	100	5	0.41	0.59	0.34	0.48	0.77	6.27
	100	5	0.74	0.26	1.88	0.67	0.43	2.72
2*	70	5	0.44	0.56	1.08	1.36	0.19	1.78
	80	5	0.45	0.55	0.98	1.20	0.34	2.30
	100	5	0.65	0.35	1.68	0.90	0.22	1.81
	110	5	0.59	0.41	1.06	0.73	0.21	2.41
	120	5	0.68	0.32	1.27	0.60	0.20	2.95
3	20	5	0.86	0.14	2.07	0.35	0.05	1.92
	50	5	0.77	0.23	0.79	0.23	0.13	3.06
	60	5	0.73	0.27	0.59	0.22	0.17	3.44
	80	5	0.64	0.36	0.33	0.19	0.09	4.21
	100	5	0.54	0.46	0.23	0.19	0.18	5.05
4	100	5	0.75	0.25	1.63	0.55	0.04	1.32
5	100	10	0.43	0.57	0.45	0.59	0.23	4.12
6	100	10	0.42	0.58	0.24	0.33	0.42	5.84
	110	10	0.39	0.61	0.20	0.31	0.46	6.10
7	100	10	0.53	0.47	0.33	0.29	0.26	4.50
	110	10	0.46	0.54	0.29	0.35	0.29	4.95
8	100	50	0.48	0.52	0.37	0.39	0.48	4.95
	100	50	0.57	0.43	0.46	0.34	0.14	4.39
9	100	50	0.73	0.27	0.62	0.23	0.08	2.90
	110	50	0.67	0.33	0.49	0.24	0.21	3.15
	120	50	0.62	0.38	0.40	0.25	0.25	3.39
10	80	50	0.63	0.37	0.53	0.31	0.17	2.74
	90	50	0.66	0.34	0.48	0.24	0.23	3.51

(continued)

NO_2W

Cell #	Vhold (mV)	Conc (μM)	P_C	P_O	Closed Lifetime (ms)	Open Lifetime (ms)	Closed Amp (pA)	Open Amp (pA)
1	100	500	0.55	0.45	0.43	0.35	0.57	4.79
2	90	500	0.64	0.36	0.41	0.23	0.27	4.41
	100	500	0.58	0.42	0.32	0.24	0.32	4.83
	110	500	0.54	0.46	0.28	0.24	0.24	5.20
	120	500	0.48	0.52	0.23	0.24	0.45	5.80
	130	500	0.43	0.57	0.19	0.24	0.58	6.29
3	90	500	0.66	0.34	0.95	0.49	0.16	3.76
	100	500	0.66	0.34	0.86	0.45	0.27	5.77
	110	500	0.58	0.42	0.58	0.42	0.24	3.55
4	80	500	0.53	0.47	0.51	0.46	0.27	6.10
5	80	100	0.66	0.34	1.05	0.53	0.31	5.80

(continued)

ClW

Cell #	V_{hold} (mV)	Conc (μM)	P_C	P_O	Closed Lifetime (ms)	Open Lifetime (ms)	Closed Amp (pA)	Open Amp (pA)
1	100	50	0.61	0.39	0.31	0.19	0.32	4.91
2	100	50	0.41	0.59	0.28	0.40	0.79	5.46
	90	50	0.36	0.64	0.20	0.36	0.57	6.07
3	90	50	0.54	0.46	0.60	0.50	0.21	3.79
	100	50	0.48	0.52	0.39	0.42	0.20	4.33
	90	50	0.43	0.57	0.32	0.43	0.31	4.70

4.4 Results

Conductance levels vary in flicker mode.

The initial guess as to the cause of the flicker mode was based on the probability of capturing an endogenous HEK 293 channel and not a GluA3 channel in the patch. The possibility that it was a Ca^{2+} activated channel prompted the removal of all Ca^{2+} from the extracellular bath: the flicker activity was still observed. However, the evidence that this activity belonged to a GluA3 channel was strengthened when the flicker mode could not be replicated when patching in the absence of agonist. This behavior was only seen when agonists of GluA3 channels, specifically glutamate, FW, ClW, or NO_2W, were present in the pipette. This behavior is reminiscent of intermediate and fast channel block on other ion channels, such as ion mediated K^+ channel block (4) and Mg^{2+} block of NMDA channels (5).

All data were idealized to one closed and one open state (Figure 4.1B). Most of the patches exhibiting flicker activity rapidly closed and opened but did not contain long closures. A small number of patches did exhibit long closures between bursts and were could be fit with two or more closed states (Figure 4.2). These closures did not make up a large percentage of the overall activity. For example, in Table 4.2, a 5 μM FW patch had a long closure with a dwell time of 405 ms which only represented 0.04% of the area of the exponential. The flicker mode was observed with every agonist tested and at all concentrations (50, 100 200 μM glutamate, 5, 10 50 μM FW, 100, 500 μM NO_2W, 50 μM ClW; Figure 4.3). Table 4.1 is a summary of all the patches acquired with flicker mode.

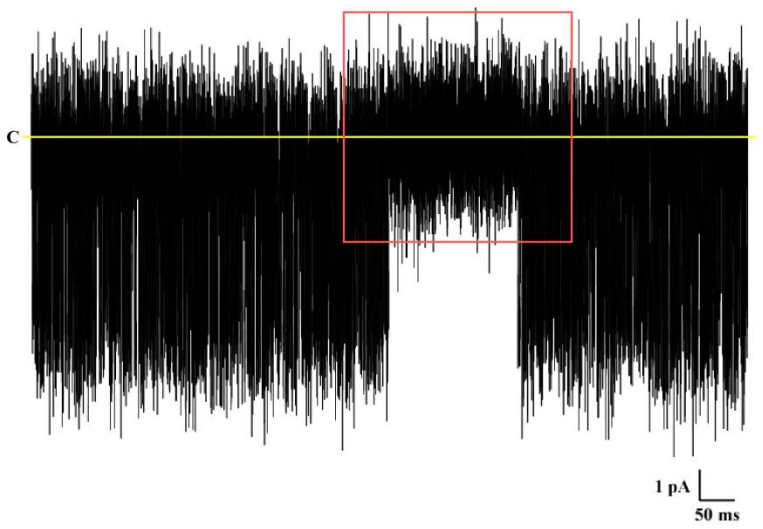

Figure 4.2

A 1 s representative trace of 500 μM NO_2W at a holding potential of 90 mV. The red box highlights longer closures in between flicker bursts. The yellow line represents the baseline.

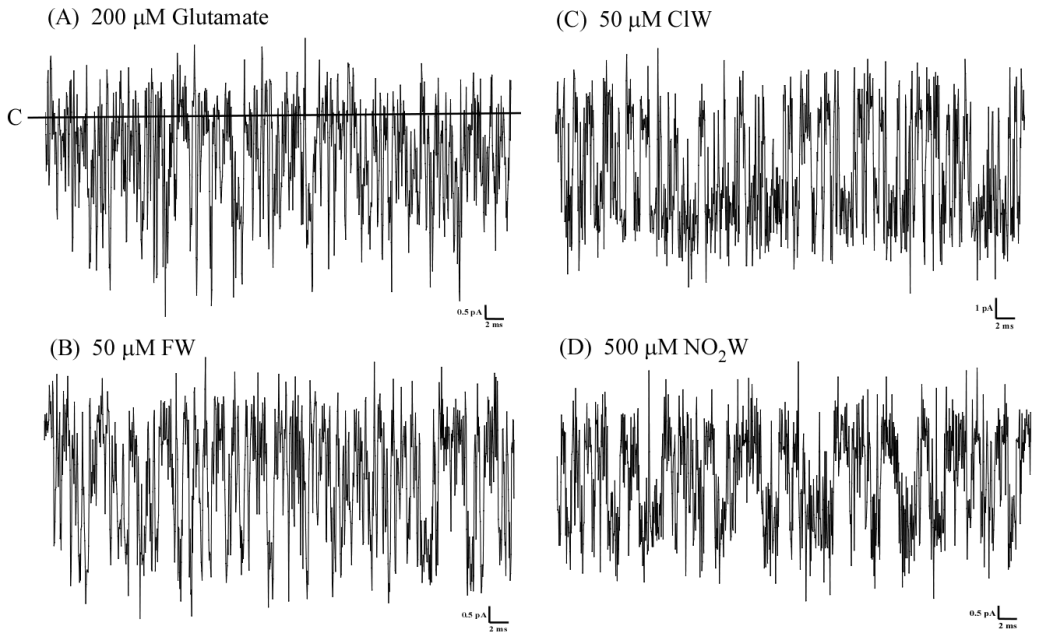

Figure 4.3

50 ms representative traces of flicker activity in the presence of **(A)** glutamate, **(B)** FW, **(C)** ClW and **(D)** NO_2W. The flicker activity ranges from more block to less block with no observable dependence on agonist or agonist concentration.

A few patches were recorded over a range of holding potentials and plotted as a current-voltage relationship to estimate the conductance, which ranged from 25 pS to 55 pS (Figure 4.4). Visual inspection of the data revealed a different degree of flicker activity which ranged from longer closings to shorter closings that showed no dependency of the agonist and agonist concentration (Figure 4.3). The patches with more dramatic flicker activity also seemed to have a decrease in channel conductance. Based on these results, it appears the flicker mode of activity does not arise from a difference in the agonist used, but rather from an unknown mechanism of channel block. This suggests the difference in conductance is possibly caused by the concentration of the blocker or by differences in membrane potential which are unknown in cell-attached patch recording.

To test whether the addition of cyclothiazide (CTZ) to the pipette buffer contributed to this blocking activity, a test patch with 5 μM FW was acquired in the absence of CTZ (Figure 4.5) and not surprisingly, the same flicker activity was observed. To further test whether this blocking effect arose from intracellular factors intrinsic to HEK 293 cells, patches with this flicker activity were pulled from the cell. The flicker mode disappeared once the patch was isolated from the cell (data not recorded). This confirmed our suspicion that the blocking activity was caused by intrinsic factor(s) present in the HEK 293 cell itself and not from the recording conditions.

Flicker mode is voltage dependent.

The activity of the channel in the flicker gating mode seemed to be affected by voltage changes (Table 4.2), in which increasing the holding potential (which corresponds to more negative membrane potentials) altered the kinetics of the flicker. The open probability (P_O) of the channel generally increased as the holding potential was increased whereas the closed probability (P_C) decreased. The mean lifetime of the

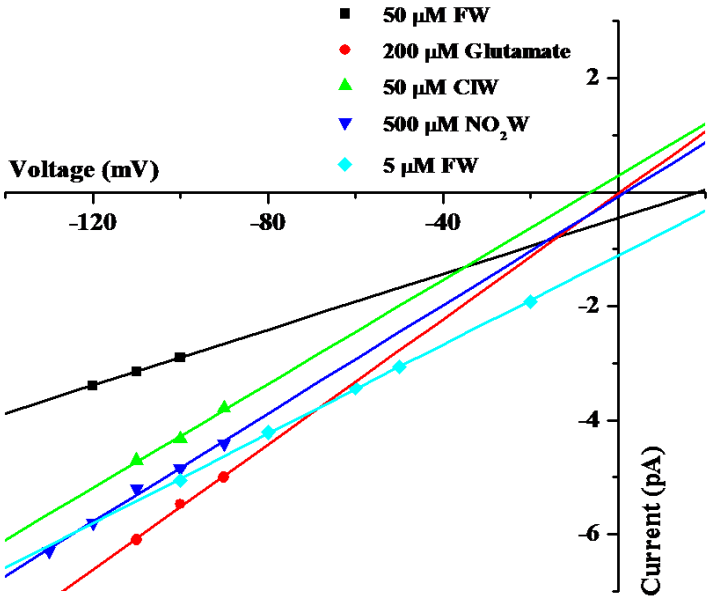

Figure 4.4

Current-Voltage relationship for glutamate, FW, ClW, and NO_2W at varying concentrations. The amplitude at each holding potential was determined by idealizing the data to one closed and one open conductance level. The conductance for each of the agonists are: 24.5 pS 50 µM FW; 54.9 pS 200 µM Glutamate; 45.6 pS 50 µM ClW; 47.5 pS 500 µM NO2W; 39.04 pS 5 µM FW.

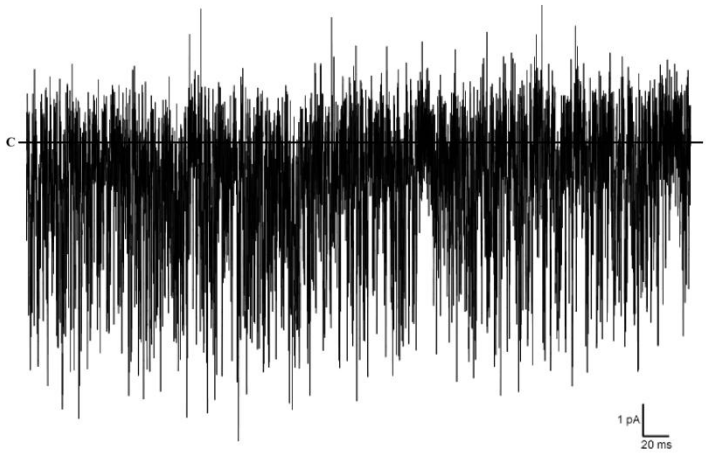

Figure 4.5

GluA3 flicker activity was acquired with 5 μM FW in the absence of CTZ.

Table 4.2

Flicker activity is voltage dependent. The kinetic values of a few patches acquired with 200 μM glutamate, 5 μM FW, and 500 μM NO_2W.

Agonist (μM)	Vhold (mV)	P_C (%)	P_O (%)	Open (pA)	τ_{C1} (ms)	Area	τ_{C2} (ms)	Area	τ_{O1} (ms)	Area
200 Glutamate	90	42	58	5	0.47	1			0.78	1
	100	42	58	5.47	0.45	1			0.78	1
	110	33	67	6.1	0.33	1			1.17	1
5 FW	20	86	14	1.92	2.81	1			0.32	1
	50	77	23	3.06	1.59	1.00	405	0.0004	0.31	1
	60	73	27	3.44	1.41	1			0.31	1
	80	64	36	4.21	0.99	1			0.38	1
	100	54	46	5.05	0.71	1			0.53	1
50 FW	100	73	27	2.9	1.26	1			0.29	1
	110	67	33	3.15	1.00	1			0.32	1
	120	62	38	3.39	0.83	1			0.38	1
50 ClW	90	54	46	3.79	0.73	1.00	246	0.0004	0.67	1
	100	48	52	4.33	0.61	1			0.70	1
	110	43	57	4.7	0.50	1			0.79	1
500 NO_2W	90	64	36	4.41	0.95	1.00	90	0.0001	0.39	1
	100	58	42	4.83	0.72	1.00	70	0.0006	0.48	1
	110	54	46	5.2	0.60	1.00	132	0.0007	0.57	1
	120	48	52	5.8	0.51	1.00	108	0.0007	0.69	1
	130	43	57	6.29	0.44	1.00	52	0.0009	0.85	1

Table 4.3

Kinetic behavior of flicker mode.

The model corresponding to the rates is: $C_2 \leftrightarrow C_1 \leftrightarrow O$.

Agonist	Vhold (mV)	K_{C-O} (s^{-1})	K_{O-C} (s^{-1})	τ Closed (ms)	τ Open (ms)
200 μM Glutamate	90	2866	1975	0.47	0.78
	100	2972	2002	0.45	0.78
	110	3777	1502	0.33	1.17
5 μM FW	20	592	3386	2.81	0.32
	50	1111	3784	1.59	0.31
	60	1270	3878	1.41	0.31
	80	1671	3376	0.99	0.38
	100	2071	2552	0.71	0.53
50 μM FW	100	1522	4343	1.26	0.29
	110	1837	4085	1.00	0.32
	120	2055	3555	0.83	0.38
50 μM ClW	90	1848	1956	0.73	0.67
	100	2222	1995	0.61	0.70
	110	2646	1885	0.50	0.79
500 μM NO2W	90	1729	3311	0.95	0.39
	100	2137	2885	0.72	0.48
	110	2437	2532	0.60	0.57
	120	2744	2180	0.51	0.69
	130	2965	1830	0.44	0.85

open state was relatively the same at all holding potentials. However, the mean closed lifetime decreased with increasing holding potential. This indicates the length of closures shortened and contributed to the overall reduction in P_C. The forward rate from C→O also increased while the backward rate O→C is decreased with increasing holding potentials (Table 4.3). This suggests that increasing the driving force of inward currents decreases the intensity of channel block. However, a complete loss of the block has never been observed with increasing membrane potentials.

There were also patches which deviated from this behavior (Table 4.1, highlighted in yellow). Although the holding potential was increased, the activity seemed to fluctuate; the P_C would increase or decrease regardless of holding potential. This was also the same with respect to P_O, amplitudes, mean closed lifetimes and mean open lifetimes (Table 4.1 highlighted in yellow). However, these patches also contained long closures in between bursts, which could signify an activity change in the channel causing nonlinear results.

4.5 Discussion

Although different modes of activity for AMPA receptors have been established on the single channel level, this is the first study which has demonstrated an open channel block. The cause of the block, however, still remains a mystery. A few potential causes of the block have been explored and ruled out. We have determined the block is not caused by any exogenous factors that were introduced to the recording system and did not notice a dependence on the agonist or the concentration of the agonist. The blocking effect is also somewhat alleviated with increasing membrane potential, though the block is never fully eliminated unless the patch is excised from the membrane. The degree of flicker activity also ranged from highly blocked, which revealed itself as a decrease in amplitude and an increase in the duration of closures, to

a lesser degree of block, which exhibited larger amplitude openings and shorter closed durations. From these results, we propose that the block is caused by a factor present in the HEK 293 cells and that the extent of blockage is dependent on the concentration of this unidentified factor. Although the data did not reveal an agonist concentration dependence on block, this possibility is still unclear and needs to be resolved in future studies.

The question now is what this factor that is causing the channel block? One possibility is a divalent cation. K^+ channels have a similar transmembrane topology but flipped 180˚ in the cell membrane. K^+ channels, like AMPA receptors, also form tetramers. Studies on various K^+ channels have demonstrated channel blockade by various divalent cations, such as Mg^{2+}, Zn^{2+} and Ni^{2+} (10-12). This same mechanism could possibly explain AMPA channel block. However, when extracellular Ca^{2+} was removed the block was still observed. The only divalent cation present in our recording buffer is Mg^{2+}, and possibly intracellular Ca^{2+}. Although these two ions are possibilities, our receptor subtype actually allows the influx of these two divalent ions. Not only that, but normal intracellular divalent ions, other than extremely high concentrations of Zn^{2+} (13), have not yet been shown to have an inhibitory effect in whole cell studies, so it is unlikely the flicker activity is caused by an ion block of the channel. Polyamines, on the other hand, are abundant in cells and have been shown to induce AMPA channel block on the whole cell level. Polyamines have blocking effects on all ionotropic glutamate receptors (3, 14). Polyamine block on NMDA receptors has also been shown in single channels and have been shown to have a voltage dependent block that is relieved by large negative potentials (14). The block by polyamines of NMDA channels is reminiscent of the block that is reported here for GluA3 channels. One method to test if polyamines were affecting GluA3 channels is to collect data in the inside-out patch configuration, in which the intracellular portion

of the receptor can be exposed directly to added polyamines. However, inside-out patches were not very stable in our system and thus not suitable for testing this hypothesis.

Ion channel block has been speculated to play a physiological role in regulating channel activity in neuronal cells. Polyamine block of Ca^{2+} permeable AMPA channels has been shown to contribute to short term synaptic plasticity in local circuits (15). During high-frequency stimulation, relief of polyamine block seems to inhibit neuronal depression (15). Identifying a pharmacological agent that mimics this block in neuronal cells might be of use in disorders such as epilepsy, in which the neuronal excitatory threshold is lower, and diseases such as amyotrophic lateral sclerosis, in which the expression of Ca^{2+} AMPA channels is increased (16, 17). There are currently several drugs that act as open channel blockers on other ion channels and are used for a range of purposes, such as local anesthetics, which block Na^{+} channels and a drug used to treat Alzheimer's disease, memantine that blocks NMDA channels. Future studies to understand the block and source of the block on the channel may open a new avenue for pharmacological manipulation of AMPA receptor function in patients with CNS related diseases and disorders.

REFERENCES

1. Dingledine, R., K. Borges, D. Bowie, and S.F. Traynelis. 1999. The glutamate receptor ion channels. *Pharmacol Rev.* 51:7-61.
2. Sommer, B., M. Kohler, R. Sprengel, and P.H. Seeburg. 1991. RNA editing in brain controls a determinant of ion flow in glutamate-gated channels. *Cell.* 67:11-19.
3. Bowie, D., and M.L. Mayer. 1995. Inward rectification of both AMPA and kainate subtype glutamate receptors generated by polyamine-mediated ion channel block. *Neuron.* 15:453-462.
4. Neyton, J., and C. Miller. 1988. Potassium blocks barium permeation through a calcium-activated potassium channel. *J Gen Physiol.* 92:549-567.
5. MacDonald, J.F., and L.M. Nowak. 1990. Mechanisms of blockade of excitatory amino acid receptor channels. *Trends Pharmacol Sci.* 11:167-172.
6. Hille, B., and B. Hille. 2001. Ion channels of excitable membranes. Sinauer, Sunderland, Mass.
7. Baum, L.E., T. Petrie, G. Soules, and N. Weiss. 1970. A maximization technique occurring in the statistical analysis of probabilistic functions of Markov chains. *Ann. Math. Statist.* 41:164-171.
8. Qin, F., and L. Li. 2004. Model-based fitting of single-channel dwell-time distributions. *Biophys J.* 87:1657-1671.
9. Qin, F., A. Auerbach, and F. Sachs. 1996. Estimating single-channel kinetic parameters from idealized patch-clamp data containing missed events. *Biophys J.* 70:264-280.
10. Claydon, T.W., D.C. Kwan, D. Fedida, and S.J. Kehl. 2006. Block by internal Mg^{2+} causes voltage-dependent inactivation of Kv1.5. *Eur Biophys J.* 36:23-34.

11. Harrison, N.L., H.K. Radke, M.M. Tamkun, and D.M. Lovinger. 1993. Modulation of gating of cloned rat and human K^+ channels by micromolar Zn2+. *Mol Pharmacol.* 43:482-486.
12. Perchenet, L., and O. Clement-Chomienne. 2001. External nickel blocks human Kv1.5 channels stably expressed in CHO cells. *J Membr Biol.* 183:51-60.
13. Bresink, I., B. Ebert, C.G. Parsons, and E. Mutschler. 1996. Zinc changes AMPA receptor properties: results of binding studies and patch clamp recordings. *Neuropharmacology.* 35:503-509.
14. Araneda, R.C., J.Y. Lan, X. Zheng, R.S. Zukin, and M.V. Bennett. 1999. Spermine and arcaine block and permeate N-methyl-D-aspartate receptor channels. *Biophys J.* 76:2899-2911.
15. Rozov, A., and N. Burnashev. 1999. Polyamine-dependent facilitation of postsynaptic AMPA receptors counteracts paired-pulse depression. *Nature.* 401:594-598.
16. Rogawski, M.A., and S.D. Donevan. 1999. AMPA receptors in epilepsy and as targets for antiepileptic drugs. *Adv Neurol.* 79:947-963.
17. Rowland, L.P., and N.A. Shneider. 2001. Amyotrophic lateral sclerosis. *N Engl J Med.* 344:1688-1700.

CHAPTER 5

Conclusions

I. Summary of findings

Research on ionotropic glutamate receptors, specifically AMPA receptors, has come a long way since the first discovery that glutamate was an excitatory neurotransmitter. We currently know the structure of the full length GluA2 receptor, without the C-terminus, bound to an antagonist (1). Many mutational, structural, and spectroscopic studies have been pieced together to formulate a better picture of how these receptors function. From these prior studies combined with the studies discussed here, we are now beginning to understand how each individual subunit contributes to the activation of an entire receptor.

Using homomeric GluA3 receptors as a model for AMPA receptor function we can elucidate structure function relationships that can extend to other AMPA subtypes and other classes of glutamate receptors. Small differences in single channel activity when averaged over hundreds of channels can yield very large differences in whole cell function. More importantly, the behaviors that are reported here can only be determined from single channel studies. Previous single channel studies were lacking for many reasons, but the most important is the inability to separate modes. AMPA receptors are very fast activators, switching between VL to VH modes on millisecond time scales. If these behaviors were not separated, then the underlying behavior could never be resolved. The studies outlined here have revealed many fundamental aspects to GluA3 receptor function; the first is that GluA3 channels exhibit different modes of activity (Chapter 2). These modal behaviors are dependent on the concentration of agonist; the lower the concentration, the more likely the receptor will activate in a low mode. These channels also display an unknown mechanism of fast open channel block. This flicker-mode is described in Chapter 4 and it appears to be due to a voltage-dependent block of the open channels from the cytoplasmic side, possibly by polyamines. The second observation is that all the agonists tested can induce the

channel to open to the same three conductance levels with differences in the open probability in each conductance level. At very high modes, the full agonist, glutamate, preferentially opens the channel to the intermediate and large conductance levels. The partial agonists, in comparison, follow in order of their efficacy; that is, when comparisons are made in the same mode, the less efficacious the agonist, the less likely the channel visits the largest conductance level (Chapter 3). Based on the single channel data collected in these studies, activation of AMPA receptors, although complex, seems to be conserved within the groups of agonists tested.

The willardiines have the ability to induce lobe closures that is similar in magnitude to glutamate induced closures, yet in whole cell studies the willardiines reveal maximal currents that are less than glutamate (2, 3). Another interesting fact is that the willardiine family itself shows a graded whole cell response (3). This observable fact has always in itself questioned the correlation between the degree of lobe closure and agonist efficacy. Structural data on the LBD and the availability of the single channel data have allowed us to make direct correlations between structure and function. The single channel results show that low concentrations of agonist can induce the channel to activate to very high modes, similar to high concentrations of agonist. However, low concentrations of agonists imply a non-saturated receptor. What method is being employed by the receptor to induce these VH modes of activity with low concentrations of agonist? We proposed that stably closed LBD's trap agonists into the binding pocket, allowing for extended periods of activation that is associated with very high modes of activation. However, this brings up many new questions, the first being, what is the cause of these stable closures? From NMR studies, we have correlated stable closures with the flipping of D655 and S656 in lobe 2 of the LBD to enable the formation of hydrogen bonds across the cleft (4). The timescale of the residues flipping into the proper conformation for H-bonding is on a

similar timescale to mode changes in single channel activity (4). The question of whether these are the only residues involved or if other residues in the ligand binding pocket play a role in stabilizing lobe closure is still uncertain and needs to be studied further.

Our studies also highlight the differences between a full agonist, glutamate, and the partial agonists, FW, NO_2W, and ClW. The single channel data reveals the efficiency of the agonists to produce full channel openings to decrease in the same order of efficacy of the agonists; glutamate > FW > NO2W > ClW (2, 3). From the structures of the LBD's bound to these agonists, the lobe closures for the willardiines ranged from less closed to more closed, with ClW being slightly more open than NO2W and FW. The less closed structures have water molecules surrounding the peptide flip region and the more closed structures do not. Interestingly, the affinity of the willardiine compounds for AMPA receptors is much higher than glutamate. This suggests the willardiines can readily bind to the LBD. We speculate these partial closures do not provide enough energy to actually induce channel opening until the LBD's fully close. Indeed, when the channel does activate, the length of time spent open in the presence of the willardiines were always longer than with glutamate, suggesting the high affinity of the willardiines for the receptor is important in the function. Within the willardiine family itself, these burst lengths also seemed to correlate with the efficacy of the agonist; FW and NO2W cause longer burst duration than ClW, and glutamate has the shortest. Interestingly, ClW being the least efficacious of the three willardiines tested, and also displaying the more open LBD conformation, also shows an alternative kinetic gating behaviors at low concentrations of agonist. That is, at VH or H modes of activation, ClW can either have a high open probability or a very low open probability in the largest conductance level that does not affect the overall channel open probability (the addition of the open

probability of all three conductance levels remains the same). These results suggest four factors play a role in channel activation: affinity of the ligand for the receptor, the ability to induce lobe closure, the stability of the closure, and the actual degree of lobe closure. The affinity of the ligand for the receptor determines the length of time an agonist can dock into the LBD; the higher the affinity, the higher the probability long bursting behaviors will be observed. Once the agonist is docked, the LBD can either begin to close, or stay open. If the closure is full, then the channel will open; if the closure is less than full, then the channel will not open. Upon lobe closure, if hydrogen bonds form between the two lobes then the closure becomes more stable and will result in VH modes of activation. Obviously, this correlation between the structural and functional studies cannot be proven unless the full length receptor is crystallized in the channel's active form, or more evidence is collected.

In order to further obtain evidence for this mechanism, mutational studies which disrupt or strengthen any of these factors could be employed. Indeed, mutation of T686 which H-bonds to E402 (in GluA2) has been characterized and shown to cause a change in activation with a shift to a lower probability of the channel opening to the largest conductance level in the presence of full agonists (5). However, that study did not examine the open channel behavior in detail. The next step would be to kinetically characterize the open channel activity and search whether these mutants also display modal gating behaviors. Structural and functional studies with partial agonists on that specific mutation can yield results which either support or refute our hypothesis. Future single channel studies with mutations on other residues hypothesized to stabilize lobe closure can also further add proof to our correlation, such as T690, or E404 which H-bonds to Y450 in GluA2. If the initial hypothesis is correct, perturbing these residues to destabilize LBD closure should result in a decrease in very high

gating modes in single channel studies and a decrease in the open probability of the largest conductance level in each mode.

Another question to address is how exactly LBD closure result in gating events in the transmembrane region. Currently, it is speculated that Lobe 2 of the LBD connects to transmembrane segment 3 (TM3) by a linker that is located between lobe 2 and TM3. Upon closure of the LBD, lobe 2 moves toward lobe 1, causing a separation of the linker which has been hypothesized to provide the energy for opening the gate of the channel (6). Until the structure of the full length receptor bound to an agonist is solved, this question will most likely remain speculated, but mostly unanswered.

II. Future Directions

Although the studies outlined here have systematically characterized the single channel behavior of wild type GluA3 channels using the neurotransmitter glutamate and 5-substituted willardiines, future studies on this subtype, and other glutamate receptors, remains to be undertaken. The first would be to determine the effects of the other willardiine compounds, IW and HW. IW is the weakest of the willardiines (3), with an efficacy that almost matches the low efficacy of kainate. Structures of IW bound to the LBD have closures ranging from 10 – 16 ° (2, 7). IW has already been shown in GluA2 receptors to exhibit three conductance levels (2), but modeling for modal behaviors has not been done. HW is a strange partial agonist; it can induce a level of desensitization that is as rapid as a full agonist, but does not cause large currents on the whole cell level (3). Structurally, HW can induce a lobe closure that is equivalent to FW. Kainate is also an interesting partial agonist to test because of the more open LBD conformation and low level of whole cell currents. If all the partial agonists have the ability to open the channel to the largest conductance level and the main difference would be in the probability of the channel opening to the largest

conductance level, then it would seem the hypothesis we put forth is more accurate at describing channel function.

From there, mutations in the LBD, which have been studied on the whole cell level, can be studied on the single channel level. One such residue to mutate would be the residue equivalent to L650 in GluA2 receptors, which is conserved in all AMPA receptors (8). This residue juts into the binding pocket and is thought to sterically clash with the isopropenyl group of the partial agonist, kainate. Mutation of this residue to a threonine in GluA2 actually increases the potency of kainate and also causes a shift in the EC_{50} to the left (8). However, a functional consequence for the full agonists was a rightward shift in the EC_{50}. AMPA had the most dramatic results with a large decrease in potency (8). In studies such as this one, it is difficult to tell what component of function is affected; does the channel still display three conductance levels or is the population of channel openings shifted so that the largest conductance level is sparsely visited? Single channel studies on these mutations will not only address this question, but provide more insight on how specific interactions in the LBD affect channel activation.

A point mutation in the delta receptor, which has been replicated in AMPA receptors, result in a channel that has a lower activation threshold (9). How these channels function on the single channel level has never been addressed. Studies on the point mutation in AMPA channels can yield some insight to the gating behavior by determining the kinetics of channel activation. A few questions to tackle is whether modal behaviors still exist, if the conductance levels are still observed and at what populations, and would there be a difference in function between full and partial agonists, as well as antagonists?

More experiments also need to be conducted to determine the cause of the flicker mode in GluA3 channels. The most obvious to test would be polyamines,

which have been shown to block Ca^{2+} permeable AMPA channels (10, 11). These experiments would have to be performed in excised patches in order to control the polyamine concentration. Even if polyamines are not the cause of the flicker mode, polyamine block on single channel function has not been characterized in AMPA receptors and would be reflective of in vivo behavior.

A question which arose from these studies regards the data in which the channel was able to open to a specific conductance level for the entire record. This behavior has been characterized but an explanation has not been determined. There is a possibility this behavior is induced by phosphorylation but the current data to support this is lacking. Phosphorylation of the C-terminus is thought to induce higher levels of activity (12). This alteration in function has not been characterized on the single channel level. Future studies which either eliminate or induce C-terminal phosphorylation should be conducted to determine how single channel function is affected. Even if phosphorylation is not the cause of this specific behavior, nonetheless studying the effects of phosphorylation has many benefits to understanding the role it plays in channel function in neuronal cells, where phosphorylation of glutamate receptors readily occurs.

Transmembrane AMPA receptor regulatory proteins, or TARP's, also play a huge role in AMPA receptor function in neurons. TARP's have been found to traffic with AMPA receptors and increase channel activation (13). Determining the single channel difference in a receptor that expresses with TARP's would be more reflective of AMPA receptor function in neurons.

A question that has been brought up but difficult to answer is how cooperativity, if any, affects channel activation. This is a difficult question to address for many reasons. Based on the full structure of GluA2 bound to an antagonist, it seems AMPA channels form dimers which then interact with another dimer pair to form a tetramer.

These interactions are further complicated by how the dimer interactions form in the N-terminal domain. The N-terminal domain dimerizes with the adjacent subunit different from the LBD dimer (subunit 1 LBD dimerizes with subunit 2 LBD, subunit 2 N-terminal domain dimerizes with subunit 3 N-terminal domain). This results in an asymmetric extracellular portion that also consists of interactions across dimer pairs (1). Dimerization of the LBD has been shown to occur after an agonist has bound and strengthening dimer contacts causes a decrease in the desensitization (14). Whether cooperativity arises from desensitization or channel activation is not yet clear. If the closure of one LBD can lead to the formation of dimer interface, with or without agonist in its dimer partner, then this might explain the single channel data in which the channel opened to only one level for long periods of time. LRET could also be used to study this (14), but determining which subunit in the tetramer had an agonist bound and which did not would be difficult to determine.

Future studies addressing any of these questions can lead to fundamental insight on glutamate receptor function and elucidate the role these receptors play in neurons. These studies can also provide a logical basis for the creation of better pharmacological agents to target specific properties of neurodegenerative diseases. Although much is known, there is much more still to be uncovered. One truth is for certain, and that is research in this field has most certainly not been exhausted.

REFERENCES

1. Sobolevsky, A.I., M.P. Rosconi, and E. Gouaux. 2009. X-ray structure, symmetry and mechanism of an AMPA-subtype glutamate receptor. *Nature.* 429:745-756.
2. Jin, R., T.G. Banke, M.L. Mayer, S.F. Traynelis, and E. Gouaux. 2003. Structural basis for partial agonist action at ionotropic glutamate receptors. *Nat Neurosci.* 6:803-810.
3. Patneau, D.K., M.L. Mayer, D.E. Jane, and J.C. Watkins. 1992. Activation and desensitization of AMPA/kainate receptors by novel derivatives of willardiine. *J Neurosci.* 12:595-606.
4. Fenwick, M.K., and R.E. Oswald. 2010. On the mechanisms of alpha-amino-3-hydroxy-5-methylisoxazole-4-propionic acid (AMPA) receptor binding to glutamate and kainate. *J Biol Chem.* 285:12334-12343.
5. Zhang, W., Y. Cho, E. Lolis, and J.R. Howe. 2008. Structural and single-channel results indicate that the rates of ligand binding domain closing and opening directly impact AMPA receptor gating. *J Neurosci.* 28:932-943.
6. Armstrong, N., and E. Gouaux. 2000. Mechanisms for activation and antagonism of an AMPA-sensitive glutamate receptor: crystal structures of the GluR2 ligand binding core. *Neuron.* 28:165-181.
7. Jin, R., and E. Gouaux. 2003. Probing the function, conformational plasticity, and dimer-dimer contacts of the GluR2 ligand-binding core: studies of 5-substituted willardiines and GluR2 S1S2 in the crystal. *Biochemistry.* 42:5201-5213.
8. Armstrong, N., M. Mayer, and E. Gouaux. 2003. Tuning activation of the AMPA-sensitive GluR2 ion channel by genetic adjustment of agonist-induced conformational changes. *Proc Natl Acad Sci U S A.* 100:5736-5741.

9. Taverna, F., Z.G. Xiong, L. Brandes, J.C. Roder, M.W. Salter, and J.F. MacDonald. 2000. The Lurcher mutation of an alpha-amino-3-hydroxy-5-methyl-4-isoxazolepropionic acid receptor subunit enhances potency of glutamate and converts an antagonist to an agonist. *J Biol Chem.* 275:8475-8479.
10. Rozov, A., and N. Burnashev. 1999. Polyamine-dependent facilitation of postsynaptic AMPA receptors counteracts paired-pulse depression. *Nature.* 401:594-598.
11. Dingledine, R., K. Borges, D. Bowie, and S.F. Traynelis. 1999. The glutamate receptor ion channels. *Pharmacol Rev.* 51:7-61.
12. Barria, A., V. Derkach, and T. Soderling. 1997. Identification of the Ca^{2+}/calmodulin-dependent protein kinase II regulatory phosphorylation site in the alpha-amino-3-hydroxyl-5-methyl-4-isoxazole-propionate-type glutamate receptor. *J Biol Chem.* 272:32727-32730.
13. Nicoll, R.A., S. Tomita, and D.S. Bredt. 2006. Auxiliary subunits assist AMPA-type glutamate receptors. *Science.* 311:1253-1256.
14. Gonzalez, J., M. Du, K. Parameshwaran, V. Suppiramaniam, and V. Jayaraman. 2010. Role of dimer interface in activation and desensitization in AMPA receptors. *Proc Natl Acad Sci U S A.* 107:9891-9896.

APPENDIX

Distinct Modulations of Human Capsaicin Receptor by Protons and Magnesium through Different Domains*

***This research was originally published in The Journal of Biological Chemistry. Shu Wang, Kinning Poon, Robert E. Oswald, Huai-hu Chuang. Distinct Modulations of Human Capsaicin Receptor by Protons and Magnesium through Different Domains. *JBC. 2010;* 258: 11547-11556.**

Abstract

The capsaicin receptor (TRPV1) is a nonselective cation channel that integrates multiple painful stimuli, including capsaicin, protons, and heat. Protons facilitate the capsaicin- and heat induced currents by decreasing thermal threshold or increasing agonist potency for TRPV1 activation (Tominaga, M., Caterina, M. J., Malmberg, A. B., Rosen, T. A., Gilbert, H., Skinner, K., Raumann, B. E., Basbaum, A. I., and Julius, D. (1998) *Neuron* 21, 531–543). In the presence of saturating capsaicin, rat TRPV1 (rTRPV1) reaches full activation, with no further stimulation by protons. HumanTRPV1 (hTRPV1), a species ortholog with high homology to rTRPV1, is potentiated by extracellular protons and magnesium, even at saturating capsaicin. We investigated the structural basis for protons and magnesium modulation of fully capsaicin-bound human receptors. By analysis of chimeric channels between hTRPV1 and rTRPV1, we found that transmembrane domain 1–4 (TM1–4) of TRPV1 determines whether protons can further open the fully capsaicin-bound receptors. Mutational analysis identified a titratable glutamate residue (Glu-536) in the linker between TM3 and TM4 critical for further stimulation of fully liganded hTRPV1. In contrast, hTRPV1 TM5–6 is required for magnesium augmentation of capsaicin efficacy. Our results demonstrate that capsaicin efficacy of hTRPV1 correlates with the extracellular ion milieu and unravel the relevant structural basis of modulation by protons and magnesium.

Introduction

The capsaicin receptor (transient receptor potential vanilloid 1 (TRPV1)), a transduction channel gated by multiple noxious stimuli, plays a central role in signal integration in pain-sensing neurons (2, 3). Noxious heat (>42 °C), acid, and capsaicin, a pungent natural product from chili peppers, all activate TRPV1 to elicit burning pain

(1, 4). Functional synergism among modalities allows TRPV1 to summate different types of subthreshold stimuli and produce a robust response (1, 5, 6). The extent of TRPV1 activation by one or a combination of stimuli determines the intensity of evoked pain (7–12).

Many mammalian TRPV1 agonists exhibit weak receptor activation, even if they may bind the receptor comparably to capsaicin (13, 14). Acidic pH potentiates responses evoked by a low concentration of capsaicin in human and rat TRPV1 alike (1, 15). In contrast, extracellular acidification can enhance only the human receptor currents when capsaicin is applied at a concentration higher than 10 μM (15). Thus, capsaicin functions as a partial agonist for hTRPV1 but a full agonist for the rat receptor. An elevation of temperature or local acidity can in principle augment the efficacies of partial agonists, transforming them from weakly or non-pain-producing ligands into noxious chemicals (16, 17). Thus, pain sensation arising from TRPV1 activation by chemical agonists in humans could conceivably be different from that in rodents, the model species frequently used in biomedical research.

Besides its involvement in pain sensation, TRPV1 displays a low level of activity at normal body temperature (18). Constitutive activity of TRPV1 is essential for regulation of body temperature, evidenced by high fever as a perilous side effect of many TRPV1 blockers during clinical trials for their efficacy in management or prophylaxis of pain (19). Modulators of TRPV1 basal activity and their sites of action are largely unknown; far less known is the variation of basal activities among species in which TRPV1 has been characterized. TRPV1 is a homotetrameric ion channel (20, 21). Hydropathy analysis predicts each subunit to be a six-pass transmembrane polypeptide (4). Earlier work suggests that capsaicin binds to the region between the second and the third transmembrane helices to gate TRPV1 (22). The region between the fifth and the sixth transmembrane segments, including a putative pore loop, forms

the ion permeation pathway (23). Several negatively charged amino acid residues in the pore have been shown to be important for sensitization or activation of TRPV1 by cations, particularly protons and magnesium (11, 24). Because of its therapeutic implication, a better understanding of how hTRPV1 opens in response to the extracellular ionic milieu is important. Notably, both protons and magnesium enhance the efficacy of capsaicin as an agonist for hTRPV1. Given its overall similar topological structure and a high percentage of identity (86%) at the amino acid sequence level to rTRPV1, we identified the structural determinants that allow these two ions to specifically sensitize the human receptor. We found that the stimulatory effects of protons and magnesium on fully liganded hTRPV1 require different modular domains. The first four transmembrane segments (TM1–4) of TRPV1 dictate whether the activity of a fully capsaicin-bound receptor can be further enhanced by protons, and a glutamate residue (Glu-536) in the linker between TM3 and TM4 of hTRPV1 is critical in the modulation by protons. TM5–6 of TRPV1 determines the species difference in magnesium modulation of both saturating capsaicin-induced currents and ligand-independent basal currents. A concerted action of the capsaicin-binding domain and the permeation pathway converges at the final stage of hTRPV1 opening.

Materials and Methods

Molecular Biology

Chimeric channels between human and rat TRPV1 were constructed by overlapped extension PCR of the sequence fragments to be transferred with *Pfu* polymerase (Stratagene, CA), followed by restriction digestion and ligations into the expression vectors containing wild type cDNAs. Thanks to a high level of sequence homology between the hTRPV1 and rTRPV1, we could select common oligonucleotide primer sets of identical sequences for PCR. We first amplified TM1-4

and TM5-6 fragments using wild type TRPV1 as templates. For TM1-4, we used a pair of oligonucleotides with the following sequences: 5'-CAGGACAAGTGGGACAGATT-3' and 5'-TAGATGCCCATCTGCTGGAA-3'. For TM5-6, the oligonucleotides have the following sequences: 5'-TTCCAGCAGATGGGCATCTA-3' and 5'-CAGGATGATGAAGACAGCCTTG-3'. The first PCR fragments were extended using external primers outside the domains to be swapped and the wild type recipient receptor plasmid as the templates. The common primer for the N-terminal region has the following sequence: 5'-AGGCTCTATGATCGCAGGAG-3', and the C-terminal common primer has the sequence 5'-GCAACTAGAAGGCACAGTCG-3' that anneals to the sequence within the vector plasmid. The extended PCR products were digested with BstEII and AflII, gel-purified, and subcloned into the gapped plasmid vectors containing the cDNA of the recipient receptor. Single point mutations were created by QuikChange mutagenesis following the manufacturer's protocol (Stratagene, CA). The sequences of mutagenic primers for the sense strand are as follows: H533Q, 5-CTGTACTTCAGCCAGCTCAAGGAGTATGT-3; E536Q, 5'-ACTTCAGCCACCTCAAGCAGTATGTGGCTTCCAT-3'; H533Q/E536Q, 5'-CTGTACTTCAGCCAGCTCAAGCAGTATGTGGC-3'. All mutants were confirmed by Sanger's dideoxy DNAsequencing.

Cell Culture and Transfection

HEK293T cells were grown in minimal essential medium plus 10% newborn calf serum with penicillin/streptomycin, incubated at 37 °C in 5% CO2, and transfected using Lipofectamine according to the manufacturer's protocols (Invitrogen). Cells were transiently transfected with 300 ng of plasmid DNA encoding TRPV1 receptor

and 100 ng of reporter plasmid encoding enhanced green fluorescent protein. Electrophysiological recordings were performed 2 days after transfection.

Electrophysiology

Outside-out patch clamp and conventional whole-cell recording methods were used. Pipettes were fabricated from borosilicate glass (World Precision Instruments) and fire-polished to a resistance of ~2 megohms. For the outside-out patch clamp experiment, the intracellular pipette solution and standard extracellular bath solution were symmetrical and contained 150mM NaCl, 10mM HEPES, 1mM EGTA, pH adjusted to 7.4 or 6.4 with NaOH. For the magnesium potentiation experiments, a 2 M MgCl2 stock solution was used as the source of Mg^{2+}. It was added into the external solution to achieve a final concentration of 5 mM Mg^{2+}. For whole-cell recordings, we used a cesium solution containing 150 mM CsCl, 10 mM HEPES, 1 mM EGTA. Capsaicin was dissolved in DMSO to make a 0.1 mM stock solution, and diluted into the recording solution at 100 μM concentration before the experiment (0.1% final DMSO). Exchange of external solutions was performed using a gravity-driven perfusion system with manually controlled solenoid valves (ValvebankTM, Automate Scientific Inc.). Voltage clamp experiments were performed at -60 mV holding potential with 320-ms voltage ramps from -120 to 80 mV at 1 Hz. Macroscopic currents were recorded using an Axopatch 200B amplifier (Molecular Devices) and filtered at 2 kHz and digitized at 1 kHz (ITC-18; Instrutech Corp.). Single channel recordings were performed in the outside- out patch clamp configuration. The holding potential was -60 mV. Data were sampled at 5 kHz and low-pass filtered at 2 kHz. Data were acquired and analyzed using Pulse-Pulsefit software(HEKA, Pfalz, Germany), QuB (Program PRE, QUB Suite, Drs. A. Auerbach, F. Qin, and F. Sachs, SUNY, Buffalo, NY), and Origin 8.0 (OriginLab Corp., Northampton, MA). A series

of voltage steps for a 150 ms duration was used to induce steady-state currents. Because the tail currents were too small to be measured accurately, the conductance (G) was derived from the steady-state currents at the ends of the voltage steps using the equation: $G = I/(V - V_{rev})$, where V_{rev} is reversal potential (equal to zero in our experiments because we used symmetric solutions). The normalized conductance (G/G_{max}) was plotted against the membrane potentials and was fitted with the following equation: $G/G_{max} = (G_{min}/G_{max} - 1)/(1+\exp(V - V_{1/2})/K) + 1$, where $V_{1/2}$ is the potential for half-maximal activation, and K is the slope factor. The dose response curve was fitted with Hill equation: $I/I\text{max} = 1/(1 + (EC_{50}/C)^n)$. I/I_{max} is the normalized current at -60 mV; EC_{50} is the half-maximal effective concentration of capsaicin, and n is the Hill coefficient. Data were presented as means ± S.E., and statistical significance was evaluated using unpaired Student's t test. A probability level of less than 0.05 was considered significant.

RESULTS

Protons Increase the Efficacy of Capsaicin as a Human TRPV1 Agonist

Extracellular acidosis has been shown to markedly sensitize rTRPV1 by increasing the apparent affinity but not the maximal activation by capsaicin (1). In contrast, the ability of capsaicin to activate hTRPV1 at saturating concentrations depends on extracellular pH. Protons have been shown to permeate capsaicin-activated TRPV1 channels and reduce intracellular pH (25). To better control both extracellular and intracellular pH values, we adopted the excised outside-out patch configuration to study the effect of protons on hTRPV1. Application of 100 μM capsaicin induced a robust strongly outwardly rectifying current typical of hTRPV1 activation, which was further enhanced when the extracellular pH was reduced from 7.4 to 6.4 (Fig. A.1, *A*

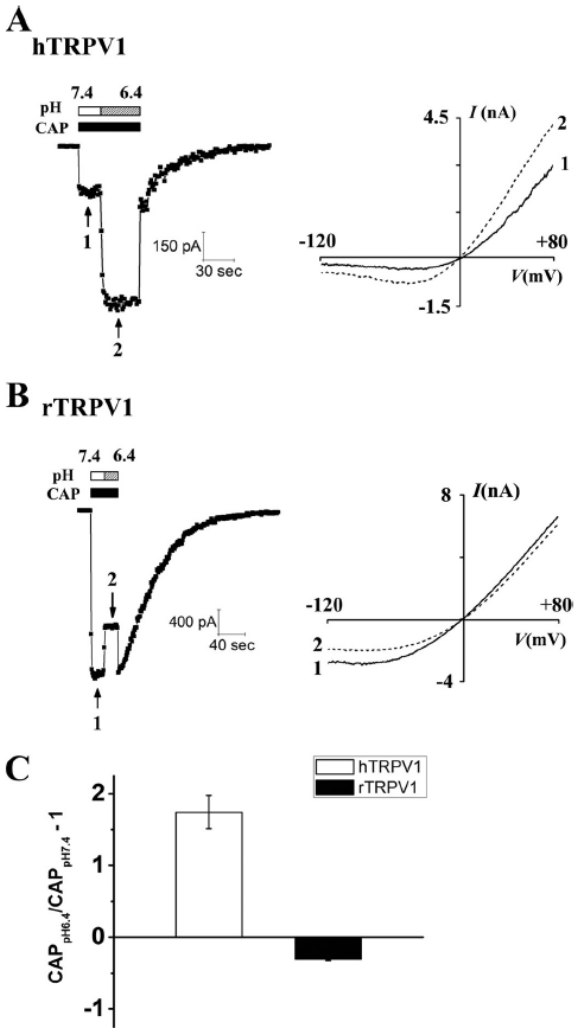

FIGURE A.1

Protons increase the capsaicin efficacy of hTRPV1 but not that of rTRPV1. A, protons increase the 100 μM capsaicin (*CAP*)-induced currents of hTRPV1. *Left*, the capsaicin currents at -60 mV; *right*, current-voltage relationships at time points indicated by numbers in the *left panel*. ***B***, protons block the 100 μM capsaicin-induced currents of rTRPV1. ***C***, comparison of the proton effect on the current amplitudes of hTRPV1 and rTRPV1 at -60 mV. CAP pH 7.4 and CAP pH 6.4 represent the amplitudes of 100 μM capsaicin (*CAP*)-induced currents at different pH values.

TABLE A.1

Proton and magnesium effects on the 100 μM capsaicin-induced currents of the wild type and chimeric TRPV1s. The proton effect was analyzed at -60 mV. The magnesium effect was analyzed at -110 mV. CAP, capsaicin.

	$CAP_{pH\ 7.4}/CAP_{pH\ 6.4} - 1$	$(CAP + Mg^{2+})/CAP - 1$
hTRPV1	1.74 ± 0.23 ($n = 7$)	1.70 ± 0.16 ($n = 4$)
rTRPV1	-0.30 ± 0.02 ($n = 9$)	-0.34 ± 0.03 ($n = 5$)
hTRPV1-rTM1–4	-0.34 ± 0.04 ($n = 7$)	0.30 ± 0.05 ($n = 7$)
hTRPV1-rTM5–6	1.62 ± 0.22 ($n = 7$)	-0.22 ± 0.05 ($n = 5$)
rTRPV1-hTM1–4	1.09 ± 0.11 ($n = 5$)	-0.21 ± 0.03 ($n = 7$)
rTRPV1-hTM5–6	-0.35 ± 0.03 ($n = 8$)	0.35 ± 0.03 ($n = 6$)

and *C*, and Table A.1). Further extracellular acidification only led to inhibition of 100 μM capsaicin-evoked rTRPV1 currents (Fig. A.1, *B* and *C*, and Table A.1). Similar results were also observed for these two receptors activated with 30 μM capsaicin (data not shown).

Acid potentiation of hTRPV1 was observed within the entire range of the voltage ramp (from -120 to +80 mV). Nevertheless, the potentiation effect is more pronounced at -60 mV (2.74 ± 0.23-fold, $n = 7$) compared with +80 mV (1.53 ± 0.03-fold, $n = 7$). Because channel numbers, single channel currents, and channel open probability jointly determine the amplitude of macroscopic currents, we asked which factor primarily contributes to the potentiation of hTRPV1 by protons. When we recorded hTRPV1 in the outside-out configuration at -60 mV with 100 μM capsaicin, protons decreased the single channel current of hTRPV1 from 2.62 ± 0.10 (pH 7.4, $n = 3$) to 1.35 ± 0.15 pA (pH 6.4, $n = 3$) (Fig. A.2). Assuming that the number of channels did not change in the membrane patch subject to acute application of protons, enhancement of hTRPV1 macroscopic current must reflect an increase of channel open probability.

Proton potentiation of hTRPV1 indicates that the saturating concentration of capsaicin alone does not activate the human capsaicin receptor maximally. In principle, any positive channel modulators, in our case protons, will not further potentiate a TRPV1 channel that is maximally activated by capsaicin. We thus examined the biophysical parameters relevant for capsaicin-induced channel activation. Our dose-response analysis of capsaicin-induced currents showed that, in our recording configuration, hTRPV1 and rTRPV1 have similar EC_{50} values for capsaicin (Fig. A.3 and Table A.2). Therefore, unlike the absence of the capsaicin-binding site in chicken TRPV1 (22), the lower activation of human TRPV1 by capsaicin is not a consequence of a lack of ligand binding but rather is an outcome of

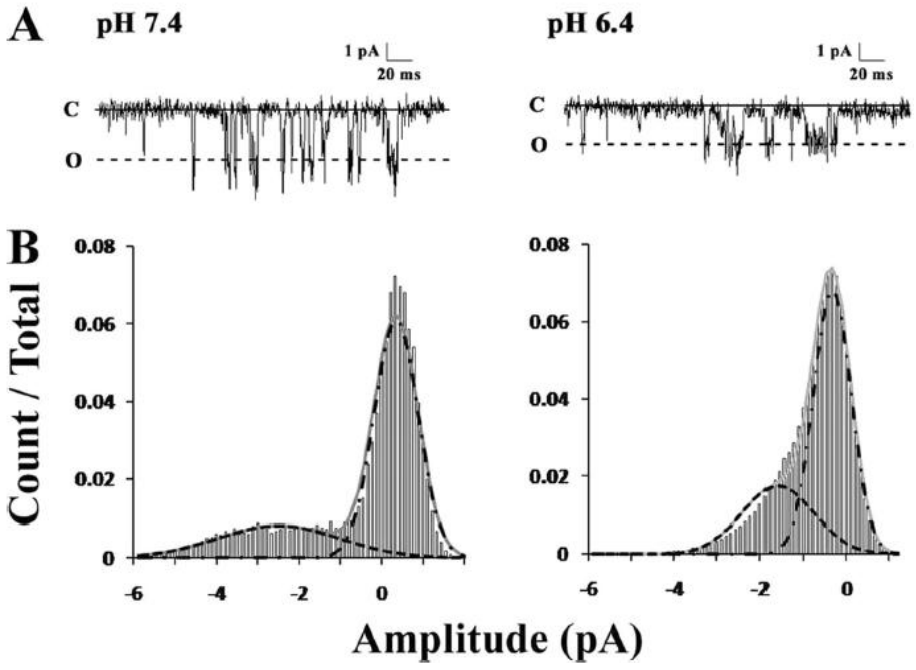

FIGURE A.2

Protons block the hTRPV1 single channel current in the presence of 100 μM capsaicin. A, representative traces of hTRPV1 single channel current from outside-out patch at pH 7.4 or 6.4 in the presence of full-dose capsaicin. Holding potential is -60 mV. *C* and *O* indicate the closed and open states, respectively. ***B***, amplitude histogram for each pH condition fitted with Gaussian functions. At -60 mV, the amplitudes of single channel current at pH 7.4 and pH 6.4 are -2.62±0.10 (*n*=3) and -1.35±0.15 pA (*n*=3), respectively.

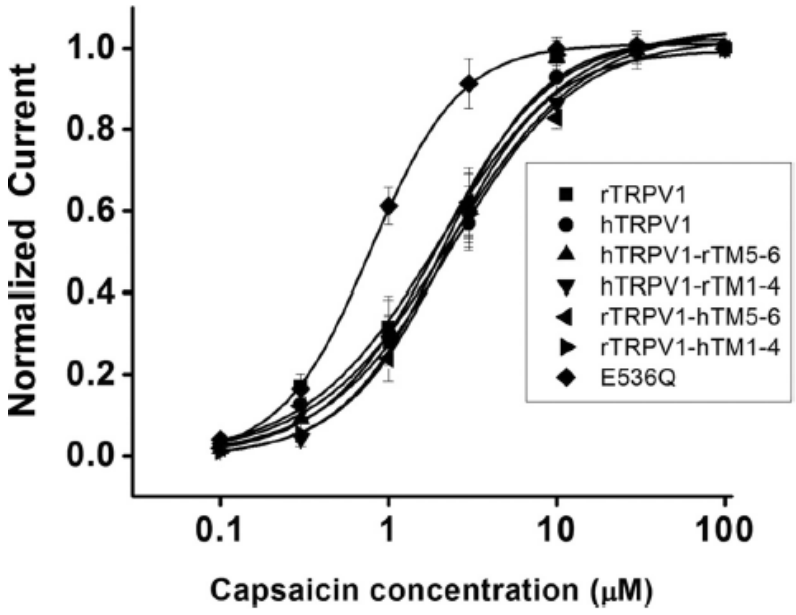

FIGURE A.3

Capsaicin dose-response curves of wild type, chimeras, and hE536Q. Hill equation was used for curve fitting. Half-maximal effective concentrations of capsaicin (EC50) are summarized in Table 2.

the inefficient gating process. Capsaicin activation of TRPV1 is more efficient at more positive membrane potentials, which is clearly observed in the voltage-dependent activation curve (the conductance-voltage plot, or *G-V* curve) of hTRPV1 currents evoked by 100 μM capsaicin. At -60 mV, the macroscopic channel conductance of hTRPV1 is less than 10% of the conductance at +190 mV in the presence of 100 μM capsaicin (Fig.A.4). In comparison, the *G-V* curve of rTRPV1 under the same recording condition is dramatically left-shifted. At -60 mV, rTRPV1 reaches higher channel opening when all the ligand binding sites are occupied by capsaicin (~50% of the maximal channel conductance, Fig. A.4). This results in almost no significant change of open probability of rTRPV1 from -60 to +80 mV (after correction for the intrinsic rectification of TRPV1 single channel conductance) in response to an increase of membrane voltage, consistent with the idea of nearly maximal activation of rTRPV1 by a high concentration of capsaicin and a consequent lack of proton potentiation. Moreover, proton modulation of hTRPV1 is reduced at more positive membrane potentials, in agreement with the model that a channel with higher open probability is less likely to be further potentiated.

First Four Transmembrane Segments (TM1–4) in Human TRPV1 Are Required for Modulation of Capsaicin Efficacy by Extracellular pH

The stimulatory effect of extracellular protons on TRPV1 arises most likely through interaction with the extracellular domain of the protein or the ion permeation pathway, which is highly water accessible. We decided to subdivide the transmembrane region of TRPV1 into ligand-binding and ion-permeation domains to locate the protons modulation site with respect to the efficacy of capsaicin. Based on analogy to the topological structure of voltage-gated potassium channels (26), we replaced the TM5–6 or TM1–4 of human receptor with the corresponding regions of

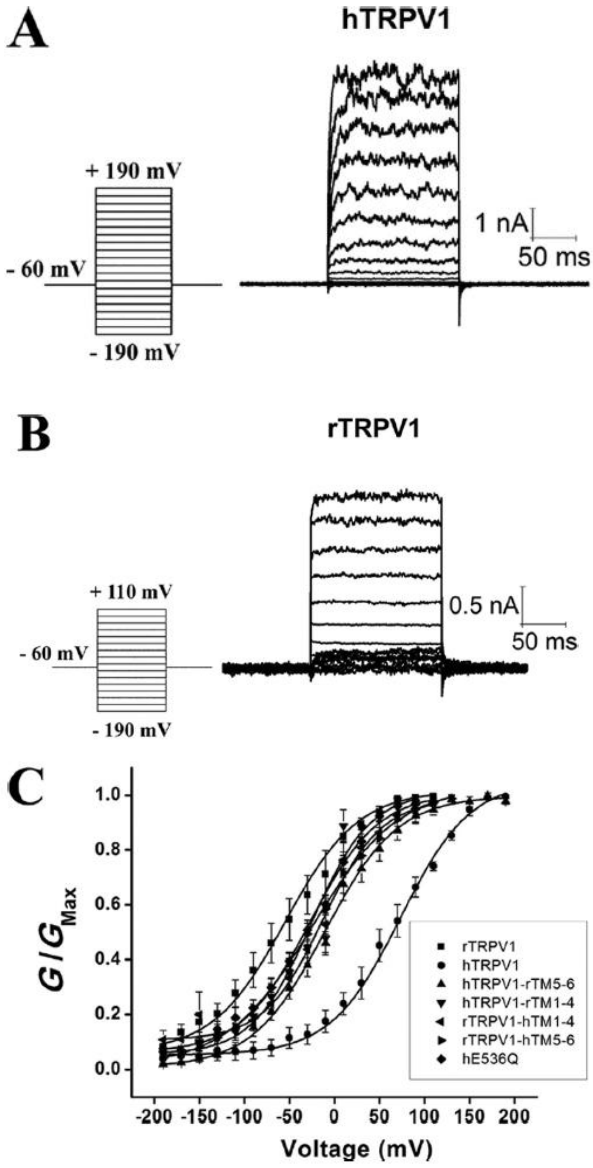

FIGURE A.4

A and ***B***, representative traces for steady-state currents of hTRPV1 and rTRPV1 induced by a series of voltage steps in the presence of 100 μM capsaicin. ***C***, conductance-voltage relationships (*G-V* curves) of wild type, chimeras, and hE536Q in the presence of 100 μM capsaicin (see also Table 2).

TABLE A.2

***Activation parameters of TRPV1 wild type and mutant receptors*.** The voltage of half-maximal activation ($V_{1/2}$) in the presence of 100 μM capsaicin and half-maximal effective concentration of capsaicin (EC_{50}) for the wild type, chimeras, and hE536Q are as summarized (n = 4–6).

	Voltage of half-maximal activation ($V_{1/2}$)	Half-maximal effective concentration of capsaicin (EC_{50})
	mV	*μM*
hTRPV1	73 ± 4	2.34 ± 0.35
rTRPV1	−54 ± 6	2.02 ± 0.48
hTRPV1-rTM1–4	−25 ± 6	2.20 ± 0.28
hTRPV1-rTM5–6	−11 ± 2	1.97 ± 0.21
rTRPV1-hTM1–4	−13 ± 3	2.13 ± 0.22
rTRPV1-hTM5–6	−24 ± 2	2.39 ± 0.47
hE536Q	−28 ± 2	0.79 ± 0.03

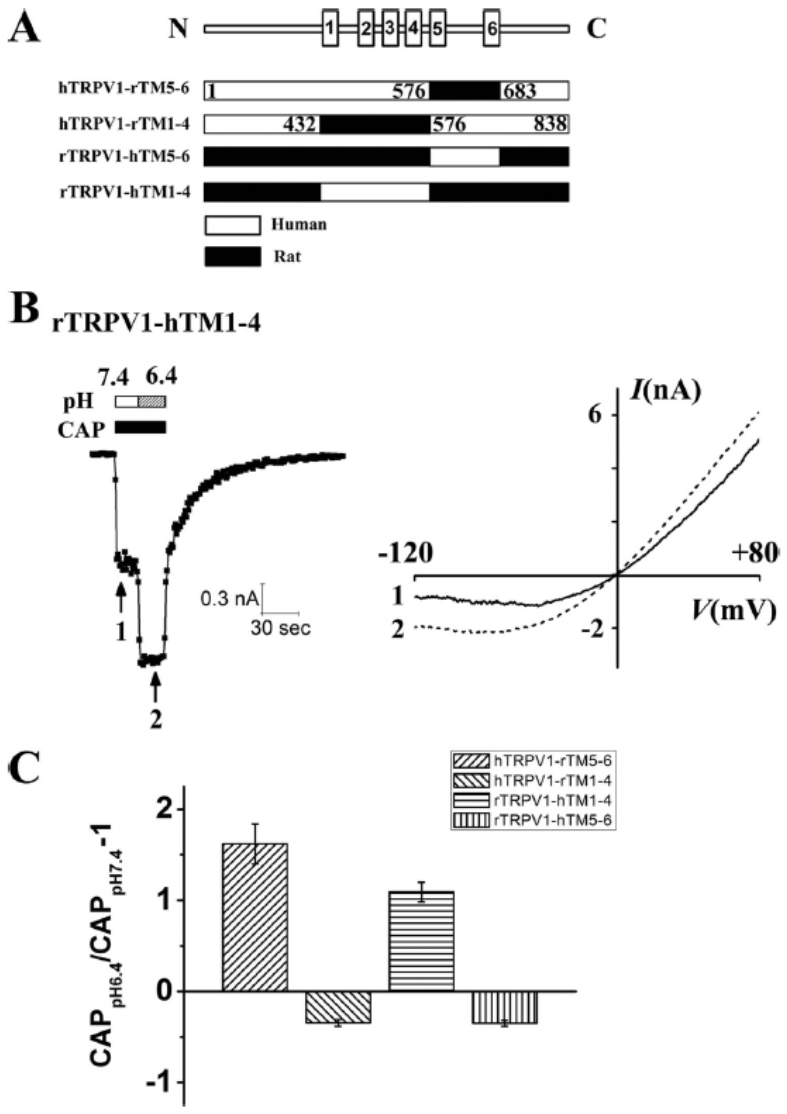

FIGURE A.5

TM1–4 in hTRPV1 determines the proton augmentation of capsaicin efficacy. A, topology of the four chimeras generated between hTRPV1 and rTRPV1. The *numbers* in individual constructs indicate the boundary residues numbers. ***B***, rTRPV1-based chimera, rTRPV1-hTM1–4, is further stimulated by protons in the presence of 100 μM capsaicin. ***C***, summary of the effect of protons on the saturating capsaicin (*CAP*)-induced currents of chimeras at -60 mV.

rTRPV1 to generate chimeric channels between hTRPV1 and rTRPV1, expecting that the former will have a pore region similar to the rat receptor, whereas the latter will show capsaicin binding and gating mimicking rat TRPV1 (Fig. A.5*A*). These two chimeric channels were named hTRPV1-rTM5–6 and hTRPV1-rTM1–4. We also constructed the reverse chimeric channels, rTRPV1-hTM5–6 and rTRPV1-hTM1–4 (Fig. A.5*A*). Because the wild type and chimeric receptors have similar EC50 values for capsaicin (Fig. A.3 and Table A.2), we used the standard recording protocol (100 μM capsaicin, -120 to +80 mV voltage ramp) to assess proton modulation. We found that only chimeras that contain the human TM1–4 are further stimulated by protons (Fig. A.5, *B* and *C*). Protons stimulated the 100 μM capsaicin-induced currents of hTRPV1-rTM5–6 or rTRPV1- hTM1–4 but blocked those of hTRPV1-rTM1–4 or rTRPV1- hTM5–6 (Fig. A.5*C* and Table A.1). Apparently, TM1–4 of hTRPV1 or rTRPV1 determines if the receptor is potentiated or blocked by protons in the presence of saturating capsaicin. This is in contrast to the proton sensitization of the TRPV1 current evoked by low doses of capsaicin, which arises from pH titration of a glutamate residue (Glu-600 in rTRPV1 and Glu-601 in hTRPV1) near the pore (24).

Titration of Glu-536 of Human TRPV1 by Protons Mediates Its Enhancement of Capsaicin Efficacy

Protons most likely exert their effect by titrating acidic residues within the TM1–4 segments of hTRPV1. To localize the precise site of proton action, we made single amino acid substitutions with nontitratable glutamine for residues with side chain p*Ka* values in the acidic range and examined the effect of protons on the mutant channels. Within the extracellular linker between TM3 and TM4, which has also been shown to be critical for direct activation of TRPV1 by strong acidic pH (27), a histidine residue

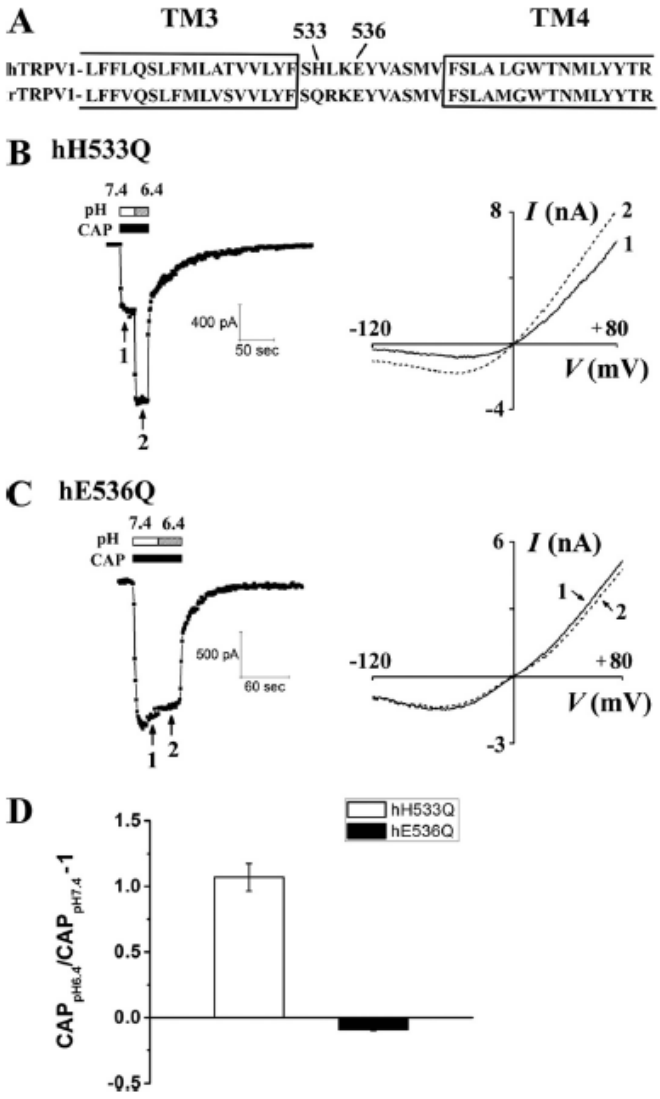

FIGURE A.6

Mutant E536Q of hTRPV1 eliminates the proton modulation of capsaicin efficacy. ***A***, hTRPV1 and rTRPV1 sequences are aligned within the TM3 and TM4 region, highlighting His-533 and Glu-536 in hTRPV1. ***B*** and ***C***, protons potentiate 100 μM capsaicin (*CAP*)-induced currents of hH533Q while slightly blocking that of hE536Q. ***D***, comparison of the proton effects on the capsaicin currents of hH533Q and hE536Q at -60 mV.

is present that is unique to the human receptor (Fig. A.6*A*). Reasoning that titration of this histidine residue (His-533) could lead to enhancement of capsaicin efficacy, we replaced it with the corresponding residue (glutamine) in the rat receptor. Surprisingly, hTRPV1 H533Q (hH533Q) remained substantially potentiated by acidic extracellular pH (Fig. A.6, *B* and *D*). We then mutated the conserved Glu-536 residue in the linker between TM3 and TM4 into glutamine. The mutation E536Q in the human receptor yields a capsaicin-gated ion channel completely resistant to proton potentiation at 100 μM capsaicin (Fig. A.6, *C* and *D*). Therefore, the protonation of Glu-536 is necessary for the acid modulation of capsaicin efficacy of hTRPV1. Upon closer inspection of capsaicin activation of hTRPV1 E536Q, we found that its EC50 value for capsaicin is reduced when compared with wild type hTRPV1 (2.34 ± 0.35 *versus* 0.79 ± 0.03 μM for wild type and mutant receptors, respectively; Fig. A.3, and Table A.2). More importantly, the voltage for half-maximal activation ($V_{1/2}$) of this mutant shifts drastically from $V_{1/2}$ of 73 ± 4 mV for wild type hTRPV1 to -28 ± 2 mV for the E536Q mutant (Table A.2). Thus, E536Q apparently exhibits a sensitized phenotype regarding capsaicin activation.

Magnesium Stimulation of Human TRPV1 Requires the TM5–6 Region of the Receptor

At the functional level, protons and magnesium share multiple mechanisms of modulation on rat TRPV1. Magnesium can sensitize rTRPV1 current evoked by low doses of capsaicin (11). At a concentration as high as 70 mM, magnesium also directly activates rTRPV1 (11). A previous study suggests that the two glutamate residues (Glu-600 and Glu-648) critical for proton modulation of rTRPV1 are the ones also involved in magnesium sensitization or activation of the rat receptor (11). Similar to protons, Mg^{2+} only increases the capsaicin efficacy of hTRPV1. As shown in Fig. A.7,

at a saturating concentration of capsaicin, Mg^{2+} enhances the hTRPV1 current while inhibiting the rTRPV1 current.

Given the highly similar nature of magnesium and proton modulation of hTRPV1, we wondered whether the opposite modulatory effects of Mg^{2+} on human and rat TRPV1 require the same domain as that of protons. We studied the magnesium effects on the same set of four chimeras: hTRPV1-rTM5–6, hTRPV1-rTM1–4, rTRPV1-hTM5–6, and rTRPV1-hTM1–4. At the holding potential of -60 mV, magnesium inhibits all four chimeric channels (data not shown). A closer inspection of the capsaicin-evoked currents at different membrane voltages, however, reveals that magnesium has more than one action on these chimeric channels. Like calcium and other divalent cations, magnesium is a permeant blocker of TRPV1. The blocking effect of magnesium appeared to be voltage-dependent in the wild type rat receptor, as the inhibition is more pronounced in the negative than in the positive membrane potential range (Fig. A.7*B*). The slight inhibition of the rat receptor by magnesium at positive membrane voltages has the characteristics of a surface potential effect from a high concentration of divalent ions, which displays a right shifted current-voltage (*I*-*V*) curve with the same slope conductance (Fig. A.7*B*). We reasoned that it may be necessary to analyze the magnesium effect at more extreme membrane potentials so that any possible stimulatory effect will not be obscured by magnesium block, for example at a voltage that magnesium block either does not occur or completely plateaus. So we studied the magnesium effect at -110 mV. We found that at a more negative membrane potential of -110 mV, magnesium actually has a small stimulatory effect on the 100 μM capsaicin-evoked currents of the chimeras with human TM5–6 (Fig. A.8, *A* and *C*, and Table 1). In contrast, the channels with the rat TM5–6 are still blocked by magnesium at this voltage (Fig. A.8, *B* and *C*, and Table 1). This result suggests that the TM5–6 region from human TRPV1 is important for magnesium

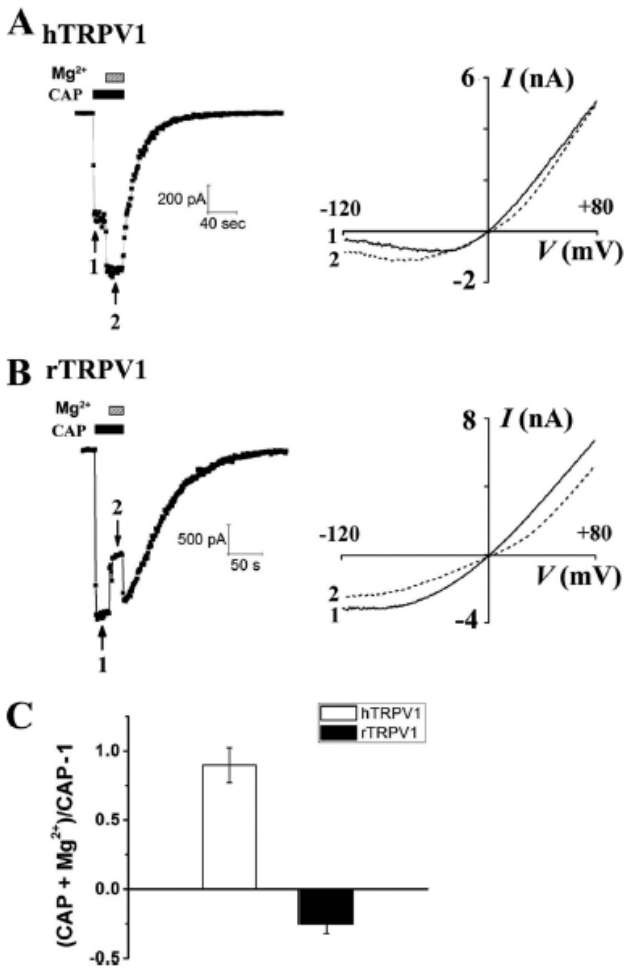

FIGURE A.7

Mg^{2+} increases the capsaicin efficacy of hTRPV1 but not that of rTRPV1. ***A*** and ***B***, *left*, at -60 mV, 5mM MgCl2 increases the 100 μM capsaicin (*CAP*)-induced currents of hTRPV1 by 0.89 ± 0.13-fold (n = 4), whereas it blocks the rTRPV1 currents by 0.25 ± 0.07 (n = 5). *Right*, current-voltage relationships at time points indicated in *left panel*. ***C***, comparison of the Mg^{2+} effect on capsaicin currents of hTRPV1 and rTRPV1 at -60 mV. Capsaicin + Mg^{2+} and capsaicin, respectively, represent the amplitudes of current induced by capsaicin with or without Mg^{2+}.

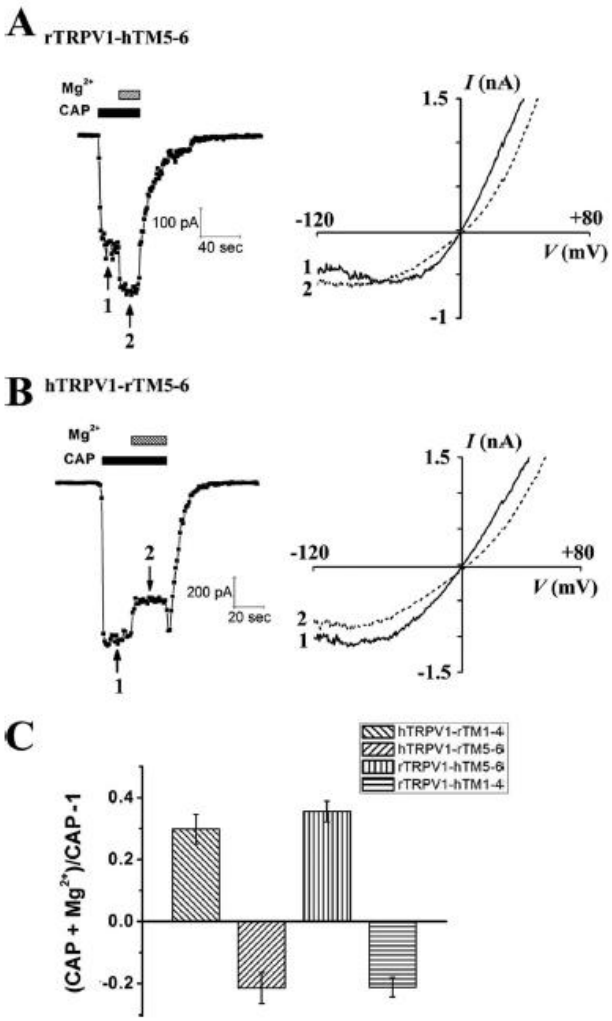

FIGURE A.8

Human TM5–6 region is required for the Mg^{2+} potentiation of capsaicin efficacy. A*, left,* at -110 mV, 5 mM Mg^{2+} potentiates the 100 μM capsaicin (*CAP*)-induced currents of rTRPV1-based chimera with human TM5–6. *Right,* current-voltage relationships show that Mg^{2+} increases the current at very negative potential. ***B****,* Mg^{2+} blocks the capsaicin currents of chimera with rat TM5–6 within the entire range of the voltage ramp. ***C****,* summary of the Mg^{2+} effect on the capsaicin currents of the four chimeras at -110 mV.

augmentation of capsaicin efficacy. Compared with the wild type human receptor, hTRPV1-rTM1–4 and rTRPV1- hTM5–6 showed much less potentiation by magnesium at -110 mV (Table A.1). The reduction of magnesium stimulation in these two chimeras may be an outcome of their higher open probabilities at -110 mV compared with the wild type human receptor (Fig. A.4). If the channel has been strongly activated at a particular voltage, magnesium is expected to have more limited stimulatory effects. To test this possibility, we used a combination of acid (pH 6.4) and 100 μM capsaicin to strongly activate hTRPV1. Under this experimental condition, magnesium stimulation of the wild type human receptor is largely diminished, with some residual stimulation seen only at more negative membrane potentials (*e.g.* -110 mV) (Fig. A.9).

In the absence of agonist, TRPV1 also displays slight basal channel activity with strongly voltage dependent outward rectification (Fig. A.10, *A* and *B*). The inward basal current is more pronounced when we used cesium instead of sodium as the charge carriers in the extracellular solution for the purpose of accurate measurement. Protons and magnesium both enhance the basal currents of either human or rat TRPV1 measured at room temperature. Magnesium potentiates hTRPV1 basal currents more effectively than rTRPV1, whereas proton enhancement of basal currents is comparable for both channels (4.84±0.78-fold *versus* 3.05±0.19- fold, $p > 0.05$, $n = 6$). Analysis of four chimeras reveals that the TM5–6 region is responsible for the species difference in magnesium modulation of basal currents (Fig. A.10*C*).

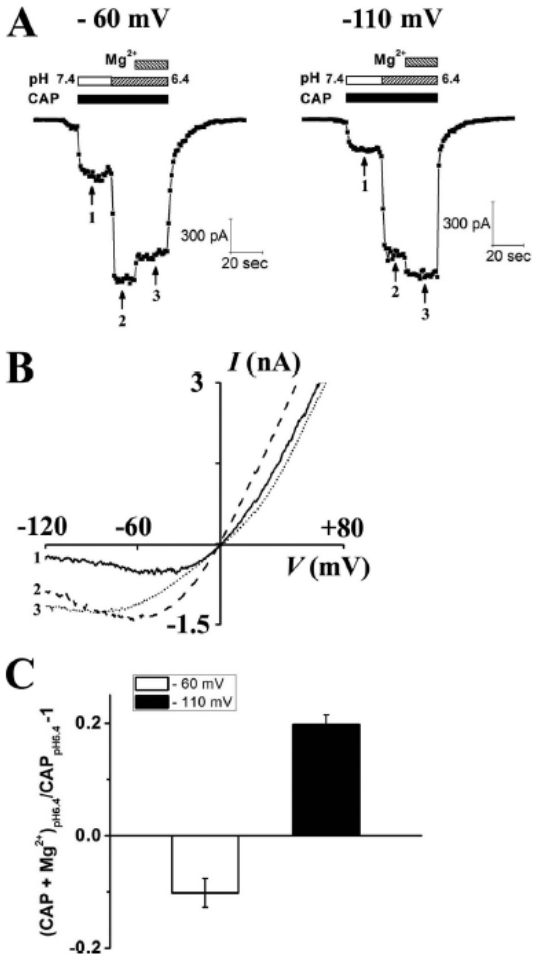

FIGURE A.9

Mg^{2+} effect on hTRPV1 is diminished when the channel is substantially opened by the combination of full-dose capsaicin and protons. ***A****, left*, at -60 mV, 100 μM capsaicin (*CAP*)-induced current of hTRPV1 is potentiated by acid (pH 6.4), 5 mM Mg^{2+} blocks the current; *right*, at -110 mV, Mg^{2+} shows small enhancing effect on the current. ***B****,* current-voltage relationships at time points indicated by numbers in *A.* ***C****,* at -60 mV, Mg^{2+} blocks the current by 0.10 ± 0.03-fold, although at -110 mV, Mg^{2+} increases the current by 0.20 ± 0.02-fold.

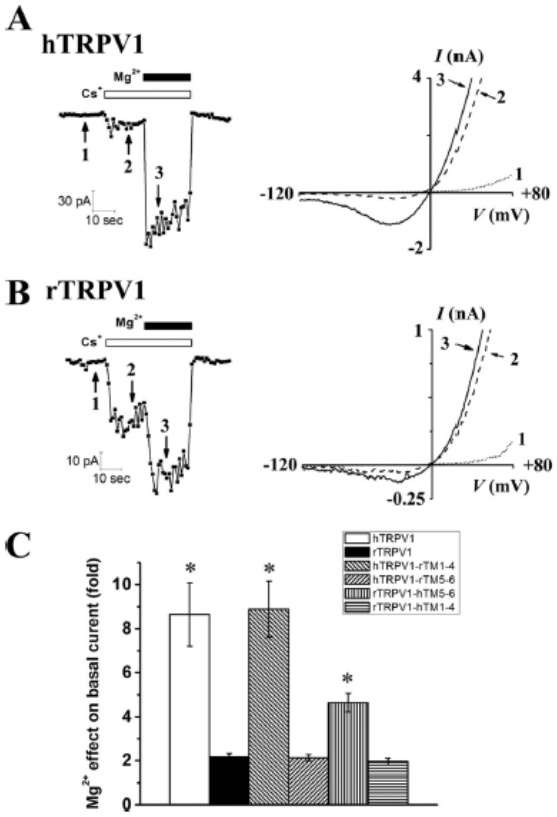

FIGURE A.10

TM5–6 determines the differential Mg^{2+} effects on the whole cell basal currents of human and rat TRPV1. ***A*** and ***B,*** *left,* hTRPV1 and rTRPV1 basal currents at -60 mV. Basal Cs^{+} current is more pronounced than Na^{+} current and 5 mM Mg^{2+} potentiates both basal currents of hTRPV1 and rTRPV1. *Right,* the current-voltage relationships at time points indicated by the *numbers* in the *left panel*. ***C,*** summary of the Mg^{2+} effect on the basal currents of wild types and chimeras at -60 mV. In the Cs^{+} solution, Mg^{2+} increases the hTRPV1 and rTRPV1 basal currents to 8.65 ± 1.45-fold (n = 12) and 2.16 ± 0.16-fold (n = 15), respectively. Mg^{2+} also potentiates the basal currents of hTRPV1-rTM1–4 and rTRPV1-hTM5–6 more effectively than that of rat receptor (*, p_0.05, compared with rTRPV1, n = 5–10). There is no significant difference between rTRPV1 and hTRPV1-rTM5–6 or rTRPV1-hTM1–4.

DISCUSSION

TRPV1 is the principal transduction channel modulating the excitability of pain-sensing neurons in vertebrate species. Although TRPV1s from all species sense noxious heat and tissue acidosis, the repertoire of chemical agonists for each species homologues displays substantial variability (22, 28–30). The efficacies of capsaicin as well as other small organic TRPV1 agonists are both species- and micro-environment-dependent (13, 17). It is therefore relevant to elucidate the molecular basis of differential sensitivity to chemical ligands or integration mechanisms between different modalities for a full appreciation of the protective and incapacitating aspects of pain sensation in physiological or pathological settings.

The similarity between human and rat TRPV1 at the primary sequence level is remarkable. The glutamate residue near the pore loop (Glu-600) responsible for enhancement of agonist potency of capsaicin is functionally conserved among species. One might expect the existence of some titratable amino acid residues unique to the human receptor accounting for proton modulation of agonist efficacy of capsaicin. However, we identified a conserved Glu-536 as the critical residue for proton stimulation of capsaicin efficacy in hTRPV1. Rather than losing its ability to be properly activated by capsaicin due to nonspecific perturbation of the overall structure of the TM1–4 domain, the hE536Q mutant channel behaves as a fully protonated wild type hTRPV1 channel. In support of this view, hE536Q has higher apparent affinity for capsaicin and shows higher channel open probability at saturating concentrations of capsaicin, mimicking a wild type hTRPV1 channel in an acidic environment (pH 6.4). However, the Glu-536 residue is also present in the rat receptor that shows no change in capsaicin efficacy by acidic pH. One possible explanation is that channel open probability of rTRPV1 by capsaicin has already reached itsmaximum within the voltage range of our recordings so that it is impossible to further enhance the rat

receptor current with any positive modulators. As long as saturating capsaicin is present, for membrane potential higher than -60 mV, rat TRPV1 open probability does not even increase in response to voltage increments, a highly effective gating factor for TRPV1 in general. Given that rTRPV1 activated by anandamide can still be potentiated by acidic pH at saturating concentrations of this agonist (13, 16), titration of the Glu-536 residue of the rat receptor may play a role in facilitating channel opening by much lower efficacy agonists, such as anandamide or oxidative lipids.

Previous studies indicate that at the transition between TM3 and the intracellular loop (TM2–3 linker), amino acid residues, including the Tyr-511 and Ser-512, are critical for capsaicin gating of the channel (22). Our results suggest that an amino acid (hGlu-536) within the extracellular loop (linker between TM3 and TM4) serves as a molecular switch to increase the open probability of ligand-bound human receptors. This linker, although short, constrains the structure of the TM1–4 domain of TRPV1 to impact its function significantly. Amino acid substitutions within this linker had been shown to obliterate the activation of TRPV1 by extremely acidic pH, even if the residues involved are not directly titratable by protons (27). Although modulatory effects of magnesium on human TRPV1 phenocopy those of protons in both the polarity and the magnitude, immediate sites of actions of these two cations are different. The stimulatory effect of magnesium is associated with pore domains in chimeras. Primary sequences of TRPV1 pore regions among species are even more conserved than other parts of the receptor, the only variation being a small hypervariable segment connecting the distal end of TM5 helix and the completely conserved "pore" loop. This segment likely contributes to refining the positions of several previously identified amino acid residues implicated in magnesium activation of TRPV1 by affecting its binding. The ligand-independent basal currents of TRPV1 from both species variants are stimulated by magnesium. However, there is a

significant quantitative difference between human and rat receptors. In contrast, protons stimulate basal currents of both receptors to a similar level.

Multimodal gating is an essential feature of TRP channels. Here, we demonstrated protons and magnesium can further stimulate fully capsaicin-bound hTRPV1 through actions on distinct structures. Various kinetic paradigms have been proposed to explain the generalized gating of the thermo-sensitive transient receptor potential channels (31–34). These models likely will need refinements when more structural or biochemical data become available to correlate with proposed functional states. These models can be quantitatively adjusted to explain differential capsaicin sensitivity of TRPV1 from different species. For example, the efficacy of capsaicin as a TRPV1 agonist is lower for the human receptor than the rat receptor. This is not because capsaicin fails to bind hTRPV1 as well as rTRPV1, as EC50 values of capsaicin for both channels are similar. Instead, capsaicin-binding processes are comparable between hTRPV1 and rTRPV1, but hTRPV1 channel is harder to open. It can be due to either a higher energetic barrier for hTRPV1 to open or because of less efficient coupling between binding and gating in hTRPV1. When we inspect the *G-V* curves of wild type and mutant channels in this study, it is obvious that maximal left shifts of these curves by capsaicin are determined by the entirety of all six transmembrane segments but not the further subdivided TM1–4 ligand-binding or TM5–6 ion-permeating domain alone. The chimeric channels, no matter with transfer of the TM1–4 capsaicin-binding domain or the TM5–6 pore domain, have the *G-V* curves fall between the boundaries defined by the two wild type receptors. However, if we compare the pair with the same TM1–6 segments, *e.g.* the hTRPV1-rTM5–6 and rTRPV1-hTM1–4, they actually have very close $V_{1/2}$ values for *G-V* curves. The human receptor has a TM1–4 domain harder to open by capsaicin. Only by substitution of the Glu-536 residue with a neutral amino acid in hTRPV1, an

equivalent of titration of Glu-536 residues in all four channel subunits, can the mutant channel reach the $V_{1/2}$ value comparable with the chimeric channels containing rat TM1–4 domain, and it acquires resistance to proton modulation. A reduced model where temperature and chemical agonists are treated as gating modifiers to shift the intrinsic voltage-dependent gate of the TRPV1 channel cannot accommodate all the data we obtained without further assumptions (31). Different positive regulators of TRPV1 gating must operate independently so that when one of them reaches its maximal capacity of modulation, the rest of them can still further increase channel opening (32–34). One apparent example is the hTRPV1 E536Q mutant, although protons essentially have no effect on full dose capsaicin-activated currents, an increase in transmembrane voltage still leads to further channel opening. It is expected that for each TRPV1 receptor, wild type or mutants, there must be an upper limit for channel openings even with all possible activators present simultaneously. This upper limit of probability for channel opening may differ from one construct to another. However, a common principle will hold for all kinds of TRPV1 channels that the relative receptor potentiation by a modulator gets smaller when other positive regulators are already present, illustrated by a reduction of Mg^{2+} effects on proton-potentiated hTRPV1. At the other extreme, one can also view capsaicin as an exceptionally strong activator for rodent receptors. Pepper plants acquire the ability to synthesize this powerful agonist for survival in their ecological niches during evolution. Being an effective deterrent against rodents, capsaicin does not require any other positive regulators to maximally activate rat TRPV1. It is thus tempting to hypothesize that different sensors for agonistic stimuli (capsaicin, heat, protons, and magnesium) are contained in different structural motifs. Although the physical natures of these sensors are currently unknown, our site mapping work will provide some candidate regions to examine once the high resolution structures of TRPV1 are available.

It is worth noting that protons have more complex effects on the capsaicin activation of human TRPV1 than that of rat TRPV1, a property attributable to relatively weak activation of hTRPV1 by capsaicin, namely partial agonism. A lower efficacy of capsaicin on human TRPV1 allows us to appreciate Nature's design of a signal integrator. Although most physiological activators, including elevation of extracellular acidity, excitatory cations, and endogenous agonists, are all weak activators of TRPV1, synergism of these stimuli can broaden the sensory dimensions of an injury-detecting receptor. Execution of the stimulatory effects through different structural domains of the sensor molecule increases the coding complexity and dynamic range of different categories of signal inputs and its overall efficiency in final receptor activation, particularly when all the stimuli are sub-threshold. This is exemplified in human TRPV1 by a plethora of interactions of protons and magnesium ions on the capsaicin-activated currents, the former through the Glu- 600 residue near the pore and the Glu-536 residue in the linker between TM3 and TM4, as well as the latter acting within the pore. It will be interesting to determine whether the same principle also applied to other endogenously produced TRPV1 agonists with even less efficacy compared with capsaicin.

REFERENCES

1. Tominaga, M., Caterina, M. J., Malmberg, A. B., Rosen, T. A., Gilbert, H., Skinner, K., Raumann, B. E., Basbaum, A. I., and Julius, D. (1998) *Neuron* 21, 531–543
2. Davis, J. B., Gray, J., Gunthorpe, M. J., Hatcher, J. P., Davey, P. T., Overend, P., Harries, M. H., Latcham, J., Clapham, C., Atkinson, K., Hughes, S. A., Rance, K., Grau, E., Harper, A. J., Pugh, P. L., Rogers, D. C., Bingham, S., Randall, A., and Sheardown, S. A. (2000) *Nature* 405, 183–187
3. Caterina, M. J., Leffler, A., Malmberg, A. B., Martin, W. J., Trafton, J., Petersen-Zeitz, K. R., Koltzenburg, M., Basbaum, A. I., and Julius, D. (2000) *Science* 288, 306–313
4. Caterina, M. J., Schumacher, M. A., Tominaga, M., Rosen, T. A., Levine, J. D., and Julius, D. (1997) *Nature* 389, 816–824
5. Trevisani, M., Smart, D., Gunthorpe, M. J., Tognetto, M., Barbieri, M., Campi, B., Amadesi, S., Gray, J., Jerman, J. C., Brough, S. J., Owen, D., Smith, G. D., Randall, A. D., Harrison, S., Bianchi, A., Davis, J. B., and Geppetti, P. (2002) *Nat. Neurosci.* 5, 546–551
6. Cornett, P. M., Matta, J. A., and Ahern, G. P. (2008) *Mol. Pharmacol.* 74, 1261–1268
7. Zhang, N., Inan, S., Inan, S., Cowan, A., Sun, R., Wang, J. M., Rogers, T. J., Caterina, M., and Oppenheim, J. J. (2005) *Proc. Natl. Acad. Sci. U.S.A.* 102, 4536–4541
8. Chuang, H. H., Prescott, E. D., Kong, H., Shields, S., Jordt, S. E., Basbaum, A. I., Chao, M. V., and Julius, D. (2001) *Nature* 411, 957–962

9. Pareek, T. K., Keller, J., Kesavapany, S., Agarwal, N., Kuner, R., Pant, H. C., Iadarola, M. J., Brady, R. O., and Kulkarni, A. B. (2007) *Proc. Natl. Acad. Sci. U.S.A.* 104, 660–665
10. Zhang, H., Cang, C. L., Kawasaki, Y., Liang, L. L., Zhang, Y. Q., Ji, R. R., and Zhao, Z. Q. (2007) *J. Neurosci.* 27, 12067–12077
11. Ahern, G. P., Brooks, I. M., Miyares, R. L., and Wang, X. B. (2005) *J. Neurosci.* 25, 5109–5116
12. Zhu, W., Xu, P., Cuascut, F. X., Hall, A. K., and Oxford, G. S. (2007) *J. Neurosci.* 27, 13770–13780
13. Ross, R. A. (2003) *Br. J. Pharmacol.* 140, 790–801
14. Hwang, S. W., Cho, H., Kwak, J., Lee, S. Y., Kang, C. J., Jung, J., Cho, S., Min, K. H., Suh, Y. G., Kim, D., and Oh, U. (2000) *Proc. Natl. Acad. Sci. U.S.A.* 97, 6155–6160
15. Hayes, P., Meadows, H. J., Gunthorpe, M. J., Harries, M. H., Duckworth, D. M., Cairns, W., Harrison, D. C., Clarke, C. E., Ellington, K., Prinjha, R. K., Barton, A. J., Medhurst, A. D., Smith, G. D., Topp, S., Murdock, P., Sanger, G. J., Terrett, J., Jenkins, O., Benham, C. D., Randall, A. D., Gloger, I. S., and Davis, J. B. (2000) *Pain* 88, 205–215
16. Olah, Z., Karai, L., and Iadarola, M. J. (2001) *J. Biol. Chem.* 276, 31163–31170
17. Sprague, J., Harrison, C., Rowbotham, D. J., Smart, D., and Lambert, D. G. (2001) *Eur. J. Pharmacol.* 423, 121–125
18. Gavva, N. R., Bannon, A. W., Surapaneni, S., Hovland, D. N., Jr., Lehto, S. G., Gore, A., Juan, T., Deng, H., Han, B., Klionsky, L., Kuang, R., Le, A., Tamir, R., Wang, J., Youngblood, B., Zhu, D., Norman, M. H., Magal, E., Treanor, J. J., and Louis, J. C. (2007) *J. Neurosci.* 27, 3366–3374

19. Gavva, N. R., Treanor, J. J., Garami, A., Fang, L., Surapaneni, S., Akrami, A., Alvarez, F., Bak, A., Darling, M., Gore, A., Jang, G. R., Kesslak, J. P., Ni, L., Norman, M. H., Palluconi, G., Rose, M. J., Salfi, M., Tan, E., Romanovsky, A. A., Banfield, C., and Davar, G. (2008) *Pain* 136, 202–210
20. Kedei, N., Szabo, T., Lile, J. D., Treanor, J. J., Olah, Z., Iadarola, M. J., and Blumberg, P. M. (2001) *J. Biol. Chem.* 276, 28613–28619
21. Jahnel, R., Dreger, M., Gillen, C., Bender, O., Kurreck, J., and Hucho, F. (2001) *Eur. J. Biochem.* 268, 5489–5496
22. Jordt, S. E., and Julius, D. (2002) *Cell* 108, 421–430
23. Owsianik, G., Talavera, K., Voets, T., and Nilius, B. (2006) *Annu. Rev. Physiol.* 68, 685–717
24. Jordt, S. E., Tominaga, M., and Julius, D. (2000) *Proc. Natl. Acad. Sci. U.S.A.* 97, 8134–8139
25. Hellwig, N., Plant, T. D., Janson, W., Scha¨fer, M., Schultz, G., and Schaefer, M. (2004) *J. Biol. Chem.* 279, 34553–34561
26. Vannier, B., Zhu, X., Brown, D., and Birnbaumer, L. (1998) *J. Biol. Chem.* 273, 8675–8679
27. Ryu, S., Liu, B., Yao, J., Fu, Q., and Qin, F. (2007) *J. Neurosci.* 27, 12797–12807
28. Phillips, E., Reeve, A., Bevan, S., and McIntyre, P. (2004) *J. Biol. Chem.* 279, 17165–17172
29. Gavva, N. R., Klionsky, L., Qu, Y., Shi, L., Tamir, R., Edenson, S., Zhang, T. J., Viswanadhan, V. N., Toth, A., Pearce, L. V., Vanderah, T. W., Porreca, F., Blumberg, P. M., Lile, J., Sun, Y., Wild, K., Louis, J. C., and Treanor, J. J. (2004) *J. Biol. Chem.* 279, 20283–20295
30. Johnson, D. M., Garrett, E. M., Rutter, R., Bonnert, T. P., Gao, Y. D., Middleton, R. E., and Sutton, K. G. (2006) *Mol. Pharmacol.* 70, 1005–1012

31. Voets, T., Droogmans, G., Wissenbach, U., Janssens, A., Flockerzi, V., and Nilius, B. (2004) *Nature* 430, 748–754
32. Matta, J. A., and Ahern, G. P. (2007) *J. Physiol.* 585, 469–482
33. Latorre, R., Brauchi, S., Orta, G., Zaelzer, C., and Vargas, G. (2007) *Cell Calcium* 42, 427–438
34. Brauchi, S., Orio, P., and Latorre, R. (2004) *Proc. Natl. Acad. Sci. U.S.A.* 101, 15494–15499